Regeneration induction in *Drosophila* limb promoted by nutrient factors

Thesis by
Yutian Li

In Partial Fulfillment of the Requirements for
the degree of
Doctor of Philosophy



CALIFORNIA INSTITUTE OF TECHNOLOGY
Pasadena, California

2027
(Defended May 19th, 2026)

© 2026

Yutian Li
ORCID: 0000-0001-8151-3518

ACKNOWLEDGEMENTS

Like *Journey to the West*, a Ph.D. is a long and demanding journey. Yet unlike a journey with a predetermined destination, scientific research is driven by exploring the unknown and pushing, little by little, the boundaries of human knowledge. I could not have wandered this far without the support of my advisor, colleagues, friends, and family.

First, I thank my advisor, Lea Goentoro, for welcoming me into the lab and for the opportunity to work on the regeneration project. Lea has been an incredibly supportive mentor who genuinely values my opinions, encourages independent thinking, and is truly invested in my development as a scientist. She has been closely involved in my work while also giving me the intellectual freedom to explore new directions. We even made occasional boba tea bets on the results of exploratory experiments, which, to my advantage, I won twice. Beyond research, Lea also genuinely cares about both my physical and mental health, and has often taken the time to check in on me. We have also had many chai lattes and snacks together, which I have come to value as moments of support and connection beyond the lab. I am truly grateful for her mentorship and support throughout these years.

I am also grateful to my lab mates in the Goentoro Lab - Zevin Condiotte, Gloria (Judah) Bates, Jesus del Rio Salgado, Christian Dimayuga, Anish Sarma, Aki Ohdera, and Natalia Huezo - for their helpful discussions and support over the years. I especially thank Zevin, Jesus, and Judah. The four of us joined the lab around the same time as graduate students and shared many of the same challenges along the way. Collecting samples from 9 a.m. to 3 p.m. for six weeks for the sequencing experiment would not have been possible without them. Christian provided great help with single-fly tracking. Anish encouraged me to try things, even if they started as tiny ideas. Aki has been calm, knowledgeable, and supportive for the whole lab throughout these years. Natalia always had great taste in meal options for group meetings. I truly appreciate the time and experiences we shared together.

I also benefited greatly from my collaborators. Fayth Tan and Martin Heithe introduced me to the *Drosophila* field. Shichen Liu helped me run the initial MiSeq. Maya Caskey helped me greatly with the data analysis. Brian Williams worked with me on fly single-nucleus

isolation, and we spent over a year optimizing the protocol together before he trained me in sequencing library preparation. Lior Pachter and Ingileif Hallgrimsdottir helped us plan the single-nucleus RNA sequencing and encouraged us to include more biological replicates. The fourth replicate, which I carried out independently during Christmas, showed slightly more noise compared to the first three, made me appreciate both the importance of experimental design and Brian's presence in the lab.

I thank my committee members, Bruce Hay, Michael Elowitz, Magdalena Zernicka-Goetz, for their guidance and thoughtful discussions that consistently brought clarity to my research direction and helped shape this work.

I am also grateful for the opportunity to mentor Caltech undergraduate students Iris Lee, Elisa Grillo, and Justin Hyon through the SURF program. Their curiosity and enthusiasm for exploring new ideas were so inspiring, and I learned a great deal from our discussions, some of which developed into new projects. I also had the privilege of mentoring Loise Wardhana, a high school volunteer, who contributed significantly to the early development of the ecdysone project.

I also appreciate the exceptional resources at Caltech. I spent a great deal of time in the Beckman Imaging Facility, where Giada Spigolon provided invaluable help with improving imaging quality. The Millard and Muriel Jacobs Genetics and Genomics Center supported us with bulk RNA sequencing, and the Single-Cell Profiling and Engineering Center provided guidance in optimizing single-nucleus RNA-seq experiments.

I could not have completed this journey without my closest Caltech friends, Yujing Yang, Meichen Fang, and Changhua Yu. Yujing, also my roommate, shared both the joys and stresses of our research experience. We also traveled together to Hawaii and now share the dream of living there. Meichen, albeit a little picky about food options, is not only a great listener but also an expert on data analysis. Changhua, whom we call Steve, rotated in the lab and started the bulk RNA sequencing experiment with me. He has also been a great meal companion and shopping partner over the years. I am also fortunate to have met so many friends here, including Yameng Zhang, Jinrui Hou, Can Li, Hanwei Liu, Michael Anaya,

Kaushiki Menon, Jialong Jiang, and many more, who have supported me in many ways throughout this time.

Before coming to Caltech, I was a student at UCSD, where I worked in the Hao Lab for three years. I deeply appreciate my advisor, Nan Hao, for welcoming me into research after I took his course and for his continued support of my development. I also sincerely thank Zohreh AkhavanAghdam and Yanfei Jiang for patiently teaching me the foundations of laboratory work and for their generous guidance in those early stages. I am grateful that I can still turn to Nan and Yanfei for advice on research, career, and life decisions.

Outside of Caltech, I am so thankful for the support from my friends all over the world. I especially thank Tianye Zhang for staying connected across time zones. I also thank Yutong Zhou, Chenyi Li, Xinyi Luo, Hanxin Zhang, Chen Chen, Qi Zhou, for visiting me in Los Angeles. I also thank my neighbor Tracey Miller and her therapy dog Beacon Miller for the comfort and late-night chats after long days.

I am also fortunate to have met my boyfriend, Kun Miao, at Caltech. He has been an indispensable part of my life throughout my PhD, first as a friend and later as my partner. He has been a constant source of emotional support and a valued peer in scientific discussions, and we have grown together throughout this journey. Supposedly, he has a stronger background in imaging than I do, but photographing me remains a challenge for him.

Finally, I would like to thank my extended family in China for always caring about me. Grandma, I hope you would be proud of me. Most importantly, I want to thank my parents, Xinming Li and Yan Zhang, for their unwavering support. They do not speak English, yet they visited me many times and always made sure I was well cared for—making sure I had enough “nutrients” in my daily life, a form of support that, in many ways, mirrors the central idea of this work. If this Ph.D. has been my *Journey to the West*, they are the reasons I was able to set out in the first place, and the home that has always supported me no matter how far I go.

ABSTRACT

Regeneration is a remarkable yet highly variable trait across tissue types and animals. This contrast raises a central question in biology: is regenerative capacity truly lost in poorly regenerating animals, or can it be reactivated under the appropriate physiological conditions? In this thesis, I investigated whether specific factors can induce appendage regeneration in animals with poor regenerative capacity, and how this regeneration activation is coordinated at both the tissue and organismal levels.

I first tested this question in animal species across the animal phylogeny: jellyfish, fruit flies, and mice. Although these animals do not normally regenerate appendages, through screening, we observed initiation of appendage regeneration when they were administered leucine, glutamine, and insulin. Although the induced regeneration is not complete, the key finding is that providing nutrient factors is sufficient to activate regeneration across evolutionarily distant species. The cross-species response suggests that regenerative programs are not fundamentally lost during evolution, but instead remain latent and can be reactivated upon favorable metabolic conditions.

Motivated by the potential use of *Drosophila* for investigating novel and conserved pathways in regeneration induction, I further characterized the regeneration induction. Although limb regrowth could take months, the decision to initiate regeneration processes is made within hours after injury, manifested in altered wound healing. At day-scale, while tissues in the injured limb segment normally degenerate, tissues in nutrient-supplemented flies survive. At week-scale, regenerative growth is preceded by a dome-shaped protrusion at the injury site. Performing single-nucleus RNA sequencing in the limb at this stage, I find widespread transcriptional modulations across cell types, and distinct cell populations within the muscle and epithelial cells that are enriched in mitotic and morphogenetic genes. This evidence across multiple time scales reveals how nutrient supplements can remodel the cells to reverse tissue loss and reactivate tissue replenishment.

Because nutrients act on the whole organism, I next investigated whether regeneration activation is accompanied by systemic remodeling, including changes at the organ level.

Indeed, regenerating flies enlarge their gut, which is a known mechanism to adapt to increased demands. In parallel, flies that activate regeneration reduce ovary size and egg chamber maturation. Consistent with the trade-off between activating regeneration and sustaining reproduction, virgin flies are more responsive to treatment. To further dissect candidate systemic regulators, I performed whole-organism transcriptomic profiling to identify the earliest processes that accompany the reactivation of regeneration. This analysis reveals steroid hormone signaling as one of the most highly upregulated signaling pathways. Because steroid hormone signaling is sensitive to nutritional status and interacts closely with insulin signaling to regulate systemic metabolism, these findings suggest that nutrient-induced regeneration involves not only local tissue remodeling, but also systemic organ remodeling and organism-wide resource reallocation.

In summary, my thesis identifies nutrient factors as a conserved strategy for inducing regeneration across evolutionarily distant species. By careful examination of gene-, cell- and tissue-level changes accompanying regeneration induction, I establish adult *Drosophila* as a tractable model to further dissect regeneration activation. Lastly, the role of nutrients further reveals that regeneration activation is a whole-body response that integrates nutrient sensing, systemic organ remodeling, and organism-wide resource reallocation.

PUBLISHED CONTENT AND CONTRIBUTIONS

Abrams MJ*, Tan FH*, **Li Y***, Basinger T, Heithe ML, Sarma A, Lee IT, Condiotte ZJ, Raffiee M, Dabiri JO, Gold DA, Goentoro L. A conserved strategy for inducing appendage regeneration in moon jellyfish, *Drosophila*, and mice. *Elife*. 2021 Dec 7;10:e65092. doi: 10.7554/eLife.65092. Erratum in: Elife. 2023 Jun 22;12:e90007. doi: 10.7554/eLife.90007.
*Equal contribution. Y.L. designed, performed experiments, analyzed data in the *Drosophila* section, and participated in the writing of the manuscript.

Li Y, del Rio Salgado J, Bates G, Condiotte ZJ, Caskey M, Williams B, Hallgrimsdottir I, Pachter L, Goentoro L. Regeneration induction in *Drosophila* by nutrient factors. Manuscript submitted.
Y.L. participated in the conceptualization of this project, designed and performed the experiments, data analysis, and wrote the manuscript.

Li Y, Bates G, Yu C, Grillo E, Wardhana L, Dimayuga CM, Goentoro L. Nutrient-induced regeneration in *Drosophila* involves coordinated organismal responses. Manuscript submitted.
Y.L. participated in the conceptualization of this project, designed and performed the experiments, data analysis, and wrote the manuscript.

Bates G, Dimayuga CM, Ammar HE, **Li Y**, Thaosatien J, Diop H, Morrissey K, Ohdera A, Goentoro L. *Lactobacillus brevis* that secretes ornithine can promote regeneration processes in *Drosophila* limb. Manuscript submitted.
Y.L. helped imaging of limb muscle.

TABLE OF CONTENTS

Acknowledgements iii
Abstract vi
Published Content and Contributions viii
Table of Contents ix
Chapter I: Introduction 1
1.1 Regeneration as a variable but widely distributed trait across animal phylogeny 1
1.2 Regenerative capacity across multiple species can be reawakened by providing extra nutrients 2
1.3 Adult *Drosophila* as an animal model for inducing regeneration 3
1.4 The role of nutrients suggests that inducing regeneration is a whole-body problem 4
Chapter II: A conserved strategy for inducing appendage regeneration in moon jellyfish, *Drosophila*, and mice 6
2.1 Summary 6
2.2 Introduction 6
2.3 Result 8
2.4 Discussion 18
2.5 Figures and tables 21
2.6 Supplemental information 32
2.7 Materials and methods 51
Chapter III: Regeneration induction in *Drosophila* limb by nutrient factors 61
3.1 Summary 61
3.2 Introduction 61
3.3 Result 62
3.4 Discussion 69
3.5 Figures and tables 71
3.6 Supplemental information 84
3.7 Materials and methods 89
Chapter IV: Regeneration activation in *Drosophila* by nutrient factors involves organismal modulations 92
4.1 Summary 92
4.2 Introduction 92
4.3 Result 94
4.4 Discussion 98
4.5 Figures and tables 100
4.6 Supplemental information 108
4.7 Materials and methods 111
Chapter V: Conclusion and future directions 114
Bibliography 117

Chapter 1

INTRODUCTION

Some animals can regenerate lost body parts after amputation, restoring complex patterned structures (Tanaka and Reddien, 2011). Humans, by contrast, are unable to regenerate limbs following injury. This striking disparity motivates a central question in biology: why some animals can regenerate complex organs or even an entire body, while others show very limited regeneration capacity, and whether the regenerative ability can be reactivated through a conserved mechanism.

1.1 Regeneration as a variable but widely distributed trait across animal phylogeny

Regeneration, the process of restoring lost tissues, organs, or even entire body structures, has long been a fundamental question in biology (Bely & Nyberg, 2010; Poss and Tanaka, 2024). The capacity to regenerate varies widely across the animal kingdom. For example, planarians can regenerate almost their entire body from a small body fragment (Tanaka and Reddien, 2011). Starfish can regenerate a whole body from a single remaining arm (Candia Carnevali, 2006). Salamanders can regenerate an entire limb, including bones, muscles, and nerves (Tanaka, 2016). These examples illustrate that some animals are capable of naturally regenerating complex structures after injury.

In contrast, many animals exhibit limited regenerative capacity. For example, *Xenopus* tadpoles lose the ability to regenerate tails during the refractory period (Beck et al., 2003). Mammals, including mice and humans, are also generally considered to be poorly regenerating animals. Regeneration in mammals is usually restricted to specific organs, tissues, or developmental stages. For example, mice can regenerate digit tips, but this regeneration is restricted to distal amputations and fails at more proximal levels (Muneoka et al., 2008; Han et al., 2007). Similarly, human digits can regenerate *in utero*, but this ability is lost as babies grow up (Yokoyama, 2007).

Importantly, increasing evidence shows that regeneration can be enhanced or reactivated in some of these limited-regeneration contexts by specific molecular or developmental signals. For example, local Bmp implantation can induce digit regeneration in mice (Yu et al., 2019). Tail regeneration in the refractory period in *Xenopus* can be partially rescued by BMP signaling (Beck et al., 2003). In addition, a multi-drug cocktail including growth factors has recently been shown to induce limb regeneration in adult *Xenopus* (Murugan et al., 2022).

Together, these findings provide further support that although regenerative capacity varies depending on species, development stage, and physiological state, it is a widely distributed trait across animals. Rather than being entirely absent in poorly regenerating systems, regenerative capacity may persist in a restricted form and can be activated under appropriate conditions. In this thesis, I first ask whether a conserved mechanism can induce regeneration in evolutionarily distant species with poor regenerative capacity.

1.2 Regenerative capacity across multiple species can be reawakened by providing extra nutrients

Injury repair is an energy-demanding process that requires extensive immune responses, cell proliferation, and tissue remodeling. Consequently, regeneration imposes substantial metabolic demands on the organism, including increased biosynthetic activity required for tissue rebuilding. To meet these demands, organisms often undergo systemic physiological changes following injury (Mahmoud, 2023). In flies, development can be delayed to allow time for repair (Worley and Hariharan, 2022). In mice and axolotls, injury induces cells in distant tissues to enter an alert state or show cell cycle activation, responses that are thought to prime tissues for future injury (Rodgers et al., 2014; Johnson et al., 2018). Severe injury in humans also triggers systemic metabolic alterations, including hyperglycemia and insulin resistance (Li et al., 2009).

Given the high metabolic demands of tissue rebuilding, nutrient availability strongly influences regenerative capacity. Indeed, limiting nutrient supply impairs the regeneration process even in highly regenerative species. When food is limiting, ctenophores stop

regenerating (Bading et al., 2017) and salamanders regenerate substantially smaller limbs (Peng et al., 2021). Starved planarians continue to regenerate normally, but require additional compensatory mechanisms (Gutiérrez-Gutiérrez et al., 2021). In axolotls, the nutrient-sensing pathway is hypersensitive, and inhibiting this pathway is sufficient to inhibit tissue regeneration (Zhulyn et al., 2023).

These observations make it expected that nutrients are necessary for supporting regeneration. However, it was surprising that simply supplying extra nutrients is sufficient to induce regeneration. As described in Chapter 2, my collaborators and I discovered that supplying specific nutrient factors, including leucine, glutamine, and insulin or sucrose, is sufficient to induce appendage regeneration in multiple animals, including mice, jellyfish, and fruit flies. Supporting this idea, increasing food supply rescues tail regeneration during the refractory period in tadpoles (Williams et al., 2021). Together, these findings suggest that nutrients are not only required to meet the energetic demands of regeneration, but also act as key physiological inputs that regulate whether regenerative programs are activated.

1.3 Adult *Drosophila* as a model for studying regeneration induction

The observation that nutrient factors can induce appendage regeneration across evolutionarily distant animals raises the question of how nutrient signals are integrated to regulate regeneration initiation in these animals. Among the species in which regeneration induction was observed, adult *Drosophila* provides a particularly powerful system for addressing this question. The fruit fly *Drosophila melanogaster* offers several practical and conceptual advantages for regeneration induction: its short life cycle and small body size can facilitate rapid testing of hypotheses. In addition, *Drosophila* has a well-developed experimental and genetic toolbox, which allows the identification of key principles in nutrient-induced regeneration.

Because visible limb regrowth occurs over weeks to months, this month scale phenotype can hamper mechanistic investigation. Therefore, motivated by the potential use of *Drosophila* for investigating novel and conserved pathways in regeneration induction, in Chapter 3, I

further characterize the early processes accompanying regeneration induction in *Drosophila*. Specifically, I examined the wound healing response, subsequent tissue survival and remodeling, and cell-level transcriptional modulations. Together, the characterized tissue-, cell-, and gene-level processes corroborate the previously observed limb growth, and facilitate the use of adult *Drosophila* as a tractable system for investigating the question of regeneration induction.

1.4 The role of nutrients suggests that inducing regeneration is a whole-body problem

Having established early markers of regeneration induction in the adult *Drosophila* limb in Chapter 3, I next investigate the processes accompanying this reactivation. The role of nutrients suggests that regeneration induction is not only controlled by tissue-specific mechanisms within the injured organ, but may also involve upstream systemic processes that regulate nutrient availability, metabolic state, and resource allocation. Indeed, even during naturally occurring regeneration processes, mounting a regeneration response impacts remote organs and organismal processes (Sun and Poss, 2023; Rennolds and Bely, 2023). For instance, tissue regeneration modifies lipid composition in distant organs (Kubler et al., 2024) and affects reproduction (Rennolds and Bely, 2024). Thus, inducing regeneration may require more than engineering local changes in the injured tissue. It may also require coordinating whole-body physiology to create a regeneration-promoting state.

This organismal perspective has potential relevance beyond the fly model. For instance, large-scale tissue loss and muscle atrophy are known complications in major injuries, including in amputees or intensive care unit patients (Kress and Hall, 2014; Sanders and Fatone, 2011). Modulating organismal nutrient pathways and metabolic organs may provide novel routes for rewiring the organism into a more regeneration-promoting state. Supporting this broader view, related work from the lab presents evidence that modulating the microbiome can also promote activation of limb regrowth (Bates et al., in review).

Drosophila is well suited for studying such organismal-scale questions. In Chapter 4, I therefore investigate systemic physiological changes accompanying nutrient-induced

regeneration, including remodeling of metabolic and reproductive organs. I further test one of the key pathways activated in the early regenerative response: steroid hormone signaling.

Together, these considerations frame the central question of this thesis: whether regenerative capacity in poorly regenerating animals can be reactivated by nutrient inputs, and how this activation is coordinated across local tissues and organismal physiology. Chapter 2 examines whether regeneration can be induced across evolutionarily distant animals with poor regenerative capacity. Chapter 3 characterizes early local processes in adult *Drosophila* limb regeneration to establish a tractable system for studying regeneration induction. Chapter 4 investigates the systemic physiological changes that accompany nutrient-induced regeneration.

Chapter 2

A conserved strategy for inducing appendage regeneration in moon jellyfish, *Drosophila*, and mice.

The content of this chapter has been published in:
Abrams MJ*, Tan FH*, Li Y*, Basinger T, Heithe ML, Sarma A, Lee IT, Condiotte ZJ, Raffiee M, Dabiri JO, Gold DA, Goentoro L. A conserved strategy for inducing appendage regeneration in moon jellyfish, *Drosophila*, and mice. Elife. 2021 Dec 7;10:e65092. doi: 10.7554/eLife.65092. Erratum in: Elife. 2023 Jun 22;12:e90007. doi: 10.7554/eLife.90007.

2.1 Summary

Can limb regeneration be induced? Few have pursued this question, and an evolutionarily conserved strategy has yet to emerge. This chapter reports a strategy for inducing regenerative response in appendage, which works across three species that span animal phylogeny. In Cnidaria, the frequency of appendage regeneration in the moon jellyfish *Aurelia aurita* was increased by feeding with the amino acid L-leucine and the growth hormone insulin. In insects, the same strategy induced tibia regeneration in adult *Drosophila*. Finally, in mammals, L-leucine and sucrose administration induced digit regeneration in adult mice, including dramatically from mid-phalangeal amputation. The conserved effect of L-leucine and insulin/sugar suggests a key role for energetic parameters in regeneration induction. The simplicity by which nutrient supplementation can induce appendage regeneration provides a testable hypothesis across animals.

2.2 Introduction

In contrast to humans' poor ability to regenerate, the animal world is filled with seemingly Homeric tales: a creature that regrows when halved or a whole animal growing from a small body piece. Two views have historically prevailed as to why some animals regenerate better than others (Goss, 1992). Some biologists, including Charles Darwin and August Weismann, hold that regeneration is an adaptive property of a specific organ (Polezhaev, 1972). For instance, some lobsters may evolve the ability to regenerate claws because they often lose

them in fights and food foraging. Other biologists, including Thomas Morgan, hold that regeneration is not an evolved trait of a particular organ, but inherent in all organisms (Morgan, 1901). Regeneration evolving for a particular organ versus regeneration being organismally inherent is an important distinction, as the latter suggests that the lack of regeneration is not due to the trait never having evolved, but rather due to inactivation—and may therefore be induced. In support of Morgan's view, studies in past decades have converged on one striking insight: many animal phyla have at least one or more species that regenerate body parts (Sánchez Alvarado, 2000; Bely and Nyberg, 2010). Further, even in poorly regenerative lineages, many embryonic and larval stages can regenerate. In regenerating animals, conserved molecular events (e.g., Cary et al., 2019, Kawakami et al., 2006) and regeneration-responsive enhancers (Wang et al., 2020) were identified. Although the hypothesis of convergent evolution cannot be fully excluded (e.g., Lai and Aboobaker, 2018), these findings begin to build the case that the ability to regenerate may be ancestral (Sánchez Alvarado, 2000; Bely and Nyberg, 2010). Regeneration being possibly ancestral begs the question: is there a conserved mechanism to activate regenerative state?

This chapter explored how, and whether, limbs can be made to regenerate in animals that do not normally show limb regeneration. In adult frogs, studies from the early 20th century and few recent ones have induced various degrees of outgrowth in the limb using strategies including repeated trauma, electrical stimulation, local progesterone delivery, progenitor cell implantation, and Wnt activation (Carlson, 2007; Lin et al., 2013; Kawakami et al., 2006; Herrera-Rincon et al., 2018). Wnt activation restored limb development in chick embryos (Kawakami et al., 2006), but there are no reports of postnatal regeneration induction. In salamanders, a wound site that normally just heals can be induced to grow a limb by supplying nerve connection and skin graft from the contralateral limb (Endo et al., 2004), or by delivery of Fgf2, 8, and Bmp2 to the wound site followed by retinoic acid (Vieira et al., 2019). In neonatal and adult mouse digits, a model for exploring limb regeneration in mammals, bone outgrowth, or joint-like structure can be induced via local implantation of Bmp2 (bone) or Bmp9 (joint; Yu et al., 2019). Thus far, different strategies gain tractions in different species, and a common denominator appears elusive.

However, across animal phylogeny, some physiological features show interesting correlation with regenerative ability (Hariharan et al., 2016; Vivien et al., 2016; Sousounis et al., 2014). First, regeneration especially in vertebrates tends to decrease with age, with juveniles and larvae more likely to regenerate than adults. For instance, the mammalian heart rapidly loses the ability to regenerate after birth and anurans cease to regenerate limbs upon metamorphosis. Second, animals that continue to grow throughout life tend to also regenerate. For instance, most annelids continue adding body segments and regenerate well, a striking exception of which is leeches that make exactly 32 segments and one of the few annelids that do not regenerate body segments (Rouse, 1998). Consistent with the notion of regeneration as ancestral, indeterminate growth is thought of as the ancestral state (Hariharan et al., 2016). Finally, a broad correlate of regenerative ability across animal phylogeny is thermal regulation. Poikilotherms, which include most invertebrates, fish, reptiles, and amphibians, tend to have greater regenerative abilities than homeotherms—birds and mammals are animal lineages with poorest regeneration. These physiological correlates, taken together, are united by the notion of energy expenditure. The transition from juvenile to adult is a period of intense energy usage, continued growth is generally underlined by sustained anabolic processes, and regulating body temperature is energetically expensive compared to allowing for fluctuation. Regeneration itself entails activation of anabolic processes to rebuild lost tissues (Hirose et al., 2014; Naviaux et al., 2009; Malandraki-Miller et al., 2018; Takayama et al., 2018). These physiological correlates thus raise the notion of a key role of energetics in the evolution of regeneration in animals. Specifically, we wondered whether energy inputs can promote regenerative state. In this chapter, we demonstrate that nutrient supplementation can induce regenerative response in appendage and limb across three vastly divergent species.

2.3 Results

Leucine and insulin promote appendage regeneration in the moon jelly *Aurelia*

We reasoned that if there was an ancestral mechanism to promote regeneration, it would likely remain intact in early branching lineages with prevalent regeneration across the species. In Cnidaria, the ability to regenerate is established in polyps, for example, hydras and sea

anemones. Some cnidarians, notably jellyfish, not only exist as sessile polyps, but also as free-swimming ephyrae and medusae (Figure 1a). In contrast to the polyps' ability to regenerate, regeneration in ephyrae and medusae appears more restricted in some species (Abrams et al., 2015; Sinigaglia et al., 2020; Schmid and Alder, 1984). We focused on the moon jellyfish *Aurelia coerulea* (formerly *A. aurita* sp. 1 strain), specifically on the ephyra, whose eight arms facilitate morphological tracking (Figure 1b). About 3 mm in diameter, *Aurelia* ephyrae regenerate the tips of arms and the distal sensory organ rhopalium, but upon more dramatic amputations such as removing a whole arm or halving the body, rapidly reorganize existing body parts and regain radial symmetry (Figure 1c). Observed across four scyphozoan species, symmetrization occurs rapidly within 1–3 days and robustly across conditions (Abrams et al., 2015). Ephyrae that symmetrized matured into medusae, whereas ephyrae that failed to symmetrize and simply healed the wound grew abnormally.

Intriguingly, in the course of our previous study (Abrams et al., 2015), we observed in a few symmetrizing ephyrae, a small bud at the amputation site. To follow this hunch, we repeated the experiment in the original habitat of our lab's polyp population, off the coast of Long Beach, CA (Materials and methods). Two weeks after amputation, most ephyrae indeed symmetrized, but in 2 out of 18 animals a small arm grew (Figure 1c). This observation suggests that, despite symmetrization being the more robust response to injury, an inherent ability to regenerate arm is present and can be naturally manifest. The inherent arm regeneration presents an opportunity: Can arm regeneration be reproduced in the lab, as a way to identify factors that promote regenerative state?

To answer this question, we screened various molecular and physical factors (Figure 2a, Table S1). Molecularly, we tested modulators of developmental signaling pathways as well as physiological pathways such as metabolism, stress response, immune, and inflammatory response. Physically, we explored environmental parameters, such as temperature, oxygen level, and water current. Amputation was performed across the central body removing three arms (Figure 2a). Parameter changes were implemented or molecular modulators (e.g., peptides and small molecules) were introduced into the water immediately

after amputation. Regenerative response was assessed for 1–2 weeks until the onset of bell growth, which hindered the scoring of arm regeneration (Figure S2).

After 3 years of screening, only three factors emerged that strongly promoted arm regeneration (Figure 2b). The ephyrae persistently symmetrized in the majority of conditions tested. In the few conditions where regeneration occurred, arm regenerates show multiple tissues regrown in the right locations: circulatory canals, muscle, neurons, and rhopalium (Figure 2c–e). The arm regenerates contracted synchronously with the original arms (Video 1), demonstrating a functional neuromuscular network. Thus, arm regeneration in *Aurelia* that was observed in the natural habitat can be recapitulated in the lab by administering specific exogenous factors.

The extent of arm regeneration varied, from small to almost fully sized arms (Figure 2b). The variation manifested even within individuals: a single ephyra could grow differently sized arms. Of the three arms removed, if regeneration occurred, generally one arm regenerated (67%), occasionally two arms (32%), and rarely three arms (1%, of the 4270 total ephyrae quantified in this study). Finally, the frequency of regeneration varied across clutches, that is, strobilation cohorts. Some variability may be due to technical factors, for example, varying feed culture conditions; however, variability persisted even with the same feed batch. We verified that the variability was not entirely due to genetic differences, as it manifested across clonal populations (Figure S3). Thus, there appears to be stochasticity in the occurrence of arm regeneration in *Aurelia* and the extent to which regeneration proceeds.

What are the factors that promote arm regeneration? Notably, modulation of developmental pathways often implicated in regeneration literature (e.g., Wnt, Bmp, and Tgfß) did not produce effect in the screen (Table S1)—although we do not rule out their involvement in other capacity, for example, in downstream patterning. We first identified a necessary condition: water current. The requirement for current for promoting regeneration is interesting because ephyrae can recover from injury by symmetrizing in stagnant water (Figure 1c). Thus, a specific physiological state is required for enabling regenerative response. Behaviorally, the presence of current promotes more swimming, while in stagnant

water ephyrae tend to rest at the bottom and pulse stationarily (Figure S4 and Video 2 show the aquarium setup used to implement current). In this permissive condition, the first factor that promotes regeneration is the nutrient level: increasing food amount increases the frequency of arm regeneration. To measure the regeneration frequency, we scored any regenerates with lengths greater than 15% of that of an uncut arm (Figure 3a). This threshold was chosen to predominantly exclude non-specific growths or buds that show no morphological structures (Figure 3b) while including small arm regenerates that show clear morphological features, that is, lappets, radial canal, and radial muscle sometimes showing growing ends (Figure 3b). Given the clutch-to-clutch variability, control and treatment were always performed side by side using ephyrae from the same clutch. The effect size of a treatment was assessed by computing the change in regeneration frequency relative to the internal control. Statistical significance of a treatment was assessed by evaluating the reproducibility of its effect size across independent experiments (Materials and methods). With these measurement and statistical methodologies, we found that although the baseline regeneration frequency varied across clutches, higher food amounts reproducibly increased regeneration frequency (Figure 3c). The magnitude of the increase varied (Figure 3g, 95% confidence interval [CI] [4.7, 12.1-fold]), but the increase was reproducible (95% CI excludes 1) and statistically significant ($p<10^{-4}$).

The second factor that promotes regeneration is insulin (Figure 3d). We verified that the insulin receptor is conserved in *Aurelia* (Figure S5). Administering insulin led to a reproducible (Figure 3g, 95% CI [1.1, 5.0-fold]) and statistically significant ($p<0.05$) increase in regeneration frequency. The insulin effect was unlikely to be due to non-specific addition of proteins, since bovine serum albumin (BSA) at the same molarity showed no statistically significant effect (Figure S7). Finally, the third promoter of regeneration is hypoxia (Figure 3e). We verified that the ancient oxygen sensor HIFα is present in *Aurelia* (Figure S5). Hypoxia led to a reproducible (Figure 3g, 95% CI [1.4, 12.0-fold]) and statistically significant ($p<0.01$) increase in regeneration frequency. To reduce oxygen, nitrogen was flown into the seawater, achieving ~50% reduction in dissolved oxygen level (Materials and methods). We verified that the effect was due to reduced oxygen rather than

increased nitrogen, since reducing oxygen using argon flow similarly increased regeneration frequency (Figure S7). The factors can act synergistically (e.g., insulin and high nutrient level), but the effect appears to eventually saturate (e.g., hypoxia and high nutrient level).

In addition to quantifying the number of ephyrae that regenerate, we further quantified the regeneration phenotypes in each ephyra, that is, the number of arms regenerating, the length of arm regenerates, and the formation of rhopalia (Figure 3—figure supplements 5 and 6). Nutrient level strikingly improved all phenotypic metrics: not only more ephyrae regenerated in higher nutrients, more ephyrae regenerated multiple arms, longer arms, and arms with rhopalia. Insulin and hypoxia, interestingly, show differential phenotypes. Most strikingly, while insulin induced more ephyrae to regenerate multiple arms, hypoxia induced largely single-arm regenerates, for example, hypoxia experiments 3 and 5 in Figure S8c. Thus, while all factors increased the probability to regenerate, they had differential effects on the regeneration phenotypes, suggesting a decoupling to a certain extent between the regulation of the decision to regenerate and the regulation of the subsequent morphogenesis.

Of the three factors identified in the screen, nutrient input is the broadest, and prompted us to search if a more specific nutritional component could capture the effects of full nutrients in promoting regeneration. Jellyfish are carnivorous and eat protein-rich diets of zooplanktons and other smaller jellyfish (Graham, 2001). Notably, all three factors induced growth: treated ephyrae are larger than control ephyrae (Figure S10). The growth effect is interesting because of essential amino acids that must be obtained from food, branched amino acids supplementation correlates positively with protein synthesis and growth, and in particular, L-leucine appears to recapitulate most of the anabolic effects of high amino acid diet (Lynch and Adams, 2014; Stipanuk, 2008). Motivated by the correlation between growth and increased regeneration frequency, we wondered if leucine administration could promote regeneration. Animals typically have a poor ability to metabolize leucine, such that the extracellular concentrations of leucine fluctuate with dietary consumption (Wolfson et al., 2016). As a consequence, dietary leucine directly influences cellular metabolism. Feeding

amputated ephyrae with leucine indeed led to increased growth (Figure S9). Assessing arm regeneration in the leucine-supplemented ephyrae, we observed a significant increase in the regeneration frequency (Figure 3f–g, 95% CI [2.5, 6.6-fold], $p<10^{-4}$). Furthermore, leucine treatment phenocopies the effect of high nutrients, improving all measured phenotypic metrics: increasing multi-arm regeneration, the length of arm regenerate, and the frequency of rhopalia formation (Figure 3—figure supplements 5 and 6).

These experiments demonstrate that abundant nutrients, the growth factor insulin, reduced oxygen level, and the amino acid L-leucine promote appendage regeneration in *Aurelia* ephyra. The identified factors are fundamental physiological factors across animals. Might the same factors promote appendage regeneration in other animal species?

Leucine and insulin induce regeneration in *Drosophila* limb

To pursue this question, we searched for other poorly regenerating systems, which fortunately include most laboratory models. *Drosophila*, along with beetles and butterflies, belong to the holometabolans—a vast group of insects that undergo complete metamorphosis, and that as whole, do not regenerate limbs or other appendages as adults (Das, 2015). Larval stages have imaginal disks, undifferentiated precursors of adult appendages such as the legs and antennae, and portions of imaginal disks have been shown to regenerate (Worley et al., 2012). Motivated by findings in *Aurelia*, we asked if leucine and insulin administration can induce regenerative response in the limb of adult *Drosophila*. We focused on testing leucine and insulin in this study because of considerations of specificity (i.e., nutrients are broad and composition of nutritional needs vary across species), pragmatism (i.e., administering hypoxia requires more complex setups), and in the case of *Drosophila* specifically, *Drosophila* being resistant to hypoxia (Haddad et al., 1997).

We amputated *Drosophila* on the hindlimb, across the fourth segment of the leg, the tibia (Figure 4a). After amputation, flies were housed in vials with standard food (control) or standard food supplemented with leucine and insulin, with glutamine to promote leucine

uptake (Nicklin et al., 2009) (treated) (Figure 4c). Each fly was examined multiple times, twice in the first week, and then once weekly over the course of 2–4 weeks.

No regrown tibia was found in the 860 control flies examined (Figure 4b–c). In the treated flies, only tibia stumps were observed in the first week after amputation. But remarkably, at 7–21 days post-amputation (dpa), a few regrown tibias were observed (1.0%, N=387; Figure 4d–e). The regrown tibias culminate in reformed joints, articulating from which appears to be the beginning of a next. segment. Control tibia stumps showed melanized clots at the tips within 1–3 dpa (Figure 4b), as expected from normal wound healing process (Rämet et al., 2002), while some treated tibias showed no clot (12.1%, N=387) and the tips stained positively with DAPI instead (14 out of 16 tibias examined; Figure 4f). Induction of regenerative response was observed across genetic backgrounds, in Oregon R, as discussed, and Canton S wild-type strains (Figure S11a). Reminiscent of *Aurelia*, not all regenerative response was patterned, few flies showed non-specific outgrowth (Figure S11b).

The bulk experiment enables us to assess a large number of flies and can capture dramatic regenerative response, that is, a fully regrown leg segment. But it can miss partial segment regrowth and therefore underestimate the extent of regenerative response. To track regenerative response in individual flies, we housed in each vial a small number of flies that were amputated in different limbs (Figure 5a). The amputated limb position, combined with sex, enabled unique identification of each fly within a vial. Each fly was imaged immediately after amputation and 1–3 additional times over the course of 2–4 weeks. The imaging frequency balanced obtaining time-lapse information with minimizing stress from repeated anesthesia.

The single-fly tracking showed pervasive regenerative response induced by nutrient supplementation. Time-lapse pictures of select control and treated flies are shown in Figure 5b–d. For each tibia stump, we measured the length over time (Figure 5e). Control tibia stumps showed near-zero percent change in length (Figure 5d; mean –0.3%, 95% CI [–3.8, 3.2%], N=116). By contrast, 49% of treated flies showed growth beyond the 95% CIs of the control distribution (Figure 5f; N=150). The rate of regrowth varied; some flies showed large

growth during the first 1–2 weeks post-amputation, while others regrow more slowly over 2–3 weeks (Figure 5c). Interestingly, four flies (2.7%) showed shortened tibia stumps, which may indicate roles of histolysis in regenerative response. Regenerative response was not only observed from amputations across the tibia, but also from more dramatic amputations across the femur (Figure 5d). We verified that the control and treated length change distributions are statistically different ($p<0.0001$***, nonparametric Kruskal-Wallis test). No sex-based differences in response were observed (Figure S12a).

In some limbs, the new growth already looks almost indistinguishable from the rest of the leg. In some limbs, the new growth showed what may be intermediate morphologies. For instance, some new growths are pigmented differently and/or have no sensory bristles (Figure 5g, Figure S12d, e,) or showed white tissues protruding from the end (e.g., Figure S12c), which was remodeled over time (e.g., Figure S12d). Finally, reproducing what was observed in the bulk experiments, five flies showed reformed tibia segments: showing a tapering end (N=150; Figure 5h), what appeared to be a joint (Figure 5i), and the beginning of the next segment (Figure 5j).

A scanning electron micrograph of a regrown hindlimb tibia (the top tibia in Figure 4e, taken 1 week later) morphologically confirms the regenerated joint as a tibial/tarsal joint. The joint-like structure shows the expected bilateral symmetry of a tibial/tarsal joint (as opposed to, e.g., the radially symmetrical tarsal/tarsal joints; Mirth and Akam, 2002) with rounded projections at the posterior and anterior end (arrows in Figure 5k). These projections, called condyles, function as points of articulation between opposing leg segments. Indeed, articulating from the regrown condyles appears to be further growth of the next tarsal segment. Finally, a unique feature of the tibial/tarsal joint of the hindlimb (but not of fore or midlimb) is an additional ventral projection between the side condyles (Mirth and Akam, 2002), which serves to restrain bending of the leg upward. The ventral projection is indeed present in the regenerated joint (arrow in Figure 5k). Altogether, these data demonstrate for the first time that patterned regenerative response can be induced from adult *Drosophila* limbs.

Leucine and sucrose induce regeneration in mouse digit

The ability of leucine and insulin to induce regenerative response in *Drosophila* limb and *Aurelia* appendage motivated testing in vertebrates. One sign that limb regeneration may be feasible in humans is that fingertips regenerate (Illingworth, 1974). The mammalian model for studying limb regeneration is the house mouse, *Mus musculus*, which like humans, regenerates digit tips. Although proximal regions of digits do not regenerate, increasing evidence suggests that they have inherent regenerative capacity. In adult mice, implanting developmental signals in amputated digits led to specific tissue induction, that is, bone growth with Bmp4 or joint-like structure with Bmp9 (Yu et al., 2019). In neonates, reactivation of the embryonic gene *lin28* led to distal phalange regrowth (Shyh-Chang et al., 2013). Thus, while patterned phalange regeneration can be induced in newborns, induction in adults so far involves a fine-tuned stimulation, for example, to elongate bone and then make joint, Bmp4 was first administered followed by Bmp9 in a timed manner. Motivated by the findings in *Aurelia* and *Drosophila*, we tested if leucine and insulin administration could induce a self-organized regeneration in adult mice.

We performed amputation on the hindpaw (Figure 6a), on digits 2 and 4, leaving the middle digit three as an internal control (Figure 6b). To perform non-regenerating amputation, a clear morphological marker is the nail, which is associated with the distal phalange (P3). Amputation that removes <30% of P3 length, that cuts within the nail, readily regenerates, whereas amputation that removes >60% of P3 length, corresponding to removing almost the entire visible nail, does not regenerate (Figure 6c; Chamberlain et al., 2017; Lehoczky et al., 2011). We therefore performed amputations entirely proximal to the visible nail—giving, within the precision of our amputation, a range of cut across somewhere between the proximal P3 and the distal middle phalange (P2) (Figure 6d)—a range that is well below the regenerating tip region. Note additional morphological markers that lie within the non-regenerating region: the os hole (‘o’ in Figure 6c), where vasculatures and nerves enter P3, the bone marrow cavity (‘m’ in Figure 6c), and the sesamoid bone (‘s’ in Figure 6c) adjacent to P2.

The digit portion removed was immediately fixed to determine the precise plane of amputation. The amputated mice were either provided with water as usual (control) or water supplemented with leucine and sucrose (treated) (Figure 6e). Both groups were monitored for 7–8 weeks. Sucrose was used because insulin is proteolytically digested in the mammalian gut. The sucrose doses used are lower or the administration duration is shorter than those shown to induce insulin resistance (Cao et al., 2007; Togo et al., 2019). We verified that control and treated mice had comparable initial weights (35.1±0.6 vs. 34.1±1.1 g, p=0.402, Student's t-test), and that as expected from amino acid and sugar supplementation, treated mice gained more weight over the experimental duration (4.5±1.0 vs. 7.8±1.0 g, p=0.028, Student's t-test).

As expected for amputation proximal to the nail, no regeneration was observed in the control mice (N=34 digits, 17 mice). Amputated digits healed and re-epithelialized the wound as expected (Figure 6f). Skeletal staining shows blunt-ended digit stumps (Figure 6i) and in many instances, as expected, dramatic histolysis, a phenomenon where bone recedes further from the amputation plane (Figure S13; Chamberlain et al., 2017). By contrast, 18.8% of the treated digits (N=48 digits, 24 mice) showed various extents of regenerative response (Figure S13). The increase in regeneration frequency due to the treatment is statistically significant (95% CI [8, 30%], p=0.0019,**, Student's t-test).

We observed, as in *Aurelia* and *Drosophila*, an unpatterned response (Figure S13), wherein skeletal staining reveals excessive bone mass around the digit stump, similarly to what was observed in some cases with BMP stimulation (Yu et al., 2019). However, we also observed patterned responses (Figure S14). The most dramatic regenerative response was observed in two digits (Figure 6g–h). In one digit, an almost complete regrowth of the distal phalange and the nail was observed (Figure 6g). Skeletal staining of the portion removed from this digit (Figure 6j) shows that it was amputated at the proximal P3 transecting the os hole. By 7 weeks, skeletal staining of the regrown digit (Figure 6j) shows that the P3 bone was almost completely regrown. The regrown P3 shows trabecular appearance that is similar in general structure but not identical to the original P3. Another dramatic response was observed from

another digit, which began reforming the nail by 7 weeks (Figure 6h). Skeletal staining of the portion removed from this digit shows that it was amputated across the P2 bone, removing the entire epiphyseal cap along with the sesamoid bone (Figure 6k). Skeletal staining of the regenerating digit shows that the epiphyseal cap was regrown, along with its associated sesamoid bone. Moreover, articulating from the regenerated P2 appears to be the beginning of the next phalangeal bone (arrow, Figure 6k). To our knowledge, the regenerative response observed in these digits represents the most dramatic extent of self-organized mammalian digit regeneration reported thus far. Distal phalange regeneration in adults has not been reported, while interphalangeal joint formation from a P2 amputation has been achieved only through sequential Bmp administration (Yu et al., 2019) and there has been no documentation of the regrowth of the sesamoid bone.

2.4 Discussion

In this study, amputations were performed on *Aurelia* appendage, *Drosophila* limb, and mouse digit. None of these animals are known to regenerate robustly (*Aurelia*) if at all (*Drosophila* and mouse) from these amputations. Upon administration of L-leucine and sugar/insulin, dramatic regenerative response was observed in all systems. The conserved effect of nutrient supplementation across three species that span more than 500 million years of evolutionary divergence suggests energetic parameters as ancestral regulators of regeneration activation in animals.

While we did not test the regenerative effect of hypoxia beyond *Aurelia*, it is notable that in mice hypoxia coaxes cardiomyocytes to re-enter cell cycle (Kimura et al., 2015) and activate HIF1α promotes healing of ear hole punch injury (Zhang et al., 2015). Notably in *Aurelia*, the amputation bisected through the body, and more than appendage was in fact regenerated, for example, circular muscle in the body is regrown (Figure 2e). Thus, nutrient supplementation may have regenerative effect in body parts beyond appendage.

The diverse physiologies of animals across phylogeny may seem difficult to reconcile with a conserved regulation of regeneration activation, especially in the view of regeneration as

recapitulation of development. Growing a jellyfish appendage is different from building a fly leg or making a mouse digit. However, there is another way of looking at regeneration as a part of tissue plasticity (Galliot and Ghila, 2010). In this view of regeneration, upstream from tissue-specific morphogenesis is a conserved regulation of cell growth and proliferation. In support of this idea, early steps in regeneration across species and organs rely one way or another on proliferation by stem cells or differentiated cells re-entering cell cycle (Cox et al., 2019). We propose that in animals that poorly regenerate, high nutrient input turns on growth and anabolic states that promote tissue rebuilding upon injury.

That regenerative response can be induced seemingly blurs the boundary between regenerating versus non-regenerating animals, because the factors identified in the study are not exotic. Variations in amino acids, carbohydrates, and oxygen levels are conditions that the animals can plausibly encounter in nature. These observations highlight two potential insights into regeneration. First, regeneration is environmentally dependent. An animal would stop at wound healing under low-energy conditions and regenerate in energy-replete conditions. In this view, for the animals examined in this study, the typical laboratory conditions may simply not be conducive to regeneration. Alternatively, the interpretation we favor, what we observed is inherent regeneration, which can be activated with broad environmental factors. We favor this interpretation because the regenerative response was unusually variable. The variability stands in stark contrast to the robust regeneration in, for example, axolotl, planaria, or hydra. Whereas wild-type processes tend to be robust, mutations produce phenotypes that are sensitive to variations in physiological parameters. Thus, just like mutant phenotypes show varying penetrance and expressivity, the variable regenerative response speaks to us as a fundamental consequence of activating a latent biological module. In this interpretation, the ordinariness of the activators suggests ancestral regeneration as part of a response to broad environmental stimuli. It would be interesting next to identify individual differences that contribute to varying propensities to mount regenerative response.

In particular, the conserved effects of nutrient supplementation suggest that regeneration might have originally been a part of growth response to abundant environments. No nutrient dependence has been observed in highly regenerating animal models such as planaria, hydra, and axolotl. Environment-dependent plasticity, however, is pervasive in development, physiology, behavior, and phenology (West-Eberhard, 2003; Moczek et al., 2011). We therefore conjecture that environment-dependent plasticity may have characterized the ancestral form of regeneration. In this conjecture, present regenerating lineages might have decoupled the linkage with environmental input and genetically assimilated regenerative response—because regeneration is adaptive or coupled to a strongly selected process, for example, reproduction. In parallel, non- or poorly regenerating animals might have also weakened the linkage with environmental input, but to silence the regenerative response. This predicts an ancient form of a robustly regenerative animal (like planaria, hydra, and axolotl) that tunes its regeneration frequency to nutrient abundance. Such plasticity has been reported in the basal lineage Ctenophora (Bading et al., 2017).

In conclusion, this study suggests that an inherent ability for appendage regeneration is retained in non-regenerating animals and can be unlocked with a conserved strategy. The treatments across species were not exactly identical, and correspondingly there might be differences in the precise molecular mechanisms—in spite of which they could be applied across species in a predictive manner. In line with our findings, the role of nutrients in promoting regeneration was reported in yet another species (in the *Xenopus tadpoles*, Williams et al., 2021). While the observed regenerative response is not perfect, this motivates further investigation into potentially more promoting factors or the possibility of combining broad promoting factors with species- or tissue-specific morphogenetic regulators. Reiterating Spallanzani's hope, Marcus Singer supposed half a century ago that '... every organ has the power to regrow lying latent within it, needing only the appropriate "useful dispositions" to bring it out (Singer, 1958).' The surprise, in hindsight, is the simplicity by which the regenerative state can be promoted with ad libitum amino acid and sugar supplementation. This simplicity demonstrates a much broader possibility of organismal regeneration, and can help accelerate progress in regeneration induction across animals.

2.5 Figures and Tables

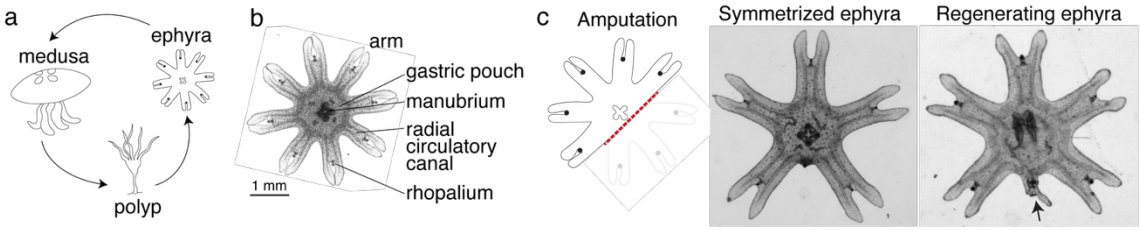


Figure 1. *Aurelia* as a system to identify factors that promote appendage regeneration.

(a) The moon jellyfish *Aurelia aurita* has a dimorphic life cycle, existing as sessile polyps or free-swimming medusae and ephyrae. Ephyra is the juvenile stage of medusa, a robust stage that can withstand months of starvation. In lab conditions, ephyrae mature into medusae, growing bell tissue, and reproductive organs, in 1–2 months.

(b) Ephyrae have eight arms, which are swimming appendages that contract synchronously to generate axisymmetric fluid flow, which facilitates propulsion and filter feeding. The eight arms are symmetrically positioned around the stomach and the feeding organ manubrium. Extending into each arm is radial muscle (shown in Figure 2) and a circulatory canal that transports nutrients. At the end of each arm is the light- and gravity-sensing organ rhopalium.

(c) In response to injury, the majority of ephyrae rapidly reorganize existing body parts and regain radial symmetry. However, performing the experiment in the natural habitat, a few ephyrae (2 out of 18) regenerated a small arm (arrow).

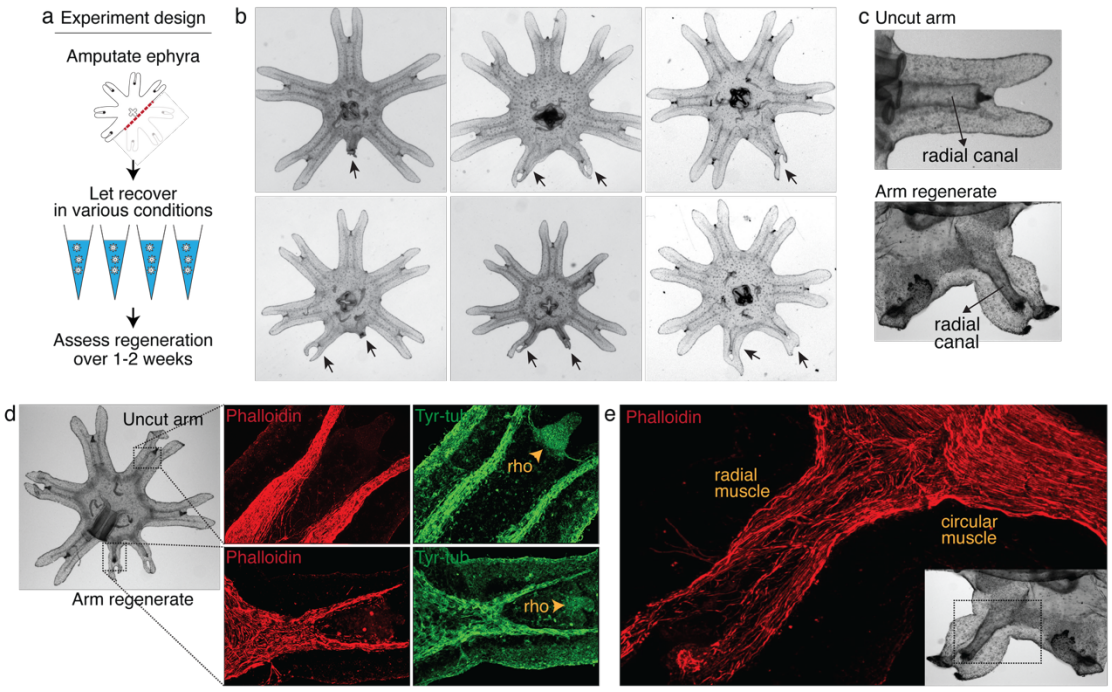
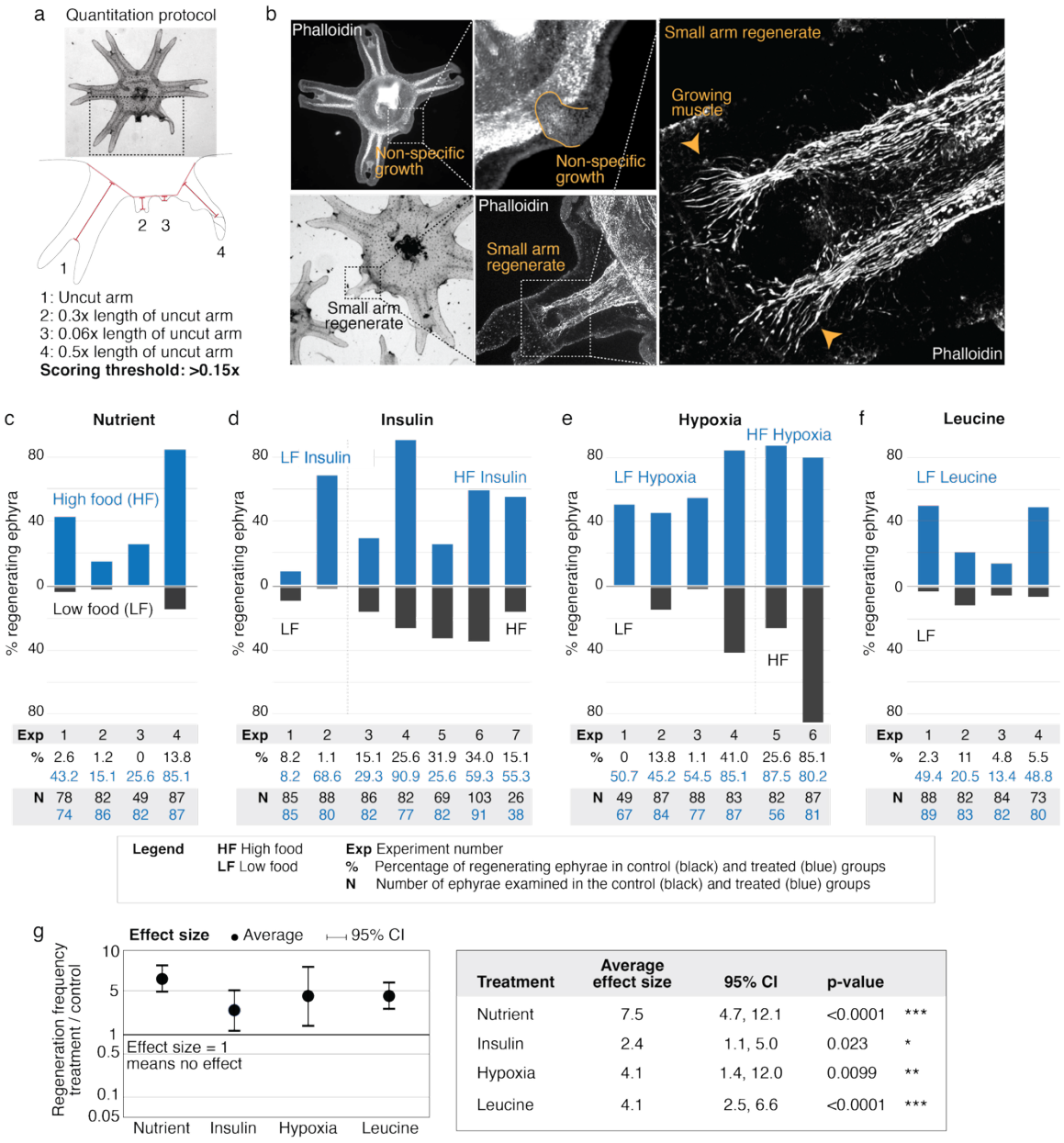


Figure 2. Arm regeneration in *Aurelia* ephyra can be induced using exogenous factors.

(a) Ephyrae were amputated (red line) across the body to remove three arms, and then let recover in various conditions. Table S1 tabulates the factors tested in the screen. Regeneration was assessed over 1–2 weeks until bell tissues began developing between the arms and obscured scoring. The ephyrae shown are from high-nutrient condition (see Figure 3). (b) Arm regeneration (arrows; from high food condition, see Figure 3a). (c) Radial circulatory canal in an uncut arm and is reformed in an arm regenerate. (d) Muscle (red), as indicated by phalloidin staining, and neuronal networks (green), as indicated by antibody against tyrosinated tubulin. The orange arrows indicate distal enrichment of tyrosinated-tubulin staining, which marks the sensory organ rhopalium (rho). Twenty ephyrae were examined and representative images are shown. (e) Higher magnification of the phalloidin staining shows the striated morphology of the regrown muscle in the arm regenerate (called radial muscle), which extends seamlessly from circular muscle in the body.



Treatment	Average effect size	95% CI	p-value	
Nutrient	7.5	4.7, 12.1	<0.0001	***
Insulin	2.4	1.1, 5.0	0.023	*
Hypoxia	4.1	1.4, 12.0	0.0099	**
Leucine	4.1	2.5, 6.6	<0.0001	***

Figure 3. Nutrient level, insulin, hypoxia, and leucine increased regeneration frequency in *Aurelia*.

(a) An ephyra is regenerating if it has at least one growth from the cut site with a length greater than 0.15 of the uncut arm length. The uncut arm length was determined in each ephyra by measuring three uncut arms and taking the average. Lappets, the distal paired flaps,

were excluded in the length measurement because their shapes tend to vary across ephyrae. The measurements were performed in ImageJ.

(b) The threshold 0.15 was chosen to balance excluding non-specific growths that show no morphological structures (e.g., as shown, lack of phalloidin-stained structures) and retaining rudimentary arms that show morphological structures, including radial muscle sometime with growing ends (shown, phalloidin stained).

(c–f) In each experiment, treated (blue) and control (gray) ephyrae came from the same strobilation. (c) Regeneration frequency in lower amount of food (LF) and higher amount of food (HF). The designation 'high' and 'low' is for simplicity, and does not presume the nutrient level in the wild. If we were to speculate, the LF amount is likely closer to typical nutrient level in the wild, based on two lines of evidence. First, regeneration frequency in LF is comparable to that observed in the natural habitat experiment. Second, in many of the wild populations studied, ephyrae mature to medusae over 1–3 months (Lucas, 2001), comparable to the growth rate in LF (by contrast, ephyrae in HF mature to medusae over 3–4 weeks). (d) Regeneration frequency in 500 nM insulin. (e) Regeneration frequency in ASW with reduced oxygen. (f) Ephyrae recovering in low food, with or without 100 mM L-leucine.

(g) The effect size of a treatment was computed from the ratio between regeneration frequency in treated and control group within an experiment, that is, the metric risk ratio RR; RR=1 means the treatment has no effect (Borenstein et al., 2009). The statistical significance and reproducibility of a treatment were assessed by analyzing the effect size across experiments using the meta-analysis package, metafor (Viechtbauer, 2010), in R with statistical coefficients based on normal distribution. See Materials and methods for details. A treatment was deemed reproducible if the 95% confidence intervals (95% CIs) of RR exclude 1. The p-value evaluates the null hypothesis that the estimate RR is 1. Reproducibility and statistical significance of each treatment were verified using another common size effect metric, odds ratio (Figure S6).

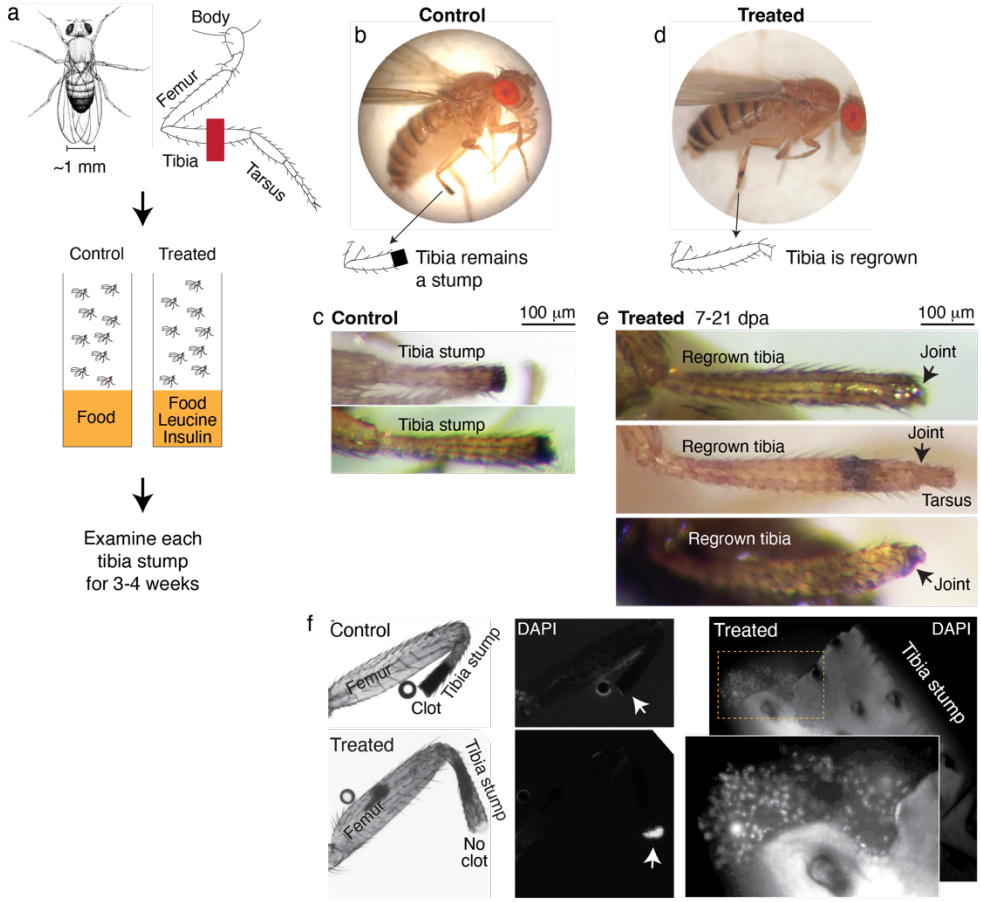


Figure 4. Leucine and insulin induced regeneration in *Drosophila* limb.

(a) Adult *Drosophila* have jointed limbs, with rigid segments connected by flexible joints. Amputation was performed across the tibial segment. After amputation, flies were housed in vials containing standard lab food (control) or standard lab food added with 1.7 mM L-Leucine, 1.7 mM L-Glutamine, and 33 µg/ml insulin (treated). Doses were determined through observing the highest order of magnitude dose of amino acid that could be fed to flies over a prolonged period without shortening their lifespan. The flies were examined at ~1, 3, 7, 14, and 21 days post-amputation (dpa).

(b) A control fly, imaged at 7 dpa.

(c) Control tibia stumps, imaged at 1–3 dpa.

(d) A treated fly, imaged at 7 dpa.

(e) At 7–21 dpa, regrown tibias, which culminate in joints, were observed in the treated population.

(f) Tibia stumps at 3–14 dpa were dissected, fixed, and mounted in Vectashield mounting medium with DAPI. Samples from 14 dpa are shown here. Insect cuticle is not dissected to restrict DAPI penetrance only to the distal tip. Clotted tips of control tibia stumps did not stain with DAPI (10 out of 10), whereas unclotted tips of treated tibia stumps were stained with DAPI (14 out of 16). Higher-resolution confocal image of an unclotted treated tibia stump at 14 dpa.

Drosophila drawing in (a) by Ashley Smart and used with permission.

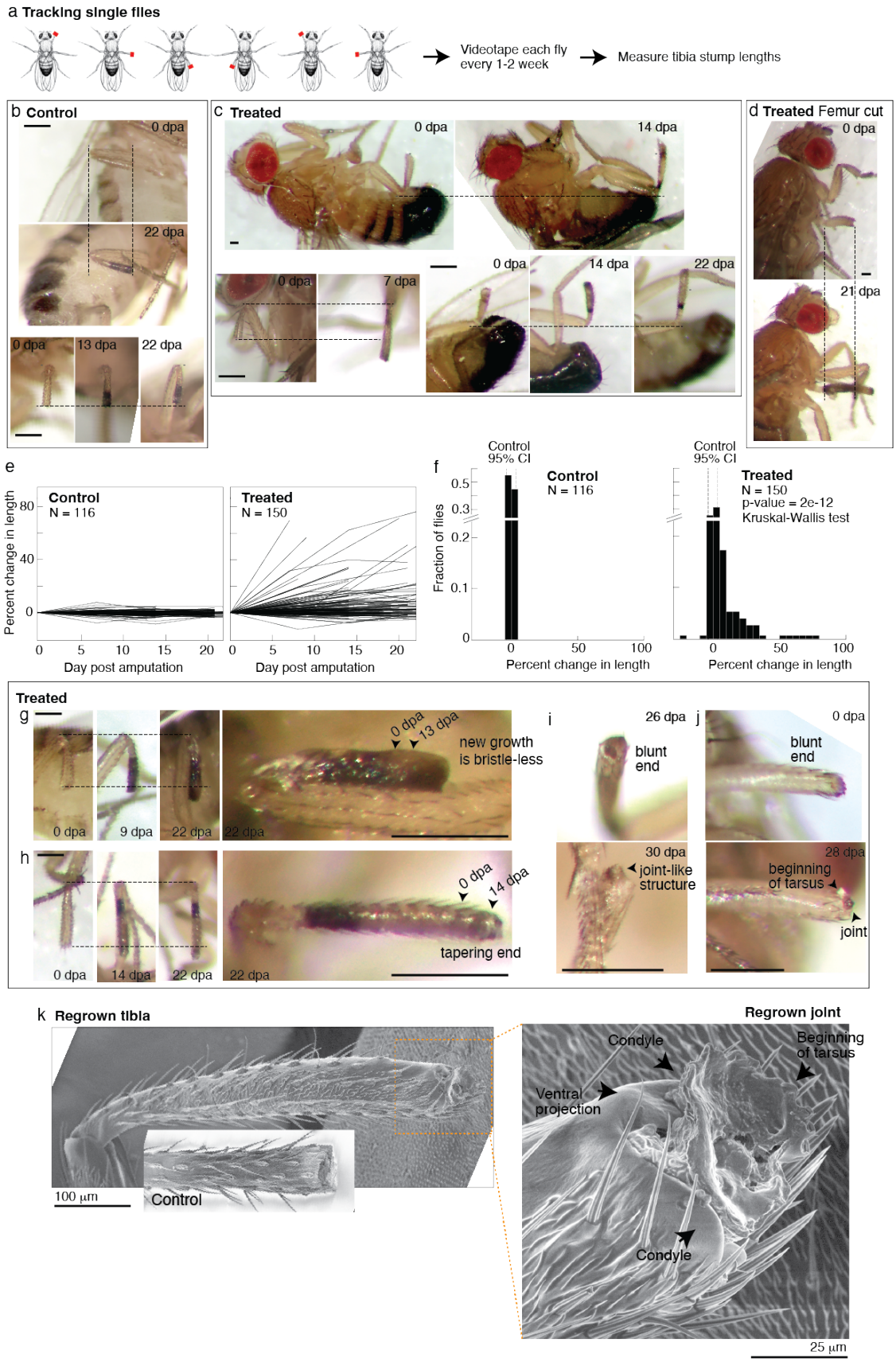

a Tracking single flies
Videotape each fly every 1-2 week
Measure tibia stump lengths
b Control
0 dpa
22 dpa
0 dpa
13 dpa
22 dpa
c Treated
0 dpa
14 dpa
0 dpa
7 dpa
0 dpa
14 dpa
22 dpa
d Treated Femur cut
0 dpa
21 dpa
e
Control
N = 116
Treated
N = 150
Percent change in length
Day post amputation
f
Control
95% CI
Control
N = 116
Treated
N = 150
p-value = 2e-12
Kruskal-Wallis test
Fraction of flies
Percent change in length
Treated
g
0 dpa
9 dpa
22 dpa
22 dpa
0 dpa
13 dpa
new growth
is bristle-less
h
0 dpa
14 dpa
22 dpa
22 dpa
0 dpa
14 dpa
tapering end
i
26 dpa
blunt
end
30 dpa
joint-like
structure
j
0 dpa
blunt
end
28 dpa
beginning
of tarsus
joint
k Regrown tibia
100 µm
Control
Regrown joint
Condyle
Beginning
of tarsus
Ventral
projection
Condyle
25 µm

Figure 5. Tracking regenerative response in individual flies.

(a) To track the regenerative response in individual flies, flies were amputated in different limbs (fore, mid, and hindlimb) and housed in small groups such that in any given vial, each fly was uniquely identifiable by sex and amputated limb. Each fly was imaged immediately after amputation and 1–3 additional times over the course of 2–4 weeks.

(b–d) Representative time lapse from control (b) and treated flies (c–d). dpa: days post-amputation. For each fly, time-lapse images are shown at the same magnification. Scale bars: 250 μm.

(e) Change in tibia stump length over time.

(f) Distribution of change in tibia stump length in control and treated flies. Percent change in length is the difference between the length at the final time point and 0 dpa, relative to the length at 0 dpa. CI: confidence interval. Statistical difference between control and treated distributions was evaluated using the nonparametric Kruskal-Wallis test. The p-value tests the null hypothesis that the data are drawn from the same distribution. We confirmed that the probability of observing growth in each condition was not biased by differences in the initial length of tibia stump (Figure S12b).

(g–i) For each fly, time-lapse images are shown at the same magnification. Scale bars: 250 μm. (g) In this treated tibia stump, the new growth showed different pigmentation and no sensory bristles. (h) In this treated tibia stump, the segment was reformed as suggested by the tapering end. (i) In this treated tibia stump, the segment was reformed and a joint-like structure grew.

(j) In this treated tibia stump, amputation was performed just before the joint. After 4 weeks, a new joint-like structure appeared, from which tissues of the next segment (tarsus) started growing.

(k) Fly with a regrown tibia at 21 dpa was mounted onto an environmental SEM with a copper stub. Inset shows a clotted tibia stump from a control fly, with the discoloration at the end corresponding to the clot. Magnification of the regenerated joint: the arrows denote the two condyles and additional ventral projection.

Drosophila drawing in (a) is by Ashley Smart and used with permission.

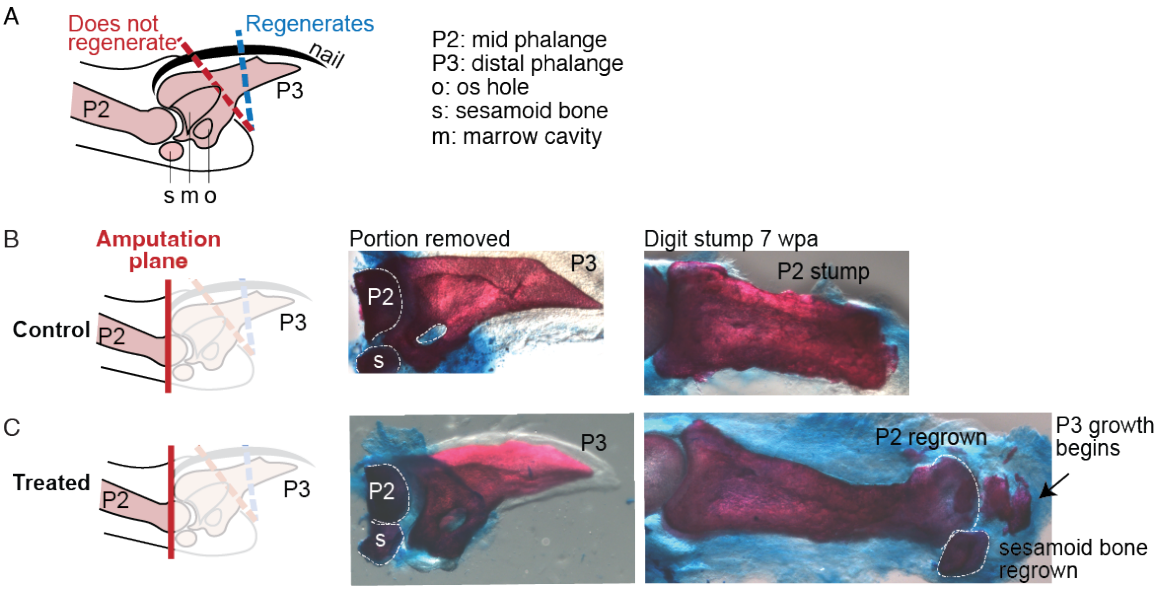


Figure 6. Leucine and sucrose induced regeneration in adult mouse digit.

(a–b) Amputation was performed on hindpaws of adult (3–6 months old) mice, on digits 2 and 4, proximal to the nail. (c) Schematic of the distal phalange (P3) and middle phalange (P2). Amputations that remove <30% of P3 (blue line) regenerate, whereas amputations that remove >60% of P3 (red line) do not regenerate. Amputations in the intermediate region can occasionally show partial regenerative response. (d) Amputations in this study were performed within the red-shaded triangle. (e) Amputated mice were given regular drinking water (control) or drinking water supplemented with 1.5% L-leucine, 1.5% L-glutamine, and 4–10% w/v sucrose (2 exps with 4%, 3 exps with 10%). Drinking water, control and treated, was refreshed weekly. (f) A representative paw from the control group. The amputated digits 2 and 4 simply healed the wound and did not regrow the distal phalange. (g) In this treated mouse, digit 2 (arrow) regrew the distal phalange and nail. Insets on the right show the digit at earlier time points. At week 1, the amputation site still appeared inflamed. At week 3, the beginning of the nail appears (arrow). At week 3, a clear nail plate was observed. (h) In this treated mouse, digit 4 (arrow) regrew and began to show nail reformation by week 4 (top inset, see arrow), that turns into a clear nail plate by week 7 (middle inset), as can be seen more clearly from the side-view darkfield image (bottom inset). (i–l) Whole-mount skeletal staining. Dissected digits were stained with Alizarin red, an anionic dye that highly localizes

to the bone. Left panels show illustration of the amputation plane, middle panels show skeletal staining of the portions removed, and right panels show skeletal staining of the digit stumps 7 weeks after amputation.

2.6 Supplementary Tables and Figures

Factor	Highest dose tested	Source	Factor	What was tested	Implementation
Modulators of signaling pathways			Nutrient	1-50 rotifers/animal 0-5 brine shrimps/animal Combination of both	Food was administered daily
Erbstatin	5 μM	Sigma D2667			
hEGF recombinant	20 ng/mL	Sigma E9644			
UO126	1 μM	Millipore 6625			
Dorsomorphin	1 μM	Sigma P5499	Water current	0 - 60 bubbles per minute	Ambient air was pumped to the cone
LiCl	250 mM	Sigma L4408			
CHIR99021	12.5 μM	Sigma SML1046	Aquarium geometry	Beaker, plate, tube, cone	Amputated ephyrae were placed in different aquaria
IWR-1	10 μM	Sigma I0161			
XAV939	2 μM	Sigma X3004			
Purmorphamine	2 μM	Sigma SML0868			
hTGF-β1	1.2 ng/mL	Peprotech 100-21	Water volume	100 mL - 1 L	
Modulators of metabolism, immune system, stress response			Animal density	10 - 100 ephyrae / L	
Diosmetin	10 μM	Sigma D7321			
17-DMAG	1 μM	TSZ Chemicals R1028			
Geranylgeranylacetone	1 μM	Sigma G5408	Temperature	18 - 25°C	Cooler or heater
KNK437	4 nM	Sigma SML0964			
MKT-077	2.5 μM	Sigma M5449	Heat shock	30 sec at 42°C 30 min at 37°C	Water bath
Bromopyruvic acid	125 nM	Sigma 16490			
6-Phosphogluconic acid	20 μM	Sigma P7877			
Antamycin A	650 nM	Sigma A8674			
3PO	10 μM	Millipore 525330			
ATP	5 μM	Sigma A3377			
3BDO	3 μM	Sigma SML1687			
D-Fructose 1.6-bisphosphate	20 μM	Sigma F6803			
DMOG	50 μM	Millipore 400091			
Rapamycin	1 μM	Sigma R8781			
L-Leucine methyl esther hydrochloride (cell permeable form)	100 μM	Sigma L1002			
Resveratrol	5 μM	Sigma R5010			
Sapanisertib	2 nM	Selleck Chemicals S2811			
MHY1485	2 μM	Sigma SML0810			
Insulin, human	3 μM	Sigma I0908			
AICAR	25 μM	Santa Cruz sc-200659A			
A769662	5 μM	Santa Cruz sc-203790			
D-Eryhtrose 4-phosphate	20 μM	Sigma E0377			
CoCl	450 nM	Sigma 60818			
Miscellaneous					
BSA	500 nM	Sigma A7906			
Ethanol	20 μL/L	VWR 89125-170			
CsCl	5 μL/L	Sigma C4036			

Table S1. Various molecular and physical modulations were screened to recapitulate arm regeneration.

Modulators were administered or physical parameters were implemented upon amputation. Some factors were dissolved in DMSO or ethanol; for these molecules, the control group was administered with an equal volume of the solvent. Since few, if at all, of the molecular modulators had been tested in Aurelia, the maximum concentrations were tested to maximize

the chance of seeing an effect. Maximum concentration was determined by solubility in saltwater or onset of adverse effects (e.g., degrowth, paralysis, death) upon overnight incubation. Where available, previously reported concentrations in cell culture or animal systems were included in the testing. A negative result means no obvious effects were observed at the maximum concentration that warrant further investigation. For factors that gave interesting effects (e.g., insulin), a range of lower concentrations were subsequently tested for optimization.

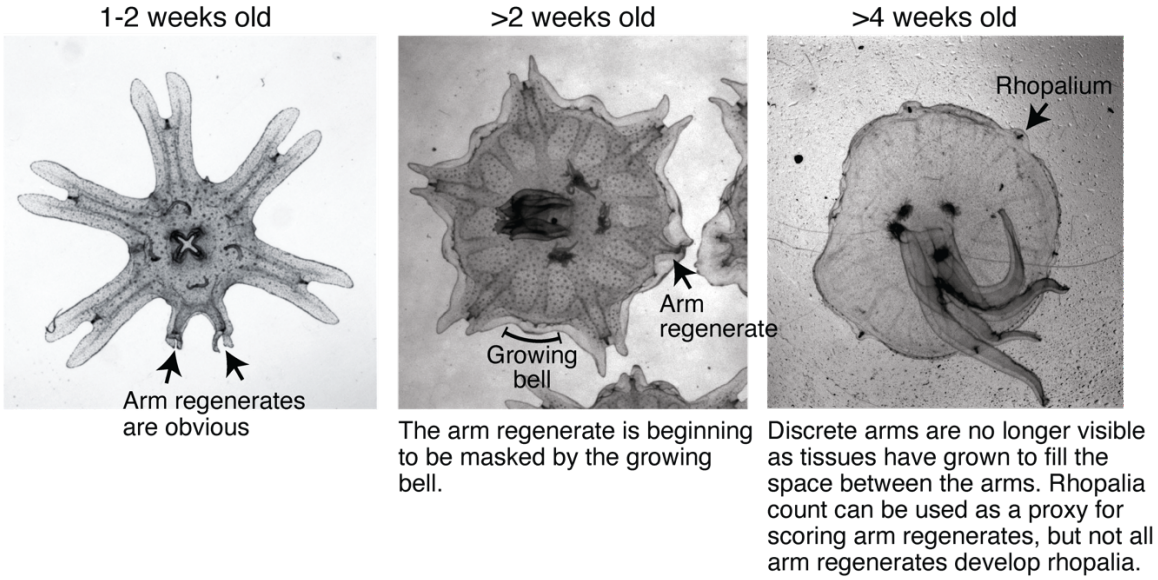


Figure S2. Bell growth limited the time window for assessing arm regeneration.

Ephyrae in the lab mature into full-belled medusae within ~4 weeks. The transition to medusa commences at 1-2 weeks after strobilation, with the onset of bell growth. Over 2-3 weeks, body tissues gradually grow and fill between the discrete arms to form a continuous bell characteristics of a medusa. Arm regeneration can be unambiguously scored in ephyrae before the bell has significantly grown. Bell growth also limited testable doses in some factors, *e.g.*, testing higher food amount than reported here led to accelerated bell growth at a rate that did not allow enough time window to quantify regeneration.

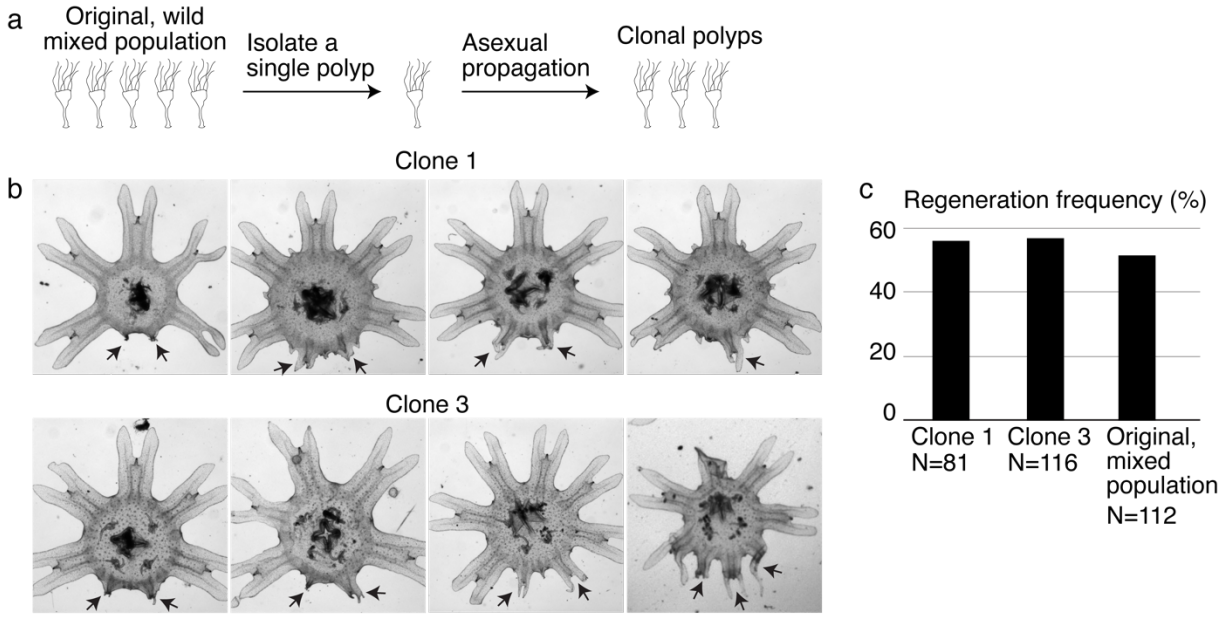


Figure S3. Variable extent of regeneration was observed in clonal lines.

(a) To develop genetically clonal lines, single polyps were isolated and settled onto tissue culture dishes. Within 1-3 months, with daily feeding of enriched brine shrimps, each dish was re-populated with polyps asexually budding from the single parental polyp.

(b) Regeneration induction with high food performed in two clonal lines. Arrows indicate arm regenerates.

(c) Regeneration frequency in the clonal and original mixed populations measured in the same experiment.

The data reported in the main text come from experiments performed in clone 3.

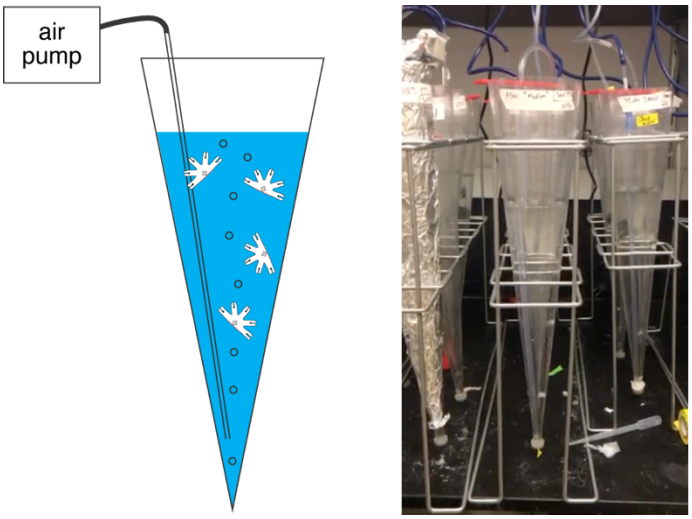


Figure S4. Water current is a permissive requirement for arm regeneration induction. Various physical environments for the ephyrae recovering from injury were tested, for example, shallow versus deep water, seawater with varying salinity, cold versus warm temperature, light versus dark, stagnant water versus current, generating water current through various means, including shaking or rotating to generate turbulent mixing and as shown here air bubbling a conical tube to generate vertical current (shown here). While symmetrization occurred robustly in all conditions, consistent induction of regeneration only occurred in the presence of columnar water current. The experiments presented in this study were performed in the 'bubbler cone' setup, where a 1 L sand settling cone was repurposed into an aquarium and connected to an air pump (Tetra Whisper 100) to generate a gentle current of ~1 bubble/s (Video 2). Each cone housed 30 ephyrae in 500 mL ASW or treated ASW, refreshed weekly, to avoid crowding and fouling. In the bubbler cone, ephyrae continually move along water current, either the upward bubble-generated current or the downward gravity-generated current. The conical geometry helps to minimize stagnant spots, where the ephyrae could get stuck.

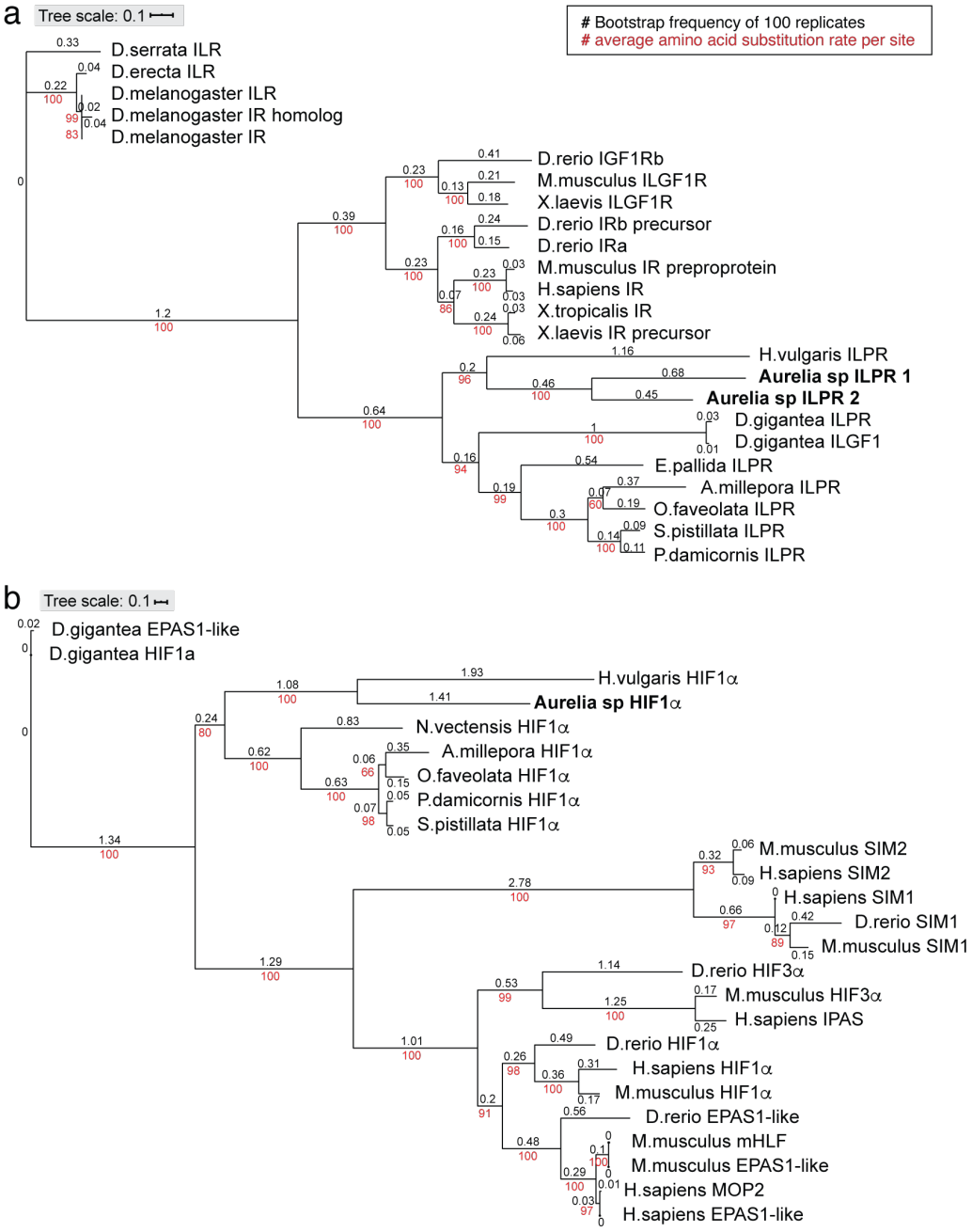
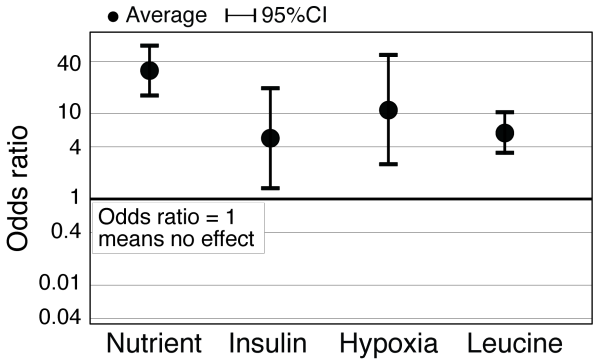


Figure S5. Conservation of insulin receptor and HIFα in *Aurelia*.

Phylogenies of insulin receptor (**a**) and HIFα (**b**) genes were constructed using the maximum likelihood inference computed with the IQ-TREE stochastic algorithm (Nguyen et al., 2015), and visualized using ITOL (https://itol.embl.de/upload.cgi). These simple trees are not meant

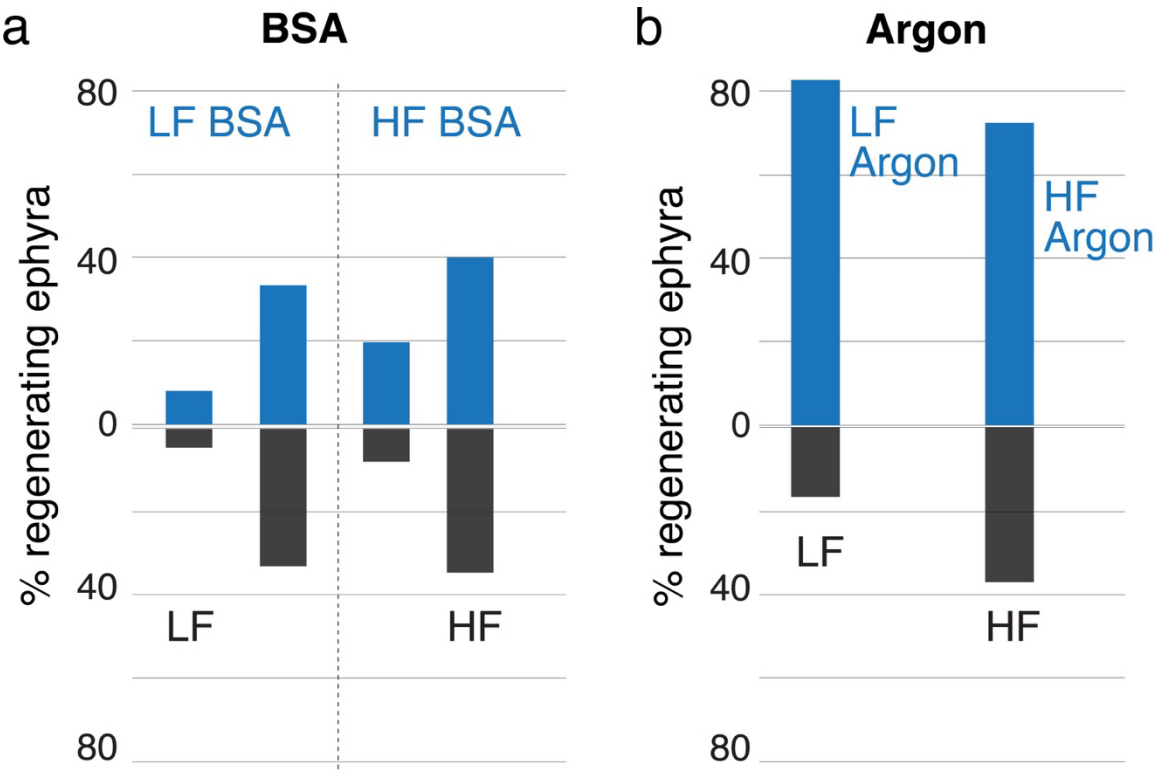
to be comprehensive, but a verification of the genes annotated as insulin-like protein receptor (ILPR) and HIFα in the *Aurelia* gene models by testing conservation with their known counterparts in other organisms. IQ-TREE parameters: Insulin receptor consensus tree is constructed from 1000 bootstrap trees; log-likelihood of consensus tree is –45,374.0; the Robinson-Foulds distance between ML and consensus tree is 0. HIFα consensus tree is constructed from 1000 bootstrap trees; log-likelihood of consensus tree is –24,414.4; the Robinson-Foulds distance between ML and consensus tree is 0.



Treatment	Odds ratio	95% CI	p-value	
Nutrient	30.9	15.8, 60.6	<0.0001	***
Insulin	5.0	1.3, 19.4	0.02	*
Hypoxia	10.8	2.5, 46,6	0.001	**
Leucine	5.8	3.4, 10.1	<0.0001	***

Figure S6. Statistical significance of regeneration induction in *Aurelia* assessed using Odds Ratio.

In addition to RR analysis presented in Figure 3g, another common measure of effect size is the Odds Ratio (OR, Borenstein et al., 2009). OR compares the odds of outcome in the presence vs. absence of treatment (Methods). Analysis of OR across experiments was performed using the metafor package (Viechtbauer, 2010) in R with statistical coefficients based on normal distribution (Methods). A treatment is reproducible if the 95% confidence intervals (95% CI) exclude 1. The p-value evaluates the null hypothesis that the estimate OR is 1.



Exp	1	2	3	4
%	4.5	32.9	7.9	34.5
	8.0	33.3	19.7	40.0
N	89	85	89	58
	25	45	66	30

Exp	1	2
%	16.7	37.1
	82.8	72.5
N	90	89
	87	69

Figure S7. Treatments using bovine serum albumin (BSA) and argon.

(a) Treatment with 500 nM BSA did not produce significant effect in regeneration frequency (95% CI [0.9, 1.9-fold change], p=0.20).

(b) Reducing oxygen using argon flow increased regeneration frequency (95% CI [1.99, 3.3-fold change], p<10–4). Effect size was computed using the metric risk ratio (see Materials and methods). LF is low food, HF is high food, Exp is Experiment ID, % is percentage of regenerating ephyra in control (black) and treated (blue), and N is the number of ephyrae in the control (black) and treated (blue) group.

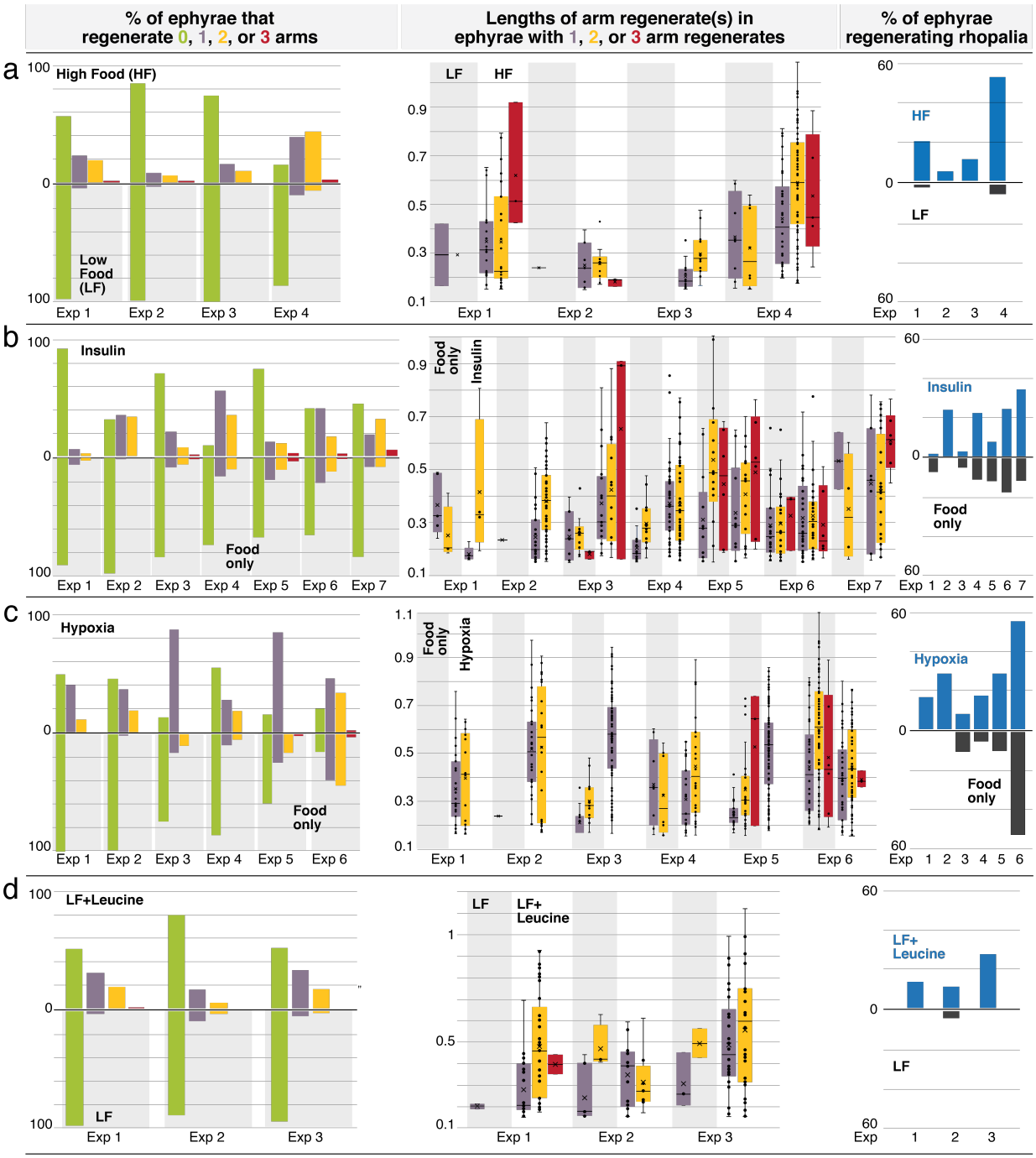


Figure S8. Regeneration phenotypes.

(a) In high amount of nutrients, (b) insulin, (c) hypoxia, and (d) L-leucine. For each treatment. Left: The percentage of ephyrae that regenerate 0 (green), 1 (purple), 2 (yellow),

or 3 arms (red). Middle: The length(s) of arm regenerate(s) in ephyrae that regenerate 1 arm (purple), 2 arms (yellow), and 3 arms (red) – normalized to the average length of uncut arms in the same ephyra. For ephyrae with multiple arm regenerates, lengths of all arms were measured and plotted individually. Boxplot: median (line), average (cross), 1st and 3rd quartiles (the box), 5^{th} and 95^{th} percentile (whiskers), and individual data points (black circles). Right: The percentage of ephyrae that reform rhopalia in control (grey) and treated (blue) groups.

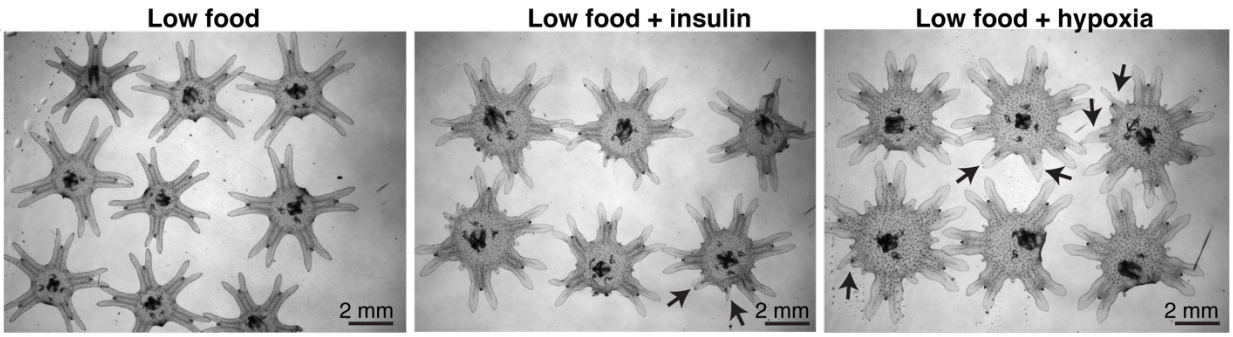
	High food				L-leucine			
	Effect size	95% CI	p-value		Effect size	95% CI	p-value	
% ephyrae regenerating	7.4	4.7, 12.1	<0.0001	***	4.1	2.5, 6.6	<0.0001	***
% ephyrae regenerating >1 arm	11.4	4.9, 5.3	<0.0001	***	6.0	1.9, 19.1	0.003	**
Length of arm regenerates	1.6	1.2, 2.0	0.0003	***	1.7	1.42, 1.9	<0.0001	***
% ephyrae regenerating rhopalia	11.8	5.3, 26.5	<0.0001	***	6.1	2.1, 17.7	0.0009	***

	Insulin				Hypoxia			
	Effect size	95% CI	p-value		Effect size	95% CI	p-value	
% ephyrae regenerating	2.4	1.1, 5.0	0.023	*	4.1	1.4, 12.0	0.0099	**
% ephyrae regenerating >1 arm	1.9	1.3, 2.8	0.0005	***	1.2	0.2, 9.0	0.833	n.s
Length of arm regenerates	1.2	0.98, 1.5	0.080	n.s	1.3	0.8, 2.1	0.239	n.s
% ephyrae regenerating rhopalia	1.3	0.7, 2.7	0.427	n.s	2.6	1.0, 6.7	0.047	*

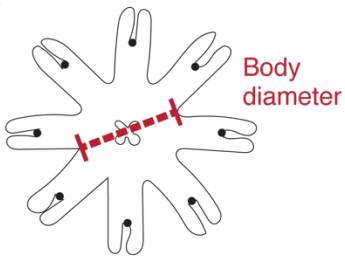
Figure S9. Statistical analysis of the regeneration phenotypes in high amount of nutrients, insulin, hypoxia, and L-leucine.

For frequency measurements, the effect size of a treatment compares the probability of an outcome in treated versus control group (i.e., risk ratio, Materials and methods). For length measurement, the effect size of a treatment compares the proportionate change that results from the treatment (i.e., response ratio, Materials and methods). Analysis of effect size across experiments was performed using the metafor package in R with statistical coefficients based on normal distribution (Materials and methods). A treatment is reproducible if the 95% confidence intervals (95% CIs) exclude 1. The p-value evaluates the null hypothesis that the estimate effect size is 1 (i.e., no effect).

a



b



Treatment	Ave. body diameter treatment/control	95% CI	p-value
High food	1.7	1.6, 1.8	<0.0001***
Insulin	1.4	1.1, 1.8	0.011 *
Hypoxia	1.5	1.3, 1.9	<0.0001**
Leucine	1.1	1.04, 1.12	<0.0001***

Figure S10. Ephyrae in high food, insulin, or hypoxia, and L-leucine tend to be bigger in size.

(a) Representative images of ephyrae growing in low food, 500 nM insulin, and hypoxia. Black arrows indicate regenerating arms.

(b) Effect size analysis of the body size increase was performed using the metafor package (Viechtbauer, 2010) in R (Materials and methods). A treatment is reproducible if the 95% confidence intervals (95% CIs) exclude 1. The p-value evaluates the hypothesis that there is no effect.

a

Strain	Condition	N	No clot	Regrown tibia
Oregon R	Control	860	0%	0%
Oregon R	Leucine & Insulin	387	12.1	1.0%
Canton S	Control	174	0%	0%
Canton S	Leucine & Insulin	284	29.9%	1.1%

b

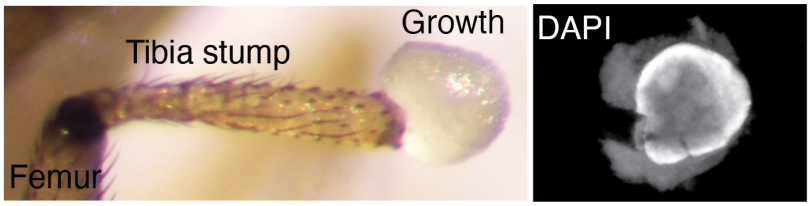


Figure S11. Regenerative response induced in *Drosophila* was observed across wild-type strain.

(a) Summary of the bulk experiment data in Oregon R and Canton S wild-type strains.

(b) Few flies showed non-patterned outgrowth from the amputation site (3 out of 387 in Oregon R, 9 out of 284 in Canton S).

a

Strain	Condition	N	No clot	Regrown tibia
Oregon R	Control	860	0%	0%
Oregon R	Leucine & Insulin	387	12.1	1.0%
Canton S	Control	174	0%	0%
Canton S	Leucine & Insulin	284	29.9%	1.1%

b

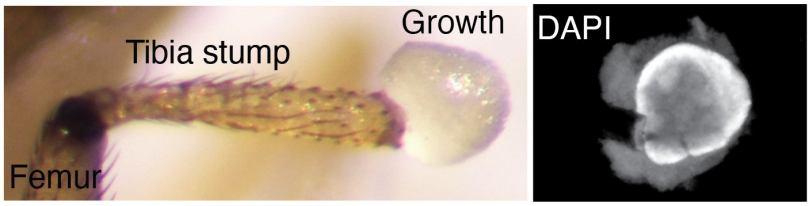


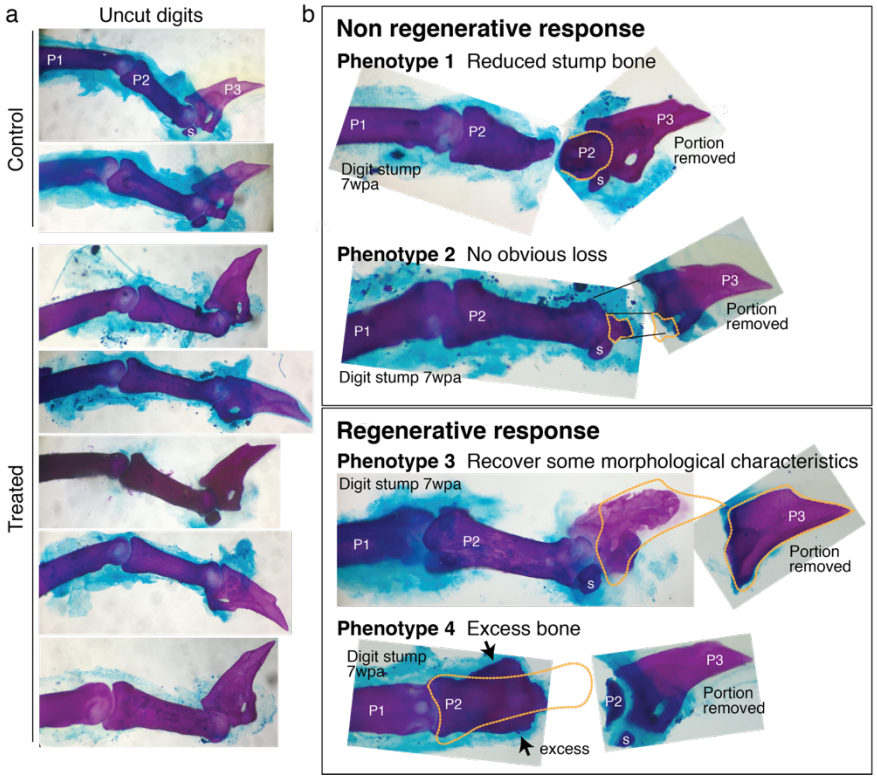
Figure S12. Tracking regenerative response in single flies.

(a) No sex-based differences were observed in the regenerative response. Distributions of changes in stump lengths in male and female flies are not statistically different (p=0.48, nonparametric Kruskal-Wallis test).

(b) Growth was observed from proximal (short tibia stump) or distal (long tibia stump) amputation across tibia.

(c) A control tibia stump.

(d–f) Treated tibia stumps showing white tissues growing from the end.



c

Phenotype	Control # digits	Control %	Treated # digits	Treated %
1	16	80.0	26	54.1
2	4	20.0	13	27.1
3	**0**	**0.0**	**6**	**12.5**
4	**0**	**0.0**	**3**	**6.3**
Total	20		48	

d P2 amputation

Phenotype	Control # digits	Control %	Treated # digits	Treated %
1	11	91.7	23	65.7
2	1	8.3	6	17.1
3	**0**	**0.0**	**3**	**8.6**
4	**0**	**0.0**	**3**	**8.6**
Total	12		35	

e P3 + joint amputation

Phenotype	Control # digits	Control %	Treated # digits	Treated %
1	5	62.5	3	23.1
2	3	37.5	7	53.8
3	**0**	**0.0**	**3**	**23.1**
4	**0**	**0.0**	**0**	**0.0**
Total	8		13	

Figure S13. Mouse digit phenotypes.

Whole-mount skeletal staining was performed with Alizarin red. wpa: week post amputation, P1: phalange 1, P2: phalange 2, P3: phalange 3, s: sesamoid bone

(a) Skeletal staining of unamputated digits (digit 3) from control and treated groups show no obvious differences in uncut digits due to the treatment.

(b) Skeletal staining of digits stumps at 7 wpa and the original portion removed from the digits. Some digit stumps show no change or even reduced bone mass (Phenotype 1 and 2). Bone histolysis, where bone mass recedes further from the amputation plane, has been observed (refs). Some digit stumps show regenerative response, either recovery of some morphological characteristics (Phenotype 3, detailed more in Figure S11) or excess, ectopic bone mass (Phenotype 4). We erred on the conservative side in scoring phenotype 3 and 4; when in doubt, digits were classified into phenotype 1 or 2.

(c-e) Phenotype counts in all digits (c), in digits amputated across P2 (d), and in digits amputated across P3 or joint (e).

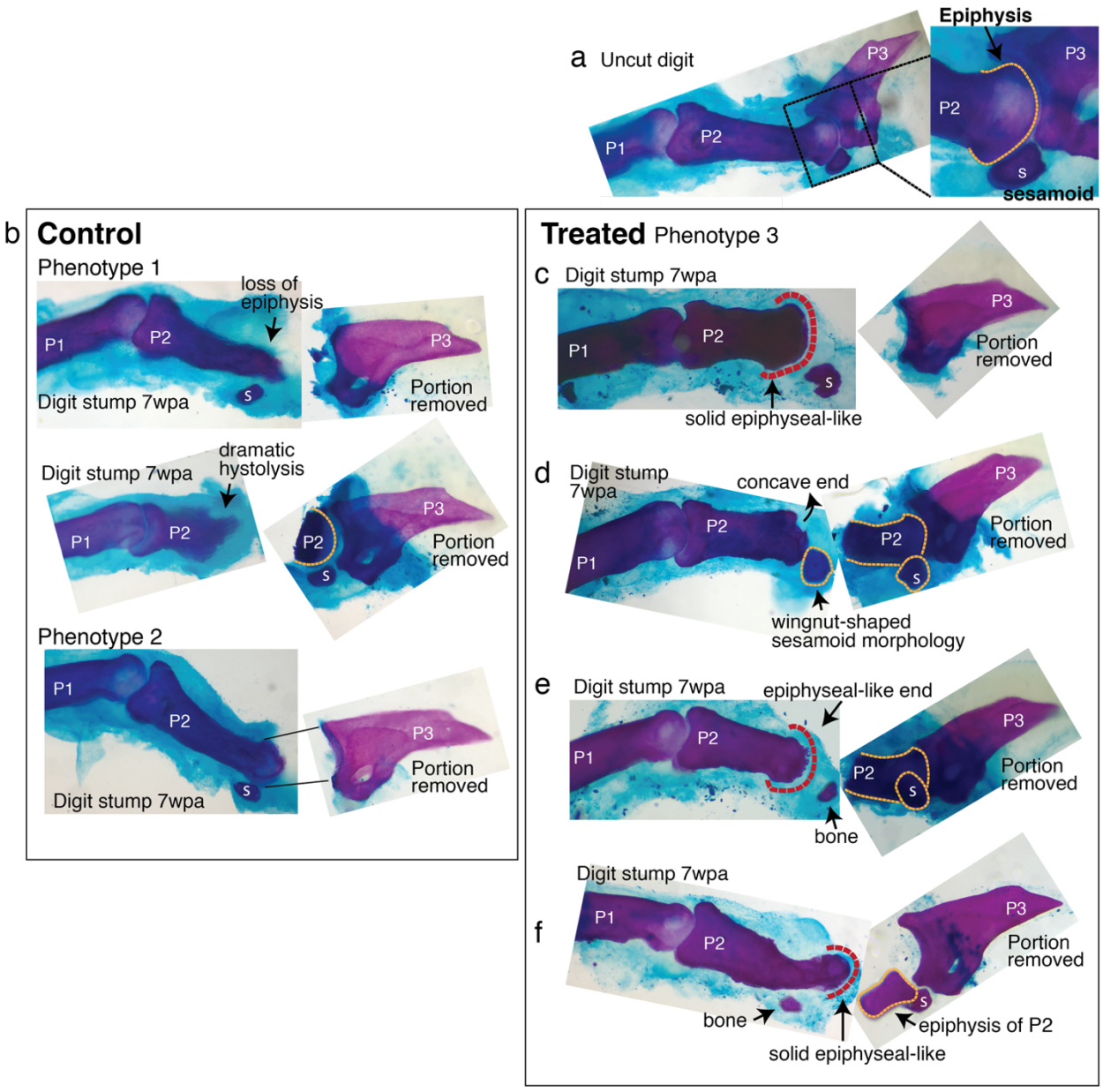


Figure S14. Regenerative response observed in mouse digit.

Six digit stumps (of total 48 examined) show regenerative response. The most dramatic two are presented in Figure 4. The remaining four are presented here. wpa: week post amputation, P1: phalange 1, P2: phalange 2, P3: phalange 3, s: sesamoid bone

(a) An uncut digit, shown for a comparison. Magnified is the P2/P3 joint area to highlight key morphological markers: the knobby shaped epiphyseal cap of P2 and the sesamoid bone embedded in the tendon on the flexor side of P2.

(b) Digit stumps from control mice show either bone stump histolysis (top and middle, phenotype 1) and no visible changes in bone stump (bottom, phenotype 2).

(c-f) Digit stumps from treated mice that show regenerative response.

(c) In this digit, the amputation removed all P3 by a cut through the joint. At 7 wpa, the P2 stump is reduced, but recovered the epiphyseal-like end (red dashed line) – marked by solid curved shape, as opposed to concave, irregular-shaped end of a histolyzing bone.

(d) In this digit, the amputation removed a significant portion of P2 along with the sesamoid bone. The P2 stump does not regain an epiphyseal end (the end is concave and irregularly shaped). However, the sesamoid bone is reformed, as identified by its location on the flexor side of P2 and wingnut shape[32] under the microscope. The recovery of sesamoid bone is non-trivial, as digit sesamoids form in juxtaposition to the condensing phalanx and eventually detach from it by formation of a cartilaginous joint.[33] If regeneration recapitulates development, it would imply that long bone condensation and cartilaginous joint deposition was ongoing in this digit.

(e) In this digit, the amputation removed a significant portion of P2 and the sesamoid bone. At 7 wpa, the P2 stump appears to be reforming an epiphyseal, rounded end (red dashed line). There is a small bone distal to P2, whose curvature appears to articulate with the end of P2, but there are not enough morphological characters to identify the bone.

(f) In this digit, the amputation removed the epiphyseal cap of P2 and the sesamoid bone. The P2 stump appears to have lost some mass, but reforms an epiphyseal-like end (red dashed line). There is an additional small bone that could be a sesamoid bone, but lacks sufficient morphological characters for identification.

2.7 Materials and Methods

Data availability

All data generated or analyzed in this chapter are included, as well as deposited to the open repository CaltechDATA.

Abrams MJ, Basinger T, Goentoro L. Regeneration data - Jellyfish [dataset]. CaltechDATA; 2021. doi: 10.22002/D1.2076.

Li Y, Sarma A, Lee I, Condiotte Z, Goentoro L. Regeneration data - *Drosophila* [dataset]. CaltechDATA; 2021. doi: 10.22002/D1.2157.

Tan FH, Heithe ML, Goentoro L. Regeneration data - Mouse [dataset]. CaltechDATA; 2020. doi: 10.22002/D1.1790.

Materials and Methods for *Aurelia aurita*

The experiments were performed in *Aurelia aurita* sp. 1 strain, also alternatively named *A. coerulea* based on recent molecular classification (Scorrano et al., 2016). Polyps were reared at 68°F, in 32 ppt artificial seawater (ASW, Instant Ocean), and fed daily with brine shrimps (*Artemia nauplii*) enriched with *Nannochloropsis* algae (both from Brine Shrimp Direct). To induce strobilation, polyps were incubated in 25 M 5-methoxy-2-methyl-indole (Sigma-Aldrich M15451) at 68°F for an hour (Fuchs et al., 2014). Ephyrae typically began to strobilate within a week. Strobilated ephyrae were fed daily with high amount of rotifers (*Brachionus plicatilis*, Reed Mariculture) until amputation time.

Experiment in the original habitat

The polyp population in the study arose from parental polyps collected off the coast of Long Beach, CA (33°46′04.2″N 118°07′44.2″W, GPS: 33.7678376–118.1289559). Ephyrae were amputated in location and immediately after submersed in the ocean. For submerging the amputated ephyrae in the ocean, a two-layered aquarium was custom-built. Ephyrae were placed in plastic canisters with a 7-cm diameter hole cut in the lid and covered with a 250-

μm plastic screen. The canisters were then placed in a thick plastic tank fitted with a 500-μm plastic screen on top. This design offers protection to the ephyrae against predators and strong waves, while at the same time allowing exchange of water, zooplanktons, and other particulates. Ephyrae were collected after 2 weeks.

Regeneration experiments

All experiments were performed at 68°F. Two to three days old ephyrae were anesthetized in 400 μM menthol and amputated using a razor blade mounted on an x-acto knife handle. Amputated ephyrae were let to recover in 1 L sand settling cones (Nalgene Imhoff, Figure S4). In each experiment, ~90 animals were amputated for each condition (e.g., 90 animals for control and 90 animals for treated). Because of the varying baseline across strobilation batches, each experiment was repeated across 2–5 strobilation batches (biological replicates). These sample sizes were chosen to obtain a 95% confidence level on the treatment effect (statistical analysis described below). Hundreds of experimental animals were first amputated, mixed together in a beaker, and then randomly allocated to the control or treatment groups. Regeneration was assessed at various times for 1–2 weeks after amputation, before onset of maturation to medusa. All data were included in the analysis.

Rationale for the amputation scheme

Among the possible amputation schemes, 3-arm amputation was chosen because it could be performed fastest. Removing one arm requires carefully cutting across the base of the arm while avoiding injuring the surrounding body. Removing two arms is less hard but still requires awkward positioning of the knife. Removing four arms again takes more time because it requires cutting through the large protruding manubrium, which also affects the animal's feeding ability. The fast 3-arm amputation facilitates testing hundreds of ephyrae per experiment.

Nutrients

Amputated ephyrae were fed daily with rotifers. The number of rotifers was estimated using a six-well plate fitted with STEMgrid (the same principle as using a hemocytometer). In this study, low food was ~10–20 rotifers/ephyra and high food was ~40 rotifers/ephyra. To replicate the study, these numbers should only be used as initial estimates, as what is 'low' or 'high' food amount may easily vary across lab cultures (e.g., rotifer culture, differences across *Aurelia* strains, etc.). Most if not all rotifers were typically consumed within an hour (determined by measuring the rotifers in the water).

Hypoxia

Immediately after amputation, ephyrae were placed in hypoxic ASW. To create a hypoxic environment, nitrogen or argon, instead of ambient air, was pumped into the bubbler cone, beginning from the day before the experiment and maintained throughout the duration of the experiment. The bubbler cone was sealed with parafilm to maintain the lowered oxygen level. The nitrogen/argon flow was adjusted to achieve 50% reduction in the dissolved oxygen level. Dissolved oxygen level was measured using a Clark-type electrode Unisense OX-500 microsensor. The measurement was normalized to oxygen level in control ASW bubbled normally with ambient air. Oxygen measurement was performed prior to the experiment and subsequently every 3 days.

L-leucine

Immediately after amputation, ephyrae were placed in ASW supplemented with 100 μM L-leucine (Sigma-Aldrich L1002, the cell-permeable methyl ester hydrochloride form). L-leucine was refreshed weekly. To determine the concentration used, a range of concentrations from one to hundreds of mM was tested. The concentration of 100 mM was chosen as it maximized the regeneration frequency without non-specific, negative effects.

Statistical analysis

To assess the statistical significance of the treatments, meta-analysis of effect size was performed (Borenstein et al., 2009). The effect size metrics used are determined by the form

of the data set. For measurements of frequencies (e.g., regeneration frequency), the data sets are in the form of a 2×2 table of dichotomous variables.

	# ephyrae that regenerate	# ephyrae that do not regenerate
Control	a	b
Treatment	c	d

For such 2 x 2 datasets, in situations where the baseline varies (*e.g.*, varying baseline regeneration across clutches), the commonly used measures of effect size are the Risk Ratio (RR),

$$RR = \frac{\left(\frac{\text{\# ephyrae that regenerate}}{\text{total \# ephyrae}}\right)\text{in treated group}}{\left(\frac{\text{\# ephyrae that regenerate}}{\text{total \# ephyrae}}\right)\text{in control group}} = \frac{\frac{c}{(c+d)}}{\frac{a}{(a+b)}}$$

and the Odds Ratio (OR),

$$OR = \frac{\left(\frac{\text{\# ephyrae that regenerate}}{\text{\# ephyrae that do not regenerate}}\right)\text{in treated group}}{\left(\frac{\text{\# ephyrae that regenerate}}{\text{\# ephyrae that do not regenerate}}\right)\text{in control group}} = \frac{\frac{c}{(c+d)}}{\frac{a}{(a+b)}}$$

RR compares the probability of an outcome in treated vs control group, whereas OR compares the odds of an outcome in treated vs control group.

For measurements of arm length and body size, the datasets are in the form of continuous variables. For such data, the commonly used effect size is the Response Ratio (R),

$$R = \frac{\text{mean arm length in treated group}}{\text{mean arm length in control group}}$$

R evaluates the proportionate change that results from a treatment, and is the meaningful effect size to use when the outcome of a treatment is measured on a physical scale, for example, length or area (as opposed to arbitrary scale, e.g., happiness level). Experiments where regeneration in one of the groups occurred in 0 ephyra were necessarily excluded.

Having computed the effect size (RR, OR, or R) within each experiment, meta-analysis of the effect size across experiments was performed. The metafor package (Viechtbauer, 2010) in R was used, with fixed-effect model (for nutrients and leucine) or random-effect restricted maximum likelihood model (for insulin and hypoxia, which had different control conditions across the experiments). Statistical coefficients were based on normal distribution.

Phalloidin and tyrosinated tubulin staining

All steps were performed at room temperature, unless indicated otherwise. Ephyrae were first anesthetized in 400 μM menthol, which minimizes curling during fixing. Next, ephyrae were fixed in 3.7% (v/v) formaldehyde (in phosphate-buffered saline [PBS]) for 15 min, permeabilized in 0.5% Triton X-100 (in PBS) for 5 min, and blocked in 3% (w/v) BSA for 2 min. For neuron staining, ephyrae were incubated in 1:200 mouse anti-tyrosinated alpha tubulin antibody (Sigma-Aldrich MAB1864-I) overnight at 4°C, and then in 1:200 goat-anti-mouse Alexa Fluor 488 (Life Technologies A11029) overnight in the dark at 4°C. Primary or secondary antibodies were diluted in 3% BSA. For actin staining, ephyrae were incubated in 1:20 Alexa Fluor 555 Phalloidin (Life Technologies A12379) overnight or for 2 hr in the dark at 4°C. For nuclei staining, ephyrae were incubated in 1:10 Hoechst 33342 (Sigma-Aldrich B2261) for 30 min in the dark.

Microscopy

Ephyrae were imaged anesthetized in menthol. Brightfield images, fluorescent images, and movies were taken with the Zeiss AxioZoom.V16 stereo zoom microscope and AxioCam HR 13-megapixel camera. Optical sectioning was performed with ApoTome.2.

Materials and Methods for *Drosophila melanogaster*

CantonS wild-type strain was a gift from Peter Lee in Kai Zinn's lab at Caltech. OregonR was a gift from James McGehee in Angela Stathopolous' lab at Caltech. OregonR and CantonS flies were reared under standard conditions at 23°C, sometime supplemented with baker's yeast.

Regeneration Experiments

Amputation was performed on adult flies 2–7 days after eclosion. Flies were anesthetized with CO2, placed under a dissection microscope, and tibia amputated using a spring scissors (Fine Science Tools, 91500-09) and superfine dissecting forceps (VWR, 82027-402). See Figure 4 for detailed description of the amputation plane. Recovering Drosophila were allocated randomly to vials with standard lab fly food (control) or standard lab fly food mixed with 1.7 mM L-Leucine (Sigma-Aldrich L8000), 1.7 mM L-Glutamine (Sigma-Aldrich G3126), and 33 μg/ml insulin (human recombinant, MP Biomedicals 0219390080). To introduce the nutrient supplements, the fly food was microwaved in short pulses, such that the topmost layer of the food was liquified. The supplements in aqueous stocks were then pipetted into this liquified layer. Food was allowed to re-set at 4°C for at least 20 min. New food was prepared fresh every 2 days, and flies were moved into freshly prepared treated food every 2 days, throughout the course of the 2- to 3-week experiment.

Single-fly Tracking

Amputation and treatment were performed as in the bulk regeneration experiments described above, with the following modifications. Canton S flies were amputated in different limbs, and were housed in small groups such that in any given vial, each fly was uniquely identifiable by sex and amputated limb. Typically, 1–6 flies are housed in each vial. 3–5 days treatment produced similar response as sustained treatment; therefore, for simplicity, treatment was performed for 3–5 days. Treated flies, but not control flies, were sometime continued on yeast supplementation. Flies were imaged immediately after amputation and 1–3 additional times over the course of 2–4 weeks. As anesthetized flies jitter, images were taken in a video format, and single frames were then selected for analysis in which the leg

stump was in focus. Tibia length was quantified in ImageJ as the diameter of the minimum enclosing circle of the leg to achieve rotation-invariant assessments. Identical imaging and analysis procedures were used for treated and control flies.

Statistical analysis and blind

Blind measurements were performed on one pair of control and treated datasets. Statistical comparison of percent change in length in control and treated leg stumps was performed using the non-parametric Kruskal-Wallis test. Samples were assigned integer ranks from smallest to largest by quantity, and then differences between conditions were assessed with respect to the ranks. The p-value tests the null hypothesis that the data are drawn from the same distribution.

DAPI staining

Fly tibias were dissected and washed in 70% ethanol (<1 min) to decrease the hydrophobicity of the cuticle and washed in PBS with 0.3% Triton-X for 10 min. The legs were fixed in 4% paraformaldehyde (in PBS) overnight at 4°C and washed five times for 20 min each in PBS with 0.3% Triton-X. The legs were equilibrated in Vectashield mounting medium with DAPI (Vector H-1200) overnight at 4°C, and imaged using Zeiss AxioZoom.V16 stereo zoom microscope with AxioCam HR 13-megapixel camera. Confocal imaging was performed using X-Light V2 spinning disk mounted on the Olympus IX81 inverted microscope.

Live fly imaging

Flies anesthetized on a CO_2 bed were imaged under a Zeiss SteREO Discovery.V8 stereomicroscope equipped with the Zeiss AxioCam 503 color camera.

Electron Microscopy

Environmental scanning electron microscopy (ESEM) was performed on a FEI Quanta 200F (FEI, Hillsboro, OR). Whole-live flies were mounted onto the SEM stub with copper tape.

ESEM images were attained at a pressure of 0.1 mbar and 5 kV at a working distance of 9–12 mm, with water as the ionizing gas.

Materials and Methods for *Mus musculus*

All studies comply with relevant ethical regulations for animal testing and research, and received ethical approval by the Institutional Animal Care and Use Committees at the California Institute of Technology.

Strain

Adult female (3–6 months old) wild-type CD1 mice (Charles River Laboratories strain 022) were used for all regeneration studies.

Regeneration Experiments

Digit amputation was performed following the established protocol in the field (Simkin et al., 2013). Mice were anesthetized with 1–5% isoflurane (in oxygen) in an induction chamber, followed by maintenance on a nosecone. The mouse was positioned on its belly with its hind paws outstretched and the ventral side of the paw facing upwards. Sustained-Release Buprenorphine was administered (Buprenorphine SR LAB) at 0.5 mg/kg subcutaneously as an analgesic. Blood flow to the hindlimb was stemmed by tying a rubber band around the ankle and clamping it with a hemostat. All surgical procedures were carried out under a Zeiss Stemi 305 dissection microscope. An initial incision, parallel to the position of foot, was made through the ventral fat pad using Vannas spring scissors (World Precision Instruments, 14003). The length of this incision was determined by the amount of ventral skin needed to seal the digit amputation wound completely. The ventral skin freed in the initial incision was peeled back using surgical forceps, and a no. 10 scalpel (Sklar, 06-3110) was used to amputate and bisect the digit completely through the second or third phalange. Digits 2 and 4 on the right hind paw were operated on in this fashion, while digit three remained unamputated as an internal control. The amputation wound was immediately closed with the ventral skin flap and sealed with GLUture (Zoetis, Kalamazoo, MI). Amputated portions

were immediately fixed as control for skeletal staining. Dissolved 1.5% L-leucine (USP grade, VWR E811), 1.5% L-glutamine (USP grade, Sigma-Aldrich G8540), and 4–10% sucrose (AR ACS grade, Avantor 8360) in drinking water was administered to mice in the experimental group ad libitum after amputation. Control mice were given untreated drinking water. Drinking water was refreshed weekly for both control and experimental groups, and treated water was made fresh on the day that drinking water was replaced. The amputated digit stumps were photographed weekly for 7–8 weeks, at which time the digits were dissected for skeletal staining.

Statistical Analysis

The sample size in the experiment balanced the aim of achieving >90% confidence level with ethical consideration of minimizing the number of animals used. Animals were randomly allocated to the control or treatment group. No restricted randomization was applied. For weight measurement, the unit of analysis is a single animal. For regeneration phenotype, the unit of analysis is a single digit. Student's t-test was used to evaluate the null hypothesis that there is no difference between the control and treated groups. 95% CIs were computed assuming normal distribution. All data were included in the analysis.

Mouse digit dissection and staining

Mice were euthanized and digits 2, 3, and 4 were removed with a no. 10 scalpel (Sklar, 06-3110) through the first phalange. Excess skin and flesh were removed with spring scissors (Fine Science Tools, 91500-09) and fine dissecting forceps (Fine Science Tools, 11254-20). All digits analyzed by whole-mount skeletal stains were prepared with a standard alizarin red and alcian blue staining protocol (McLeod, 1980). Digits were dehydrated in 95% ethanol for 1 day, and incubated in staining solution (0.005% alizarin red (Beantown Chemical, BT144735), 0.015% alcian blue (Acros Organics, AC40046-0100), 5 % acetic acid, 60 % ethanol) for 1 day at 37 °C. Tissue was cleared in 2 % potassium hydroxide at room temperature for 1 day, 1% potassium hydroxide for 1 day, and then taken through an increasing glycerol series (25%, 50%, 75%, and 100%). The stained samples were imaged

on Zeiss AxioZoom.V16 stereo zoom microscope with a Zeiss AxioCam 503 color camera or a Zeiss Stemi 305 dissection microscope with an iPhone six camera.

C h a p t e r 3

Regeneration activation in *Drosophila* limb promoted by nutrient factors

The content of this chapter is adapted from a submitted manuscript:
Li Y, del Rio Salgado J, Bates G, Condiotte ZJ, Caskey M, Williams B, Hallgrimsdottir I, Pachter L, Goentoro L. Regeneration activation in *Drosophila* promoted by nutrient factors.

3.1 Summary

Nutrients have been shown to promote regeneration processes across species, including in *Drosophila*. To characterize how nutrients promote regeneration, we assessed in *Drosophila* limb early processes that mark regeneration induction. At hour-scale, nutrient treatment alters wound healing, which correlates with the subsequent tissue remodeling processes. At day-scale, while tissues in the injured limb segment normally degenerate, tissues in treated animals survive. At week-scale, muscle bundles remodel and a dome-shaped protrusion forms at the injury site. Performing single-nucleus RNA sequencing at this stage, we find widespread transcriptional modulations across cell types. Strikingly, distinct muscle and epithelial populations emerge that are enriched in mitotic and morphogenetic genes, including those associated with regeneration in larval tissues. This chapter demonstrates, at gene, cell, and tissue level, how nutrient treatment promotes dramatic reversal of tissue loss and activation of processes to replenish.

3.2 Introduction

Although some animals have remarkable ability to regenerate, some others including humans have more limited ability to regenerate. Building on insights from highly regenerating animals (Tanaka and Reddien, 2011; Sánchez Alvarado, 2000; Poss and Tanaka, 2024), increasing studies have begun to examine systems that poorly regenerate and ask whether and how regeneration can be induced. Excitingly, across species, evidence is emerging that regeneration processes can be induced. For instance, in frogs, limb regeneration can be

induced by activating the Wnt pathway (Kawakami et al., 2006), injecting progenitor cells (Lin et al., 2013), or administering a cocktail of drugs (Murugan et al., 2022). In mice, digit regrowth can be induced by administering Bmp proteins (Yu et al., 2019) or modifying a heterochromatic gene (Shyh-Chang et al., 2013). While the induced regeneration is not complete, these studies demonstrate that regeneration processes can be promoted at all, and provide experimental systems with which to further identify factors that limit regeneration.

In addition to developmental molecules, a role for nutrients is emerging. Nutrients are not only necessary for supporting regeneration (e.g., Zhulyn et al., 2023; Gutiérrez-Gutiérrez et al., 2021), supplying extra nutrients or specific nutrient factors, unexpectedly, is sufficient to induce regeneration. In moon jellyfish, increasing nutrient availability promotes activation of appendage regeneration (Abrams et al., 2021). In frog tadpoles, increasing nutrient availability rescues tail regeneration (Williams et al., 2021). In adult fruit flies, supplying insulin and amino acids promote limb growth (Abrams et al., 2021; Figure 1). Finally, in adult mice, feeding sucrose and amino acids promotes digit growth (Abrams et al., 2021). Insulin and amino acids normally signal to the animals a highly abundant environment. These findings suggest that the nutrient environment may be fundamental in the evolution of regeneration.

To investigate how nutrients promote regeneration processes, in this study, we seized on the observation in the *Drosophila*. While the growth occurs over weeks to months, in this study, we characterized how reprogramming already occurs within hours and days.

3.3 Results

At hour-scale, nutrient treatment modifies wound healing

Amputation of the adult limb and treatment were performed as described in Figure 2A-B. Although the developing limb discs in the larval stage can regenerate and recover normal development (Worley and Hariharan, 2022), regeneration display gradually diminishes as

the discs further differentiates and adult fly limbs do not regenerate. Accordingly, as expected, in control adult flies, the amputation wound simply heals and no growth is observed (Figure 1B-C). The wound heals similar to what has been described in wound studies in larvae (Galkow and Krasnow, 2004; Bidla et al., 2005; Álvarez-Fernández et al., 2015). Within minutes, hemolymph flow stops. Within 12–72 hours, a thick, melanized scab forms over the wound site (Figure 2C-D).

Interestingly, we noticed in the control flies, a small fraction (median 8.6%) that heals without forming a melanized scab (e.g., Figure 2E-F). Hemolymph flow still stops within minutes, consistent with the previous report that soft clot formation is independent from the subsequent hardening of the clot into a scab (Bidla et al., 2005). The scabless healing is interesting because the treatment significantly increases the fraction of flies that heal scabless (to a median of 44%, Figure 2G). Melanization may occur in proximal regions (e.g., Figure 2E bottom) or the distal tissue may melanize darker later on (e.g., Figure 5A). The frequency of scabless healing, baseline and treated, can vary across experiments. We do not fully understand the basis of the variation, but since the treatment is nutrient signals, underlying variations in metabolic states (e.g., Pettersen et al., 2018) may play a role. Despite the variation, we verified that the treatment reproducibly increases the fraction of flies that heal scabless (Figure S1).

In summary, within 12–72 hours after amputation, nutrient treatment alters wound healing. The nutrient treatment appears to allow what is normally a marginal response in the population to emerge in many more flies. As described next, the way the wound heals correlates with the tissue processes at day-scale.

At day-scale, nutrient treatment modifies tissue survival.

To characterize tissues, we first attempted staining. Because of the thick adult cuticle, present histological protocols involve chemical clearing and shaking incubation over multiple days. While they work for intact tissues, the extensive handling damages tissues in the scabless

limbs. While we continue developing staining strategies, in this study, we utilized fluorescent reporters.

To visualize tissues in the limb, we analyzed the Mef2>RFP line, which expresses red fluorescent protein (RFP) driven by the promoter of Mef2. Mef2 is a transcription factor in differentiation, maintenance, and repair in diverse cell types (Potthoff and Olson, 2007; Liu et al., 2014). We first assessed the technical aspects of utilizing transgenic lines. First, genetic background may influence response to treatment. We verified that Mef2>RFP flies respond to treatment (Table S1). Next, fluorescent imaging is often hampered by the thick cuticle. Fortunately, a recent study (Koyama et al. 2020) characterized how mounting in Elmer's glue optically clears the adult cuticles. With the glue mounting, Mef2>RFP can be readily imaged in freshly dissected limbs. Finally, autofluorescence is a marker of tissues with increased metabolic activities (e.g., Monici, 2005; Morrow et al., 2024), which can mark response to injury. Autofluorescence is indeed slightly elevated in the injured limbs, but the low, diffuse autofluorescence is distinguishable from the strong, structured Mef2>RFP signal (Figure S2).

Having established the technical aspects, we now analyzed Mef2>RFP signals after amputation. As alluded earlier, tissue responses correlate with the way the limbs heal and treatment. In limbs that heal scabbed, control or treated, Mef2>RFP signals gradually diminish over days and disappear within 10 days after amputation (Figure 3A, B, D). The loss of tissue signals is largely contained within the injured leg segment (the tibia); femur signals are occasionally also affected. Tissue loss in major injury is not unexpected; it is also a major problem in human amputees (Finco et al., 2022).

In treated limbs that heal scabless, Mef2>RFP shows dynamic expression. After amputation, the Mef2>RFP signal is at first reduced within 3–4 days after amputation. Afterward, the Mef2>RFP signal returned, and stayed strong for the duration of the experiments (3-4 weeks; Figure 3C, and quantitation in Figure 3D). The treatment is required for observing the week-scale signal. In control limbs that spontaneously heal scabless, although a similar early dynamic takes place, i.e., disappearance and return, the return is not sustained and the

Mef2>RFP signal disappears by 10 days (see scabless control data in Figure 3D). To further verify tissue survival, we analyzed a known signaling pathway in muscle repair, Notch (Bi et al., 2016). We observed Notch reporter activation in the treated, scabless limbs (Figure S3).

In summary, within days after amputation, nutrient treatment reverses large-scale tissue loss. While tibia tissues in the untreated flies degenerate, tibia tissues in the treated flies survive. The tissue analysis also reveals how in the minority of controls flies that spontaneously heal scabless, Mef2>RFP appears to briefly return, but it fails to sustain. The treatment enables the Mef2>RFP signal to sustain in more flies, and, as described in the next section, to progress further.

At week-scale, nutrient treatment promotes morphological changes.

Next, we examined the Mef2>RFP signals more closely. Shown in Figure 4A-B is a close-up of the Mef2>RFP signals hours after amputation (Figure 4A) and 5 days later after the return (Figure 4B). From ~7dpa onward, small muscle bundles begin appearing near the amputation plane (dashed box in Figure 4C). Imaging deeper into the tissues (Figure 4C1-C2) revealed how the small bundles appear to be defraying at one end (e.g., see arrows). None of these were apparent in limbs earlier than 7 dpa (Figure 4A-B).

Around the same time, a protrusion begins appearing (Figure 5). The onset of the protrusion varies from limb to limb. At any given time (we assayed 7, 10, and 14 dpa), we would observe protrusion in ~5–15% of the limbs (N=444). The shape of the protrusion ranges from a small dome to a long, cylindrical shape (Figure 5A). Finally, assaying Mef2>RFP, small muscle bundles can be detected within the protrusion among highly diffuse signals (Figure 5B, B1).

In summary, at week-scale, morphological changes begin occurring near the amputation plane. Small muscle bundles appear and a protrusion forms over the amputation plane. While it is tempting to call the protrusion blastema, not all regrowth is preceded by a blastema formation. For instance, heart regeneration involves widespread dedifferentiation and

proliferation of the cardiomyocytes (Jopling et al., 2010; Porello et al., 2011). Determination of blastema or the lack of it would have to await assessment of specific blastema markers. To facilitate such next studies, we performed in the next section single-nucleus RNA sequencing.

At week-scale, nutrient treatment promotes widespread modulation across cell types.

To analyze cells in the adult, the Fly Cell Atlas (Li et al., 2022) relies on isolated single nuclei because recovering intact cells is difficult from cuticular body parts. Additionally, nucleus analysis is the only approach for multinucleated cells such as muscles. Accordingly, we performed single-nucleus RNA-sequencing. Limbs were collected at the stage in which they begin showing protrusion (Figure 5). As a control, we collected the same region of limbs from uninjured, untreated flies (Figure 6A). Four control-treated pair replicates from four independent fly cohorts were collected. We analyzed a total of 27,859 nuclei in the control samples (from four replicates: 4,235, 6,625, 9,225, 7,774 nuclei) and 32,635 nuclei in the treated samples (from four replicates: 7,340, 6,877, 10,005, 8,413 nuclei). For each nucleus, the average number of reads was ~$1x10^5$, and the average UMI count was ~$1x10^3$.

First, we performed principal component analysis (PCA; Figure 6B). The samples clustered by condition, with PC1 capturing 70.1% of the variance. PC2, which correlates with technical batches, captures only 7% of the variance. This analysis verifies that the difference between control and treated samples are predominantly biological, with minimal batch-to-batch effects. Indeed, performing the PCA at the cell-level, we verified the same population structures, but with a strong shift, between control and treated samples, suggesting widespread transcriptional modulations between the two conditions (Figure 6C). Top contributors in the variance between control and treated samples include upregulation in multiple heat shock proteins (*Hsp23*, *Hsp68, Hsp70's*) and genes in the JAK/STAT signaling pathway (*upd2* and *upd3*). As we will analyze next, these genes are indeed upregulated across multiple cell types.

To assess cell types, we performed clustering analysis. First, we verified that the control analysis reproduces the Fly Cell Atlas (Figure 6D). The control samples recover all major cell types in the limb: epithelial (marked by *grh*), muscle (*Mhc*, *sls*, *bt*), hemocyte (*Hml*), neuron (*fne*, *futsch*), tracheal (*trh*), and glial (*repo*). Not only does the control analysis recover the marker gene separation, the top genes in each cluster reproduce those in the Fly Atlas (Table S2). One cell type in the Fly Atlas is missing in our dataset: the chordotonal organ, which is expected since the upper femur was not included in the sample. Moreover, with almost four times the number of nuclei than the limb atlas, the present analysis can further distinguish: (1) Another population of epithelial cells marked by a lower expression of *grh* and whose top markers include *slf* and *knrl* (Epithelial 2, Figure 6D); (2) Following the marker genes identified in Hopkins et al., 2023, two populations of sensory support cells, mechanosensory (*sv*) and chemosensory (*nompA*); and (3) A small cluster (marked by *Wnt6*, *Lim1*), that was not identified in Fly Atlas. With the control analysis robustly recovering the published benchmark, we moved to analyze the treated samples.

The treated samples recover the major clusters of epithelial, muscle, hemocyte, and neuron cells (Figure 6E). There are changes in the proportion of the clusters, and the chemosensory support cells are not recovered. Notably, there is an increase in the proportion of the muscle and epithelial cells. Importantly, the treated samples recover a distinct muscle cluster and a distinct epithelial cluster (orange bars in Figure 6E). These new clusters are not small. The new muscle cluster comprises 21.3% of the total muscle cells. The new epithelial cluster comprises 43.5% of the total epithelial cells. In each cluster, the canonical fate markers (*e.g.*, *Mhc* for muscle or *grh* for epithelial) rank lower and are replaced by different top genes (Table S2), discussed next. We verified that these distinct clusters cannot be recovered from the control cells even when we over clustered (Table S2). We next analyzed these treated-specific clusters in more depth.

Starting with the muscle cluster, we compared gene expression in the new muscle cluster in treated vs the muscle cluster in control samples (Figure 7A, Table S3). Top upregulated genes in the new muscle clusters are dominated by multiple genes in the heat shock and antioxidant

glutathione pathways (Figure 7A). Expression of heat shock proteins in muscle has been shown to promote proteostasis and protection from stress, even conferring non-autonomous protection to surrounding cells (Kawasaki et al., 2016). Also notably enriched in the upregulated genes are the mitotic GO terms (Figure 7B, Table S4). 11% of the differentially expressed genes are annotated in mitotic-related GO terms, such as cell division, spindle assembly, and cell cycle. Upregulated cell cycle genes include *Ran*, *trbl*, *Gadd45*, *Cyclin B*, *Cyclin A*, *Cdk1*, *Cks30A*, *polo*, *geminin*, *aurora B*. By contrast, downregulated genes are enriched in GO terms in differentiation (Table S4), which include markers of differentiated muscle, i.e., *Mhc*, *sals*, *sls*, *Zasp52*, *Zasp66*.

Next, we compared gene expression in the new epithelial cluster in treated vs the corresponding epithelial cluster in the control sample (Figure 8A). Top upregulated genes in the new epithelial clusters are again dominated by the aforementioned heat shock proteins as well as genes in the JAK/STAT pathway, *upd2* and *upd3*. Enriched in the upregulated genes are GO terms related to cytoskeleton organization, cell migration, and JNK pathway, as well as GO terms in development and morphogenesis, including imaginal disc morphogenesis, post-embryonic organ development, and epithelial morphogenesis (Figure 8B). The analysis notably recovers the GO terms of tissue regeneration. Although small, the genes driving this enrichment include, all upregulated, *regeneration* (*rgn*, by 4-fold), *Augmented of liver regeneration* (*Alr*, 3-fold), and *imaginal disc growth factor 1* (*Idgf1*, 2.8-fold), all of which key genes in imaginal disc regeneration (McClure et al., 2008; Katsuyama et al., 2015). Consistent with this enrichment is upregulation in *Ets21C* (24-fold), a stress-induced transcription factor that sustains a pro-regenerative transcriptional program in imaginal disc (Worley et al., 2022). While the regeneration GO term enrichment is found in particular in the epithelial cluster, the genes themselves are upregulated across multiple cell types (Table S3).

In addition to promoting formation of new cell clusters, nutrient treatment promotes marked gene expression modulation in the remaining cell types. Different cell types respond differently. For instance, glial (*repo*+) cells from treated samples show upregulation in

ribosome biogenesis, protein folding, and glial cell development. In tracheal (*trh*+) cells, top upregulated GO terms are immune response, cytoskeleton organization, and tracheal system development. Finally, to verify that the conclusions of the differential expression analysis are not sensitive to clustering parameters, we performed combined analysis, comparing all treated cells vs all control cells. The combined differential expression analysis indeed recovered, albeit more diluted, the key genes and key GO terms (Table S3–S4).

3.4 Discussion

This study is motivated by previous observations that nutrients can promote partial limb regrowth (Abrams et al., 2021, and reproduced in related studies by Li et al. and Bates et al.). To understand how nutrients promote regeneration, this study characterizes cell and tissue processes. We find that nutrient treatment alters wound healing, reverses large-scale tissue loss, and promotes widespread transcriptional modulation in all cell types (Figure 9). Strikingly new clusters emerge in the muscle and epithelial cells that are enriched in mitotic and morphogenetic genes, including those known to drive regeneration in the larval tissues. Thus, while limb growth occurs over month scale, these results demonstrate that reprogramming to regenerate already occurs within hours and days. Moreover, while not all animals show dramatic limb regrowth, the detailed analysis here reveals a more pervasive reprogramming at cell and tissue level. Thus, while regrowing a complete organ may still be a longer goal in the field, studies of inducing regeneration can in the shorter term identify useful regenerative strategies at cell and tissue level.

What is such a marvel for us to observe is how malleable the cell processes are. Increasing nutrients can promote large-scale reversal of tissue loss and a dramatic cell reprogramming leading to organ regrowth. The role of nutrients brings into the problem of inducing regeneration the question of energy and resource limitation. This can be consistent with increasing findings that metabolic reprogramming can induce regeneration, for instance in cardymyocytes (Liu et al., 2026). We propose that the role of nutrients signifies broader energetic requirements. In a related paper (Li et al.), we find that the nutrient treatment not only transforms local processes in the injured organs, but also promotes remodeling of distant

metabolic organs, endocrine signaling, and resource allocation. The role of nutrients accordingly opens up new dimensions for therapeutic opportunities beyond targeting the injured organs. In another related study (Bates et al.), we find that we can target the microbiome, and identify a specific bacterium that can strongly promote regeneration processes. Understanding how to induce regeneration may guide us into the fundamental energetics of cellular and organismal states.

3.5 Figures and Tables

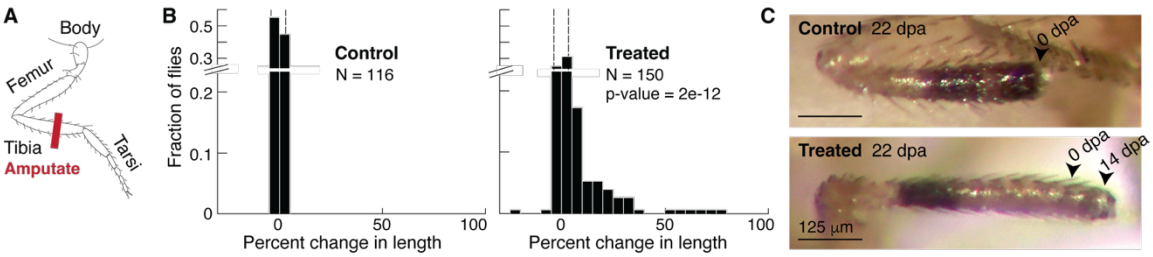


Figure 1. Adult flies begin regenerating limbs when provided with insulin, leucine, and glutamine.

(A) As an injury model, we amputated the limb across the tibia segment. Treated flies were supplemented with insulin, leucine, and glutamine.

(B) The tibia length was measured immediately after amputation and 3–4 weeks later. The change in the tibia length is plotted here, in control (left) and treated flies (right). Dashed lines are the 95% confidence intervals (CI) of the control distribution. 49% of the tibias from treated flies show growth beyond the control 95% CI.

(C) Tibias at 22 days post amputation (dpa). Arrow heads indicate the lengths at previous time points. Top: A limb from a control fly. The length remains the same at 0 and 22 dpa. Bottom: A limb from a treated fly that is growing. Reproduced from Abrams et al., 2021. More examples of growth can be found in the next chapter and Bates et al..

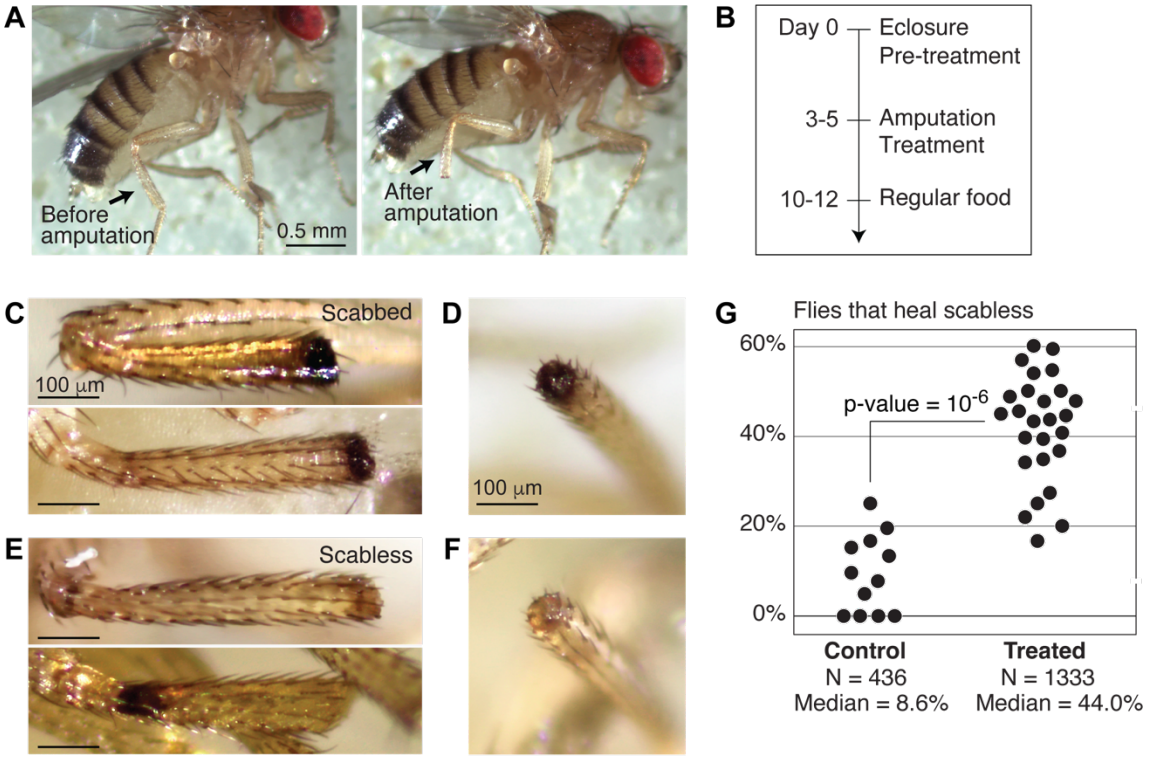


Figure 2. Treatment alters the way the wound heals.

(A) Flies were gently anesthetized and amputated across the tibia segment. Shown is a fly before (left) and after (right) amputation.

(B) For treatment, newly eclosed flies were placed on yeast supplement for 3–5 days, and then amputated. After amputation, flies were treated with insulin, leucine, glutamine, and yeast supplement for a week, after which they were moved to regular food. Control flies remain in regular lab food the entire time.

(C-D) Flies normally heal wounds by forming a melanized scab.

(E-F) Flies that heal wounds without a melanized scab.

(G) Each data point is an independent experiment, with 30–40 flies examined in each experiment. N: the total number of flies analyzed. Statistical test: Kruskal-Wallis.

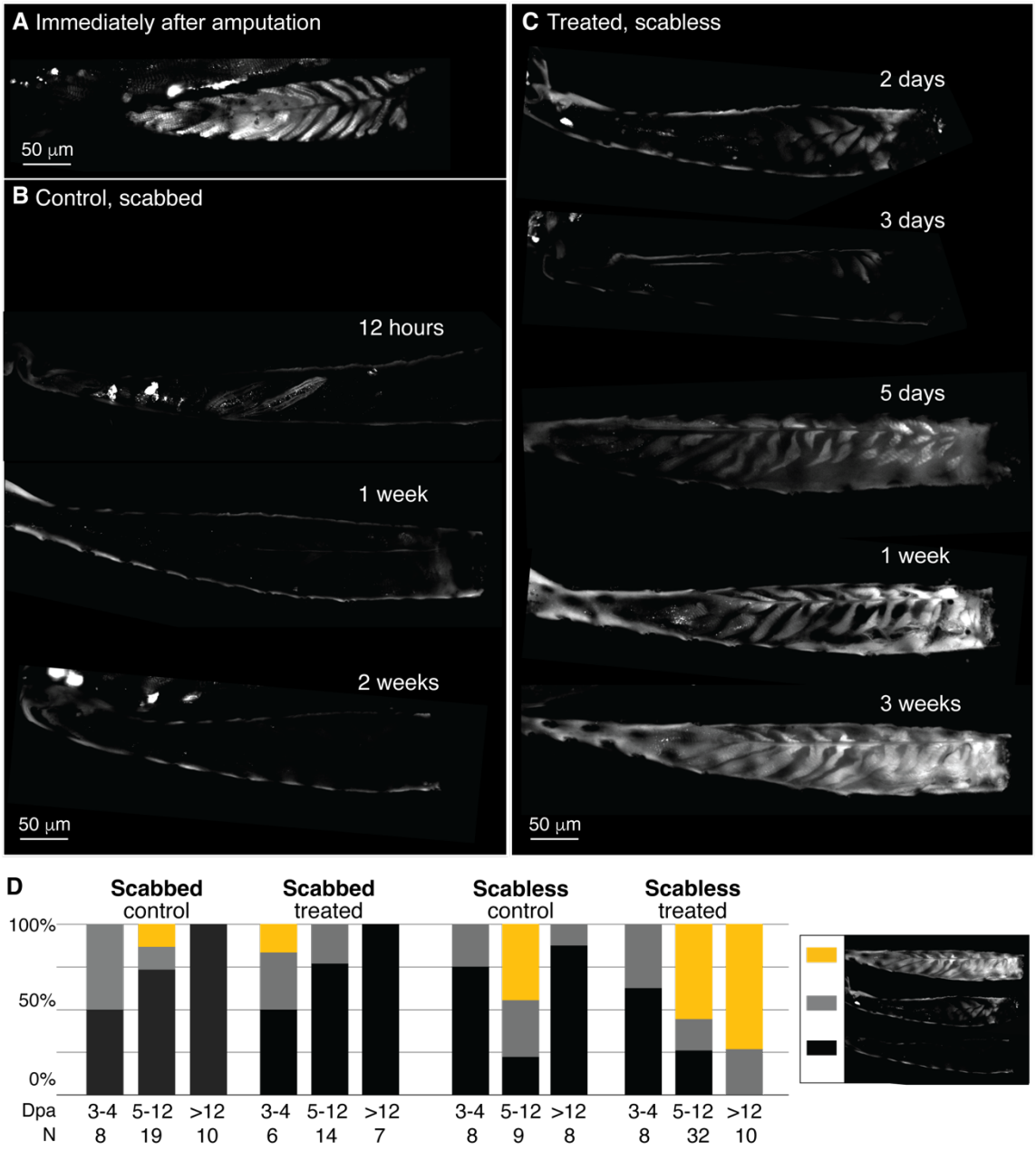


Figure 3. Tibia tissues survive in treated flies that heal scabless.

Mef2>RFP flies were amputated and treated as described in Figure 2B. To image, the limbs were dissected at the indicated time after amputation, mounted, and imaged using a confocal microscope.

(A) A tibia immediately after amputation.

(B) Representative tibias from control flies that heal scabbed.

(C) Representative tibias from treated flies that heal scabless.

(D) Summary of the samples analyzed. Black: no signal. Grey: low signal. Yellow: full signal.

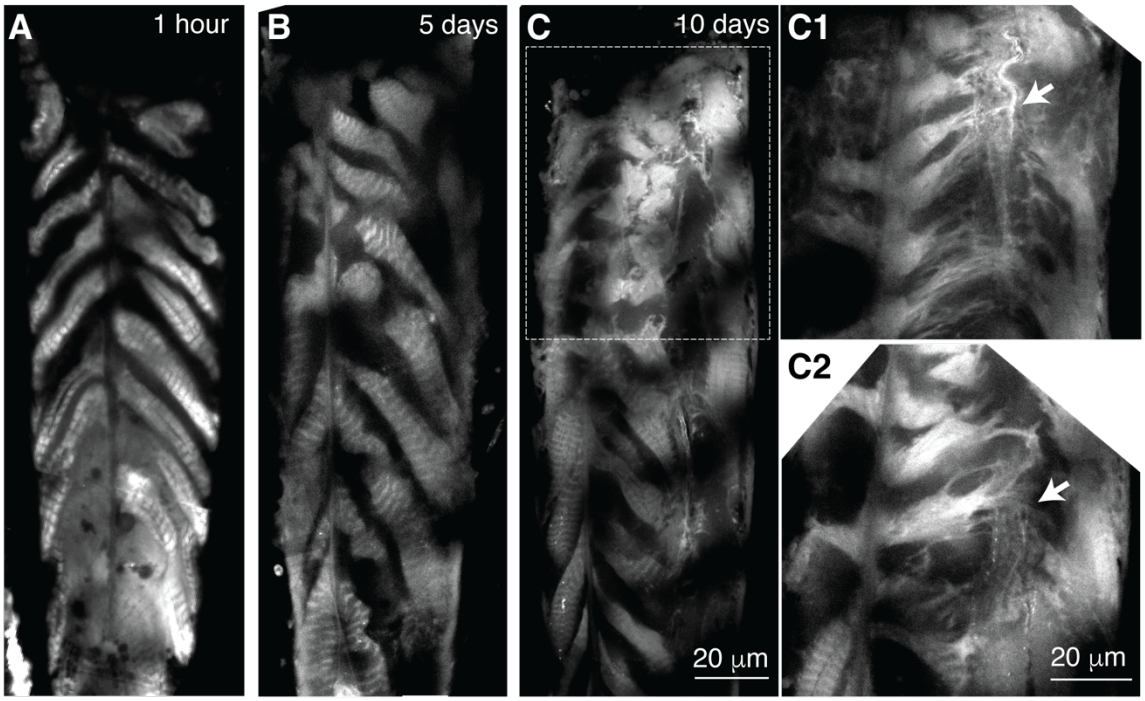


Figure 4. Around 7–10 dpa, tissues near the amputation plane began showing morphological changes.

In these experiments, Mef2>RFP flies were dissected at the indicated time after amputation, and imaged using confocal microscopy. Figure **C1** and **C2** are magnification of the boxed region in **C**, taken at z-sections deeper into the tissues.

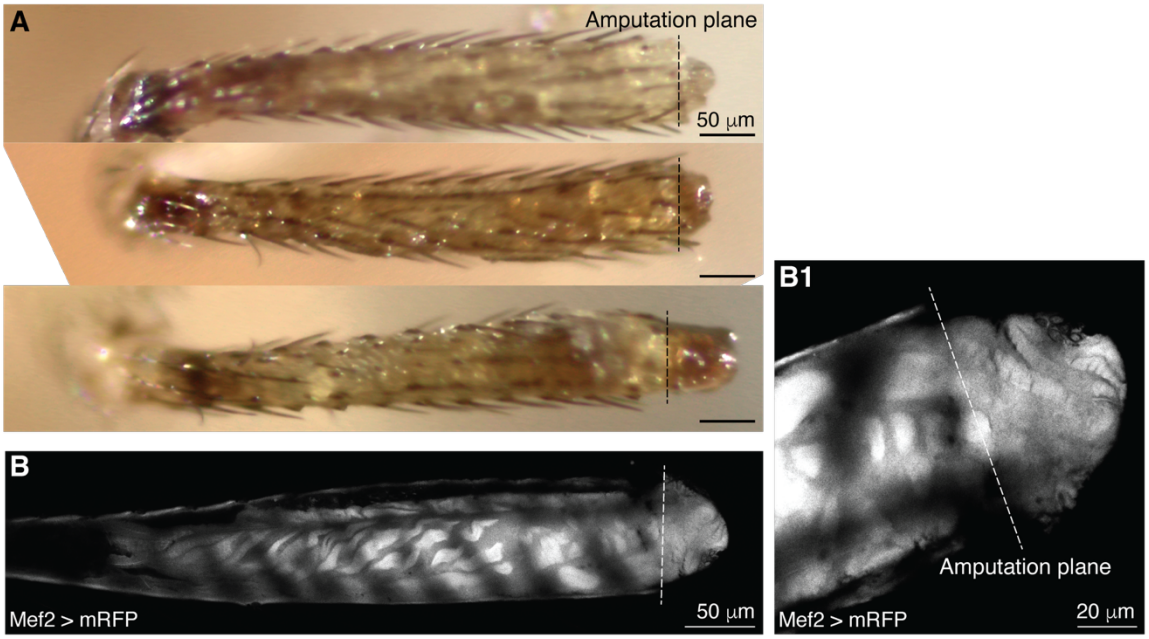


Figure 5. Around 7–10 dpa, protrusion began to form over the amputation plane.

(A) Three different limbs, showing varying shape of protrusion.

(B, B1) The protrusion is positive for Mef-RFP. B1 is a magnification of the distal region in B. Dashed line indicates the end of the cuticle.

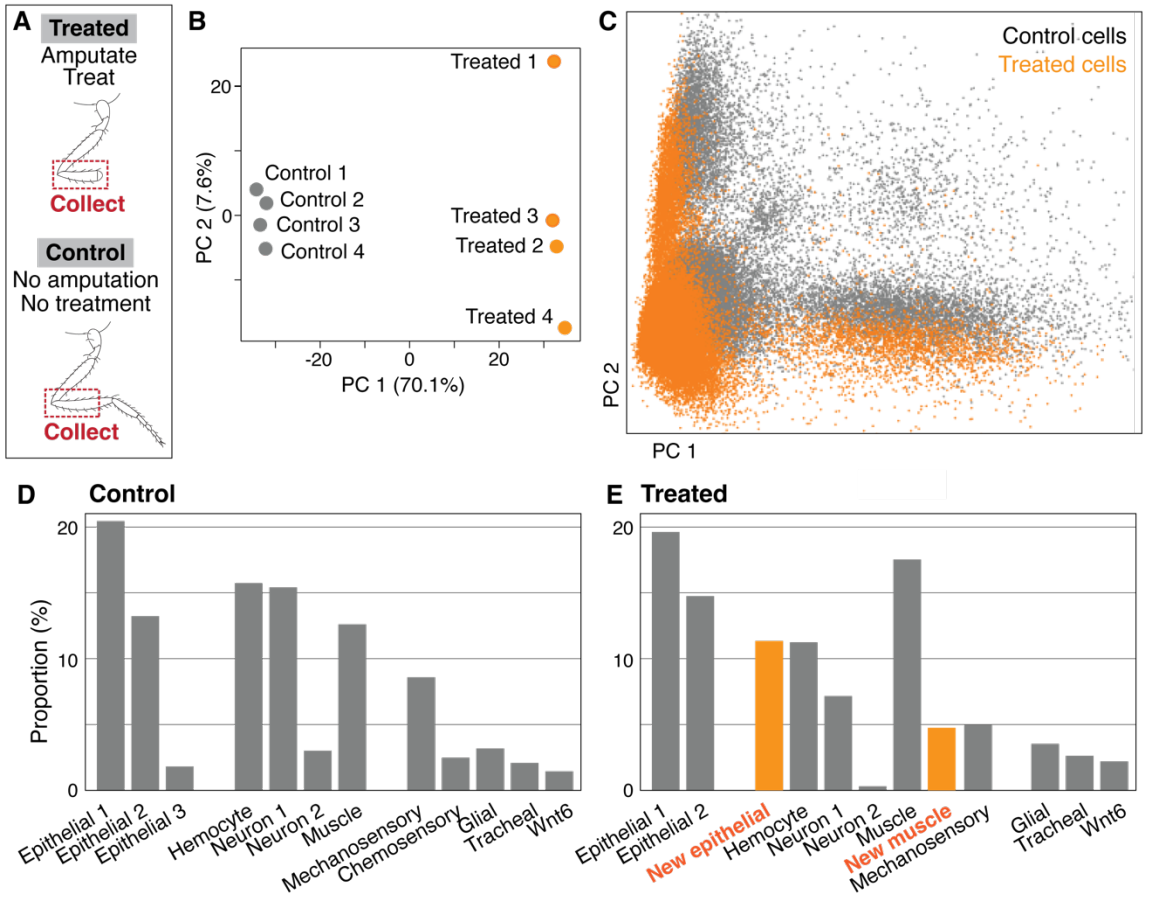


Figure 6. Single-nucleus RNA-seq analysis recovers two distinct cell clusters in regenerating limbs.

(A) Sample collection design. We collected tibias at the protrusion stage (Figure 5). The red dashed box indicates the region collected. As a control, we collected the same region of tibias from uninjured, untreated flies. A minimal bit of femur had to be included to enable handling. Four replicates were collected, with each control-treated pair collected side-by-side from the same fly cohort. The four replications were performed in 4 different weeks, to ensure we sampled independent fly cohorts.

(B-C) Principal component analysis at the sample-level **(B)** and cell-level **(C)**.

(D-E) Cell clusters in limbs from control **(D)** and treated **(E)** flies. Orange cell clusters are recovered only in limbs from treated flies.

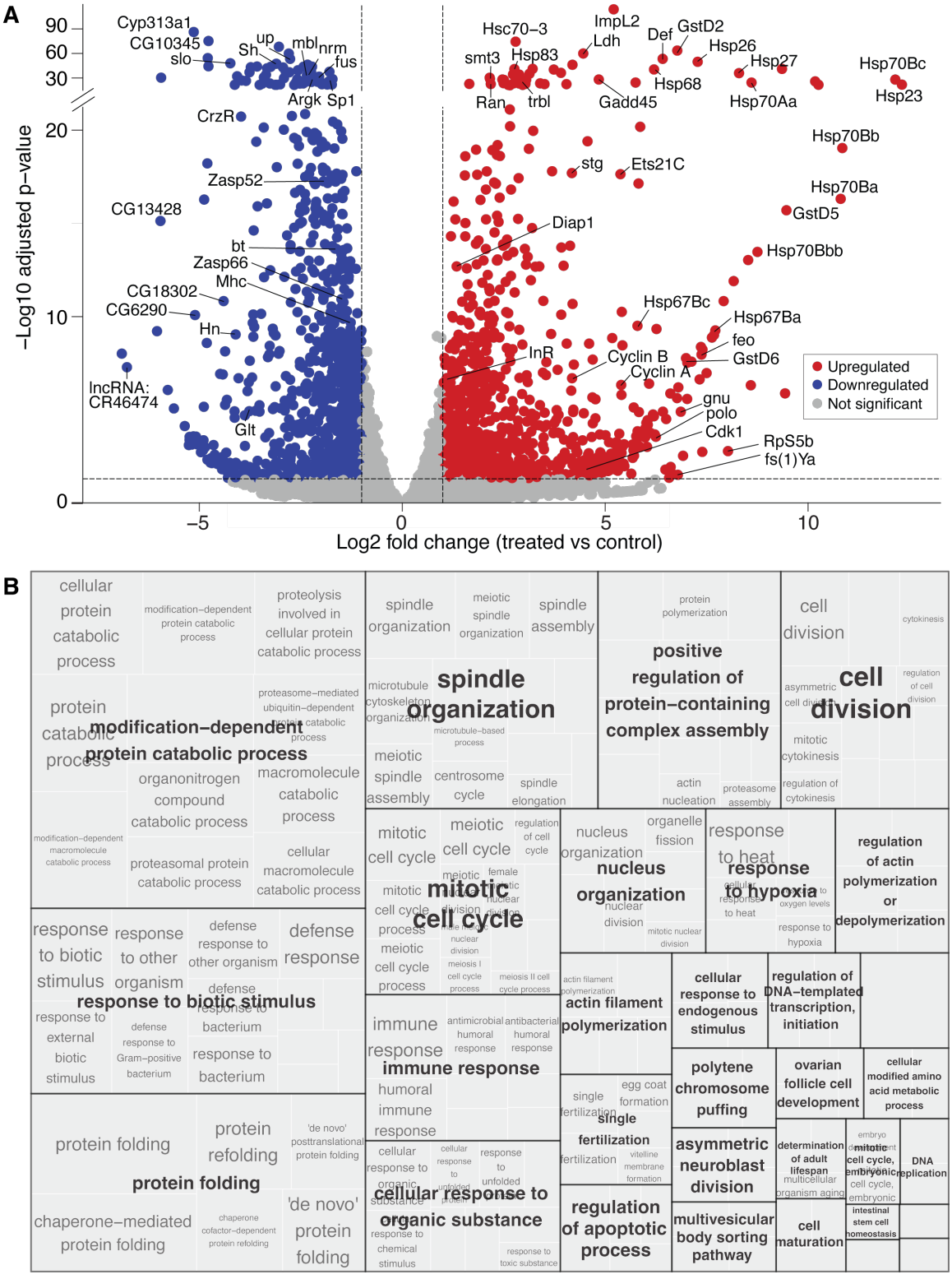


Figure 7. Genes differentially expressed in the new muscle cell cluster.

Differential expression (DE) analysis was performed between the newly clustered muscle cells in the treated sample and the muscle cluster in the control sample.

(A) Volcano plot of DE genes with cut-off adjusted p-value > 0.05, fold change > 1.

(B) GO terms enriched in the DE genes.

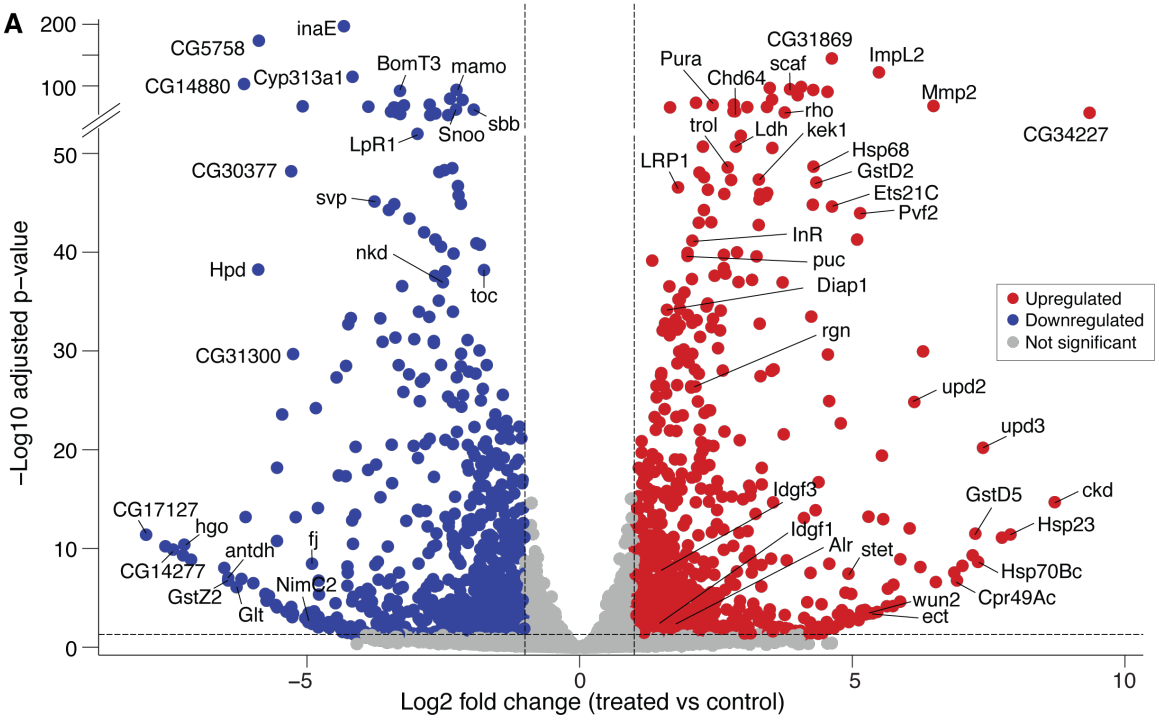


Figure 8. Genes differentially expressed in the new epithelial cell cluster.

Differential expression (DE) analysis was performed between the newly clustered epithelial cells in the treated sample and the corresponding epithelial cluster in the control sample.

(A) Volcano plot of DE genes with cut-off adjusted p-value > 0.05, fold change > 1.

(B) GO terms enriched in the DE genes.

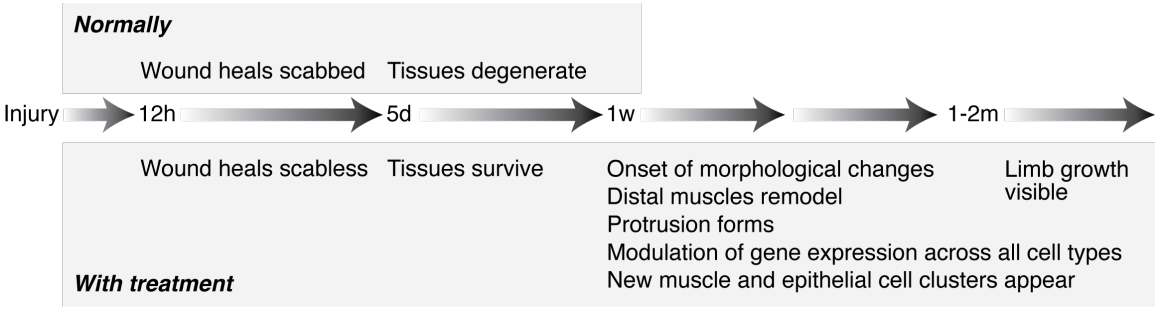
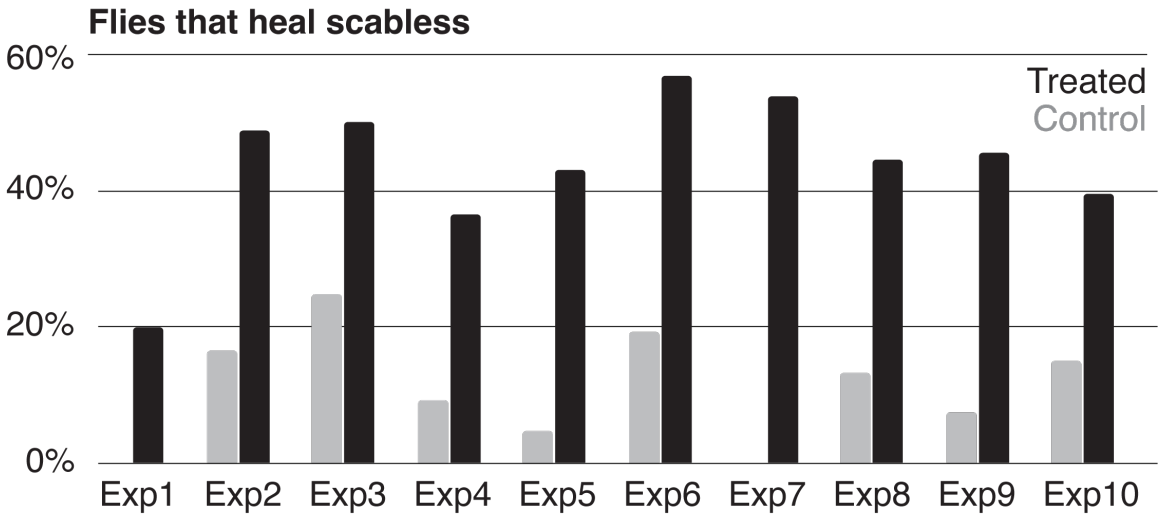


Figure 9. Hour-, day-, and week-scale markers of regeneration induction.

h: hours, d: days, w: weeks, m: months. The times shown are the earliest times the differences can be observed, but as described in the result section, there can be fly-to-fly variation in the timing. Proceeding through each succeeding step may also involve distinct regulations or checkpoints, which would be interesting to further investigate.

3.6 Supplemental information



Estimate fold change	95% CI	p-value
3.4	2.4, 4.8	<0.0001 ***

Figure S1. Despite variation, the nutrient treatment reproducibly increases the percentage of flies that heal wounds scabless.

These experiments were performed in the wild-type CantonS flies. Shown here are ten independent experiments, in which control (grey) and treated (black) conditions were set up side-by-side. Independent experiments are experiments performed using different fly cohorts in different weeks (a fly cohort are flies that emerge in the same stock bottle, i.e., from the same set of parentals). For Exp1 and Exp7, the grey bar is missing because the scabless frequency in control is 0. Statistical significance and reproducibility were assessed by analyzing the effect size across experiments using meta-analysis (Borenstein et al., 2009), implemented using the metafor package in R (Viechtbauer, 2010), with fixed-effect model and statistical coefficients based on normal distribution. The effect size of the treatment was computed as the fold change between the scabless frequency in treated and control within an experiment (the metric risk ratio RR in Borenstein et al., 2009). Fold change = 1 means the treatment has no effect. A treatment is reproducible if the 95% confidence intervals (95% CI)

of the effect size exclude 1. The p-value evaluates the null hypothesis that the fold change is 1.

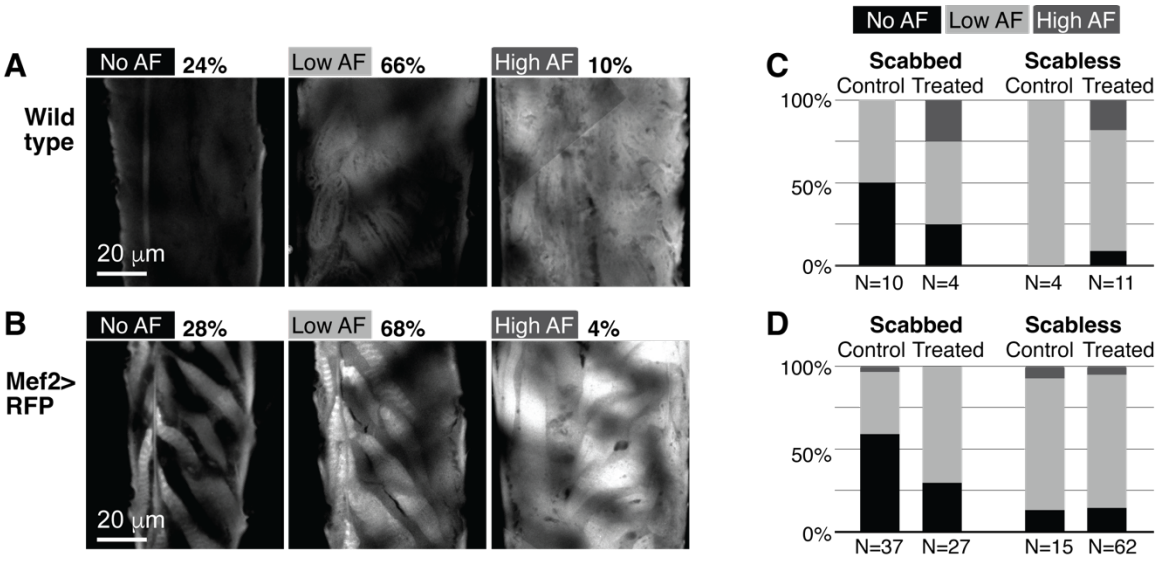


Figure S2. Analysis of autofluorescence in injured limb segments.

Autofluorescence (AF) is a common marker of increased metabolic activities. Major sources of endogenous tissue AF are high-energy molecules, such as NADPH and flavins (Monici, 2005; Morrow et al., 2024). **(A, C)** To assess the extent of AF, we examined wild-type flies using imaging parameters identical to those used to analyze Mef2>RFP. Since the wild-type flies carry no exogenous fluorescent constructs, all signals observed can be attributed to endogenous AF. Low AF is detected in 66% of the limbs analyzed. AF is confined to the injured segment; no or low AF signals were observed in the femur. **(B, D)** Mef>RFP signals can be readily distinguished from the low AF. While the AF signal is diffuse with some weak tissue outlines **(A)**, Mef2>RFP signals are higher in intensity and show a sharp pattern of muscle bundles with striation **(B)**. In addition, we also find in 4-10% of the limbs analyzed signs of unhealthy tissues, e.g., delamination from cuticle, holes in tissues, which correlates with very high autofluorescence (high AF). These limbs were excluded from the analysis.

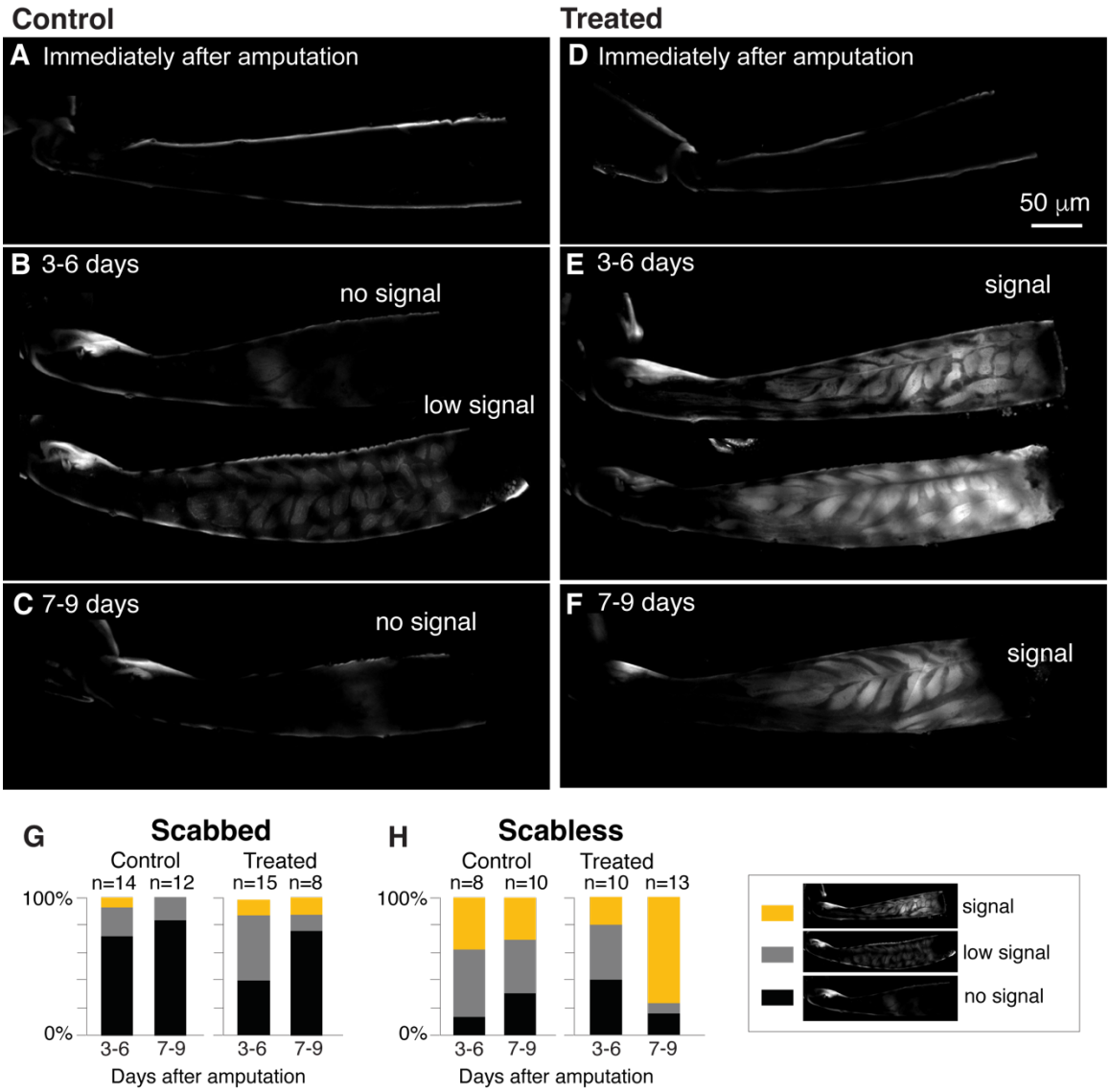


Figure S3. Notch reporter is activated in the treated, scabless limbs.

Notch activation in the muscle bundle is required for muscle repair; in aged and muscular dystrophic mice, Notch activation improves repair myogenesis (Bi et al., 2016). To assess Notch signaling, we used the established reporter for Notch signaling, NRE-EGFP, in which EGFP expression is driven by the Notch Response Elements (NRE; Zacharioudak and Bray, 2014). Time in the images is days after amputation. NRE-EGFP is not active in the intact limbs or upon amputation **(A**, **D)**, and remains inactive or low in limbs that heal scabbed (**B-C**, **G**). NRE-GFP is strongly activated in treated, scabless limbs (**E**, **F**, **H**).

Fly line	BDSC stock number	Baseline rate of scabless healing	Rate of scabless healing with treatment
Some lines that respond to treatment			
Mef2>mRFP	26882	9% (N=266)	31% (N=405)
NRE-EGFP	30727	21% (34)	66% (N=40)
His2B-RFP	Gift from David Glover lab	12% (N=189)	35% (N=272)
Some lines that did not significantly respond to treatment			
Zasp-GFP	6824	6% (N=34)	13% (N=103)
nls-GFP	1691	13% (N=16)	6% (N=33)
A line with a high baseline of scabless wound healing, and did not significantly respond to treatment			
puc-GFP	56276	60% (N=45)	60% (N=10)

Table S1. Wound healing and response to treatment are influenced by genotype. The genotype of a reporter line differs from wild type because of the inclusion of the reporter construct itself, as well as the balancer chromosomes and marker mutations. To use a reporter line, we first verified that the line can recapitulate the wild-type in responding to treatment. Shown are the averages. N is the total number of flies examined. Some reporter lines do not respond to treatment (e.g., ubi-FUCCI, nls-GFP) or appear to have a wound healing phenotype (e.g., puc-GFP), and therefore could not be used for this study. BDSC: Bloomington *Drosophila* Stock Center.

Supplemental table S2, S3 and S4 is available at: https://doi.org/10.22002/3e51h-09526

3.7 Materials and methods

Data Availability. Raw data, RNA sequencing data, and codes are deposited in CaltechDATA (doi: 10.22002/g4x3b-x1n64). Additionally, codes for analysis of single-cell data are available at https://github.com/pachterlab/Goentoro.

Fly lines. The following fly lines were used in this study: wild-type CantonS (a gift from Kai Zinn lab at Caltech), Mef2>RFP (BDSC #26882), NRE-GFP (BDSC #30727). Flies were kept at room temperature, with a 12h/12h light/dark cycle.

Amputation. Flies were gently anesthetized with CO_2, <3-4 liter per minute, which leaves the flies immobilized but still jittery, and the tibia was cut using fine spring scissors (Fine Science Tools t#91500-09).Flies were anesthetized <5 at a time to keep the anesthesia time <1 minute. Amputation was performed in midlimb and hindlimb, except for single-nucleus RNA sequencing, in which only midlimbs were used for consistency in tissue collection. After amputation, flies were placed in treated food (see Treatment) at 4–6 flies/vial.

Treatment. To supplement food with leucine, glutamine, and insulin (LGI), we made a stock LGI solution at 1.7 mM L-leucine (Sigma L8912), 1.7 mM L-glutamine (Sigma G8540), and 0.03 mg/mL insulin (Sigma I0908). Fly food was briefly microwaved to melt the top layer, then 200 μL of the LGI solution was mixed into the melted top layer. To supplement food with yeast, dried yeast granules (Saf-Instant Yeast) were added to cover 30–40% of the food area. Treatment protocol is described in Figure 2A. Duration, dose, and combination of molecules were previously tested in Abrams et al., 2021; the protocol used here gives the strongest response so far.

Imaging. Brightfield imaging was performed using Zeiss Axio V16 dissection scope and Axiocam 208 color camera. For confocal fluorescent imaging, limbs were dissected and then mounted in a small drop of Elmer's clear glue (Koyama et al., 2020). A #1.5 cover glass was gently pressed down on the limb. Mounted limbs were immediately imaged with Zeiss LSM 980. Mef2>RFP was imaged with 10% 561 nm laser and 750V PMT gain. NRE-EGFP was

imaged with 10% 488 nm laser and 750V PMT gain. Within a figure, images are shown with identical dynamic range for consistent comparison.

Single-nucleus isolation. Female flies were used. Treated limbs were collected at 7–10 days after amputation, selecting for those with protrusion. Control limbs were collected from the same region of limbs from uninjured, untreated flies. For each replicate, ~1500 flies were amputated to enable collection of ~100 limbs with the desired morphological stage within the collection time window. Dissection was performed following the Fly Cell Atlas (Li et al., 2022). Samples were homogenized with a dounce. Homogenized samples were sequentially filtered through 40 μm, 10 μm and 5 μm cell strainers. In each filtering step, 300 μL of homogenization buffer was added to rinse the strainer, followed by centrifugation at 300g at 4°C for 30 seconds. The final solution was centrifuged at 300g for 10 minutes at 4°C to pellet the nuclei. ~30,000 nuclei/sample were loaded into 10X Chromium X for droplet generation. Libraries were prepared using the 10X V4 Chromium GEM-X Single Cell 3' Kit v4, and sequenced on a NovaSeq X Plus with a 25B flow cell.

Single-nucleus RNA sequencing analysis. Raw sequencing reads were demultiplexed by UCSF CAT. Kallisto reference genome index was built with kb-python (v0.29.5) using the Drosophila melanogaster BDGP6.54 genome FASTA and corresponding GTF annotation. Alignment and quantification were performed using kallisto (v0.51.1, Bray et al., 2016; Melsted et al., 2021; Sullivan et al., 2025). Count matrices were imported into Python (v3.9.5) and analyzed using Scanpy (v1.10.3; Wolf et al., 2018). Cells were filtered using the stringent threshold of Fly Cell Atlas, i.e., cells were required to have a minimum of 500 UMI, 200 genes, and <5% mitochondrial content. Genes were required to be in at least 3 cells to be included in the analysis. Cells with Scrublet doublet score >0.3 were removed (Wolock et al., 2019). Filtered datasets were concatenated into control and treated groups, and normalized to 106 counts and log1p-transformed. Highly variable genes were calculated using the Seurat method with sc.pp.highly_variable_genes (min_mean=0.01, max_mean=8, min_disp=1, n_bins=20, flavor="seurat"; Satija et. al., 2015). Principal component analysis (PCA) at cell-level is performed using sc.tl.pca (svd_solver=arpack). PCA at sample-level

was performed by summing raw counts within each biological replicate to generate sample-level expression profiles, followed by normalization, log1p transformation, and PCA using the sklearn PCA implementation. Neighborhood analysis was performed using sc.pp.neighbors (n_neighbors=30, n_pcs=20). Clustering was performed using the Leiden algorithm (Traag et al., 2019; see Table S2). We identified a small cluster in control that consisted predominantly of cells from replicate 4, which was further verified using CellSweep algorithm (Caskey et al., 2026) to contain only ambient RNAs, and was therefore excluded from downstream analysis. Cluster-specific top marker genes were computed using sc.tl.rank_gene_groups (method=Wilcoxon). Differential gene expression analysis was performed with DESeq2 (v1.34.0; Love et al, 2014). GO enrichment analysis was performed using clusterProfiler (v4.2.2; Yu et al., 2012) with the gene background defined as all genes expressed in the analyzed cells. GO term similarity clustering was performed using rrvgo (v1.6.0; Sayols, 2023).

C h a p t e r 4

Characterization of regeneration activation in *Drosophila* limb promoted by nutrient factors: local modulations

The content of this chapter is adapted from a submitted manuscript:
Li Y, Bates G, Yu C, Grillo E, Wardhana L, Dimayuga CM, Goentoro L. Regeneration activation in *Drosophila* by nutrient factors involves organismal modulations.

4.1 Summary

Inducing regeneration must involve reprogramming of the injured tissues, but it is less understood how the organismal state also needs to be modulated. In the previous chapters, we found that nutrients can promote regeneration processes in multiple species, including in *Drosophila*. In this chapter, we assessed systemic changes that accompany regeneration induction by nutrients. At the organ level, flies that activate regeneration enlarge their midguts, a known mechanism to adapt to increased demands. In parallel, flies that activate regeneration reduce ovary size and egg chamber maturation. Consistent with a trade-off between regeneration and reproduction, virgin flies are more responsive to treatment. At the transcriptomic level, within hours after injury, flies that activate regeneration already show a distinct global profile. Early divergence is confined to 150 genes, suggesting that the switch to a regeneration-promoting state is localized to few specific pathways. Strikingly upregulated is the response to the steroid hormone. Administering the steroid hormone can indeed recapitulate nutrient factors in promoting limb regrowth to commence. This study suggests that inducing regeneration involves not only modulating the injured tissues, but also organismal processes to support the demands.

4.2 Introduction

Why some animals regenerate so well, when some others do not regenerate as well, is a fascinating question. Excitingly, increasing studies demonstrate that regeneration processes

can be induced. For instance, in frog limb, regrowth can be promoted by administering progenitor cells (Lin et al., 2013) or a cocktail of small molecules (Murugan et al., 2022) into the limb stump. In mouse digit, regrowth of bone and joint can be induced by administering Bmp proteins into the digit stump (Yu et al., 2019). In mouse heart, cardiac regeneration can be enhanced by hypoxia (Nakada et al., 2017) or activating the Hippo pathway in the cardiomyocytes (Xin et al., 2013). Although the induced regeneration is not perfect, the key finding is that regeneration processes can be promoted at all, providing systems to further investigate factors that limit regeneration.

Coping with injury and rebuilding lost tissues is demanding. Accordingly, a role for nutrients was recently observed. Nutrients are not only necessary for promoting regeneration (e.g., Zhulyn et al., 2023; Gutiérrez-Gutiérrez et al., 2021), supplying nutrients can, unexpectedly, promote regeneration processes to commence. Supplying extra nutrients or specific nutrient factors promotes tail regeneration tadpoles (Williams et al., 2021), appendage regeneration in jellyfish, digit regrowth in adult mice, and partial limb regrowth in adult flies (Abrams et al., 2021; and related studies by Li et al and Bates et al.). The conserved influence of nutrients suggests that upstream from the tissue-specific mechanisms in the injured organ is a conserved regulation involving nutrients. Thus, inducing regeneration may not only involve engineering changes in the injured tissues, but also coordinating upstream systemic processes.

Indeed, even in regeneration that naturally occurs, mounting regeneration impacts remote organs and organismal processes (Sun and Poss, 2023; Rennolds and Bely, 2023). For instance, tissue regeneration delays development in flies to give time to repair injury (Colombani et al., 2012; Garelli et al., 2012); modifies lipid composition in distant organs (Kubler et al., 2024); triggers cells in distant tissues to enter an alert state or cell cycle (Rodgers et al., 2014, Johnson et al., 2018); and affects reproduction (Rennolds and Bely, 2024). Thus, naturally occurring regeneration does not only locally affect the injured tissues, but appears to systemically impact the organism. Systemic regulations may broaden therapeutic avenues to induce regeneration. Motivated by this, in this chapter, we

investigated in *Drosophila* the systemic modulations that accompany induction of regeneration processes.

4.3 Results

Flies that activate regeneration have larger midguts

As an injury model, we amputated the limb as described in Figure 1A. Fly limbs do not normally regenerate. The wound heals forming a thick melanized scab (Figure 1C), as expected from previous wound healing studies (Galkow and Krasnow, 2004; Bidla et al., 2005; Álvarez-Fernández et al., 2015). Nutrient treatment was performed as described in Li et al. (Figure 1B). To assess systemic changes, we began by assessing some organ changes. A key organismal adaptation to changing physiological demands is midgut plasticity (Buchon et al., 2009; O'Brien et al., 2011). In response to increased demands, midgut enlarges to facilitate adaptation in nutrient intake, storage, metabolism; microbiome composition; and systemic immune and hormonal profiles (Stojanovic et al., 2022).

To assess the midgut, as characterized in a previous study (Abrams et al., 2021), a one-week pulse of nutrient treatment can capture the effect of continuous treatment. As further characterized in a related study by Li et al., reversal of tissue loss occurs within the first week. Accordingly, we focused in this study on early systemic changes in the first week after amputation. To identify flies that activate regeneration at this early time, as characterized in Li et al., regeneration activation is marked by the way the wounds heal scabless (Figure 1C). Finally, nutrient treatment may have broad effects that are not specific to regeneration. To address this, we took advantage that within the treated population, some flies activate regeneration and some flies fail to do so. Comparing these two treated populations eliminates broad treatment effects and focuses us on changes more likely to be specific to regeneration activation.

Implementing these experimental designs, we find that the midgut is remodeled. Midguts from flies that heal wounds scabless are larger than those from flies that heal wounds scabbed

(Figure 1D-E). Quantifying the midgut area, we find a statistically significant difference, with a median shift of 35.6% (Figure 1F). Since we are comparing two injured populations, the effect measured here is not due to the limb injury, but correlates with regeneration activation. Midgut enlargement is consistent with inducing regeneration being demanding to the organism. As described next, another demanding organismal process is indeed affected.

Flies that activate regeneration have smaller ovaries

A major expenditure in organismal processes is reproduction. Consistent with reproduction and responding to injury being both demanding, there have indeed been reports in *Drosophila* that injury negatively influences egg production (Sepuvelda et al., 2008; Dixon et al., 2025). In this study, we further assessed the effects of activating regeneration. To distinguish the effect of injury from regeneration activation, as in the midgut assessment, we compared injured, treated flies that activate regeneration and injured, treated flies that do not (Figure 1B).

We find that the ovary is remodeled in flies that activate regeneration. Ovaries from treated flies that heal wounds scabless are smaller than ovaries from flies that heal scabbed (Figure 2A). Quantifying the ovary size, we find a median size difference of 19.9% (Figure 2B). To assess where the reduction in ovary size comes from, we examined the egg chambers. Scabbed and scabless flies show no significant difference in the total number of egg chambers and number of ovarioles (Table S1), suggesting that egg production still proceeds However, strikingly, the fraction of the late-stage egg chambers is halved in the scabless flies (Figure 2C). Thus, maturation to late stages appears to be slowed down. The late stages interestingly correspond to nurse-cell dumping and chorion formation that accompany large growth to mature size (Figure 2D).

The altered ovary size and reduced late-stage egg chambers suggest that inducing regeneration requires allocating resources from reproduction. To assess this hypothesis, we examined virgin flies, which have lower egg production than mated females (Chapman et al., 2003). Consistent with a trade-off between regeneration and reproduction, virgin females

indeed more readily modulate wound healing in response to the treatment (Figure 2E). As described next, this trade-off is further supported by the transcriptomic analysis.

Flies that activate regeneration show early transcriptional divergence

The organ assessment shows that systemic changes accompany and can influence regeneration induction. To facilitate further characterization of a systemic regeneration-promoting state, and to identify candidate systemic signals, we characterized transcriptomic changes in whole flies. As characterized in a related study by Li et al., flies that mobilize regeneration processes can be identified as early as within 12 hours after amputation from the wound healing. To capture the earliest divergence between regenerating and non-regenerating states, we accordingly analyzed this time point (Figure 3A).

The analysis identifies 170 transcripts (150 genes) that are differentially expressed with fold change > 2 (and 249 transcripts, 223 genes with fold change > 1; Figure 3B). *Drosophila* has 13,907 protein-coding genes (Adams et al., 2001; Kaufman, 2017). Thus, only 1.6% of the genes are modulated between flies that activate regeneration and flies that do not. The low number of differentially expressed genes suggests that shifting to a regeneration-promoting state involves few, specific processes.

Top upregulated genes (Figure 3B) are populated by genes in metabolic (*glutamine synthetase 2*, *for*, *Edem1*) and growth regulation (*gigas*/*Tsc2*, *eIF4H1*, *hppy*, *Csk*, *Tao, syd, lilli*). Consistent with metabolic and growth processes being modulated, multiple ribosomal proteins are upregulated (e.g., *RpL23A*, *RpL10*, *mRpL28*), and enrichment analysis identifies GO terms in RNA processing, stem cell regulation, and mitosis (Figure 3B, Figure S2). Indeed, major translational regulators (*eIF4H1*, *pumilio*, *Cnot4*) and mitogenic signaling pathways (Wnt, epidermal growth factor) are among the differentially expressed genes.

The differentially expressed genes also support signatures of organ remodeling. Top downregulated genes are strikingly populated by markers of differentiated muscle (e.g., *sals, Zasp52*, *ewg*; Figure 3A, Figure S2). Muscle remodeling would be consistent with response

to changing metabolic demands (Bassel-Duby and Olson, 2006). Also notably enriched in downregulated genes is mating behavior (Figure S2), consistent with the ovary remodeling observed in the previous section (Figure 2). Further, the global transcriptomic analysis identifies modulation in immune processes, with downregulated genes enriched in the stress-response JNK/MAPK pathway and Toll/NF-κB pathway (Figure S2) and upregulated genes enriched in the JAK/STAT pathway and Imd/NF-κB pathway (Figure 3B). Finally, the analysis uncovers a striking enrichment in an endocrine process, the response to the steroid hormone ecdysone (Figure 3B), which we will investigate further in the next section.

In summary, this analysis identifies global transcriptional signatures that accompany the induction of regeneration. As described in the next final section, we followed up on the process most enriched in the regenerating state, the steroid hormone signaling.

Steroid hormone can recapitulate nutrient factors in promoting regeneration

Systemic changes suggest the action of signals that coordinate activities at organismal level to support regeneration activation. One candidate is insulin itself, which is indeed part of the treatment. Another endocrine candidate is presented by the global sequencing analysis. Strikingly enriched in the upregulated genes is response to the steroid hormone, ecdysone (Figure 3B). Multiple known targets of ecdysone are upregulated, including *mical, crol*, *rols*, *broad*, as well as the receptor itself, *EcR* (Figure 3A). Although perhaps more known for its role in metamorphosis, ecdysone receptors are expressed in almost all adult fly tissues (Schwedes et al., 2011). In adult, ecdysone functions closely with insulin in coordinating nutrient status and physiological demands with organ functions (Nijhout et al., 2014; Zipper et al., 2020; Ahmed et al., 2021; Koyama et al., 2020; Belles and Piulachs, 2015). To verify the role of ecdysone, we assessed the extent to which ecdysone can recapitulate nutrient signals in promoting regeneration.

We verified that, as with nutrient treatment, ecdysone treatment modulates wound healing. Ecdysone treatment more than doubles the proportion of flies that heal wounds scabless (Figure 4A). Motivated by this early indicator of regeneration activation, we further assessed

how far ecdysone can promote regeneration processes. To do so, we tracked individual flies for 1–2 months after amputation to assess for limb growth. To mimic the one-week pulse of nutrient treatment, ecdysone was administered for one week only after amputation.

We observed in ecdysone-treated flies activation of limb growth (Figure 4C-E). Quantifying the tibia length over time, we find that 36% of the treated flies show a statistically significant increase beyond the 95% confidence interval of the control set (Figure 4B). The extent of growth varies across flies. Some examples of the growth observed are shown in Figure 4D-F. Interestingly, some of the new growths are enclosed in cuticles (e.g., Figure 4E), and some are not (e.g., Figure 4D, F). This motivates our current working hypothesis that the latter may represent an intermediate stage, consistent with the observation in a related study (Li et al., Figure 5) that growth proceeds with tissue protrusion. In summary, this analysis shows that the steroid hormone ecdysone can recapitulate the nutrient factors in promoting regeneration.

4.4 Discussion

This study characterizes how induction of regeneration by nutrient treatment involves systemic changes. The experiments identified specific changes in distant metabolic organs, a trade-off with reproduction, and transcriptomic signatures of the regeneration-promoting state. In particular, the study identifies a role for the steroid hormone signaling, whose direct administration can promote limb regrowth to commence. Thus, inducing regeneration processes does not only involve reprogramming in the injured tissues, but also systemic coordination of organismal processes.

The nutrient factors used in this study—insulin, leucine, and glutamine—are those whose abundance normally signals to the animal a high-sugar and high-protein environment and activates endogenous pathways that support growth. Consistently, the systemic changes identified in this study—enlargement in midgut, reduction in reproduction, activation of the steroid hormone signaling—are consistent with a ramp-up in energetic activities and resource allocation. The nutrient/insulin/steroid hormone signaling axis is indeed a deeply conserved

systemic regulation that coordinates organ functions with nutrient status and physiological demands. Presenting nutrient signals of high abundance may push the organism into a growth state that is normally inaccessible, and enables regeneration processes to emerge. Because the shift is systemic, it can plausibly impact multiple organs.

Within the same time frame of the systemic changes characterized here, a related study by Li et al. shows that extensive changes are also occurring in the injured limb, which include alteration in wound healing, dramatic reversal of tissue loss, and formation of distinct cell clusters. Together, these studies provide a local-systemic framework that can guide further studies in *Drosophila* and other systems to investigate the full extent to which organisms can be rewired to promote regeneration. The local-systemic framework for regeneration induction opens up broader therapeutic opportunities beyond targeting the injured organs. In a related study (Bates et al.), we identified that microbiome modulation can strongly promote regeneration processes.

Early divergence between regenerating and non-regenerating states in *Drosophila* is confined to only 1.6% of the genes. The unexpectedly small number of changes suggests that we can map the local-systemic interactions underlying a regeneration-promoting state to a satisfying degree. Systemic changes associated with injury and regeneration are little understood, but of medical significance. Hyperglycemia and insulin resistance are enigmatically common in critical illnesses and pregnancy (van den Berghe et al., 2001; Marik and Raghavan, 2004; Sweeting et al., 2022). In some severe diseases or after major surgeries, systemic muscle wasting is a serious complication (Wyart et al., 2020; Sayer et al., 2024). Inducing regeneration, the ultimate goal of regenerative medicine, can critically depend on manipulating the interplay between local and systemic regulations.

4.5 Figures and tables

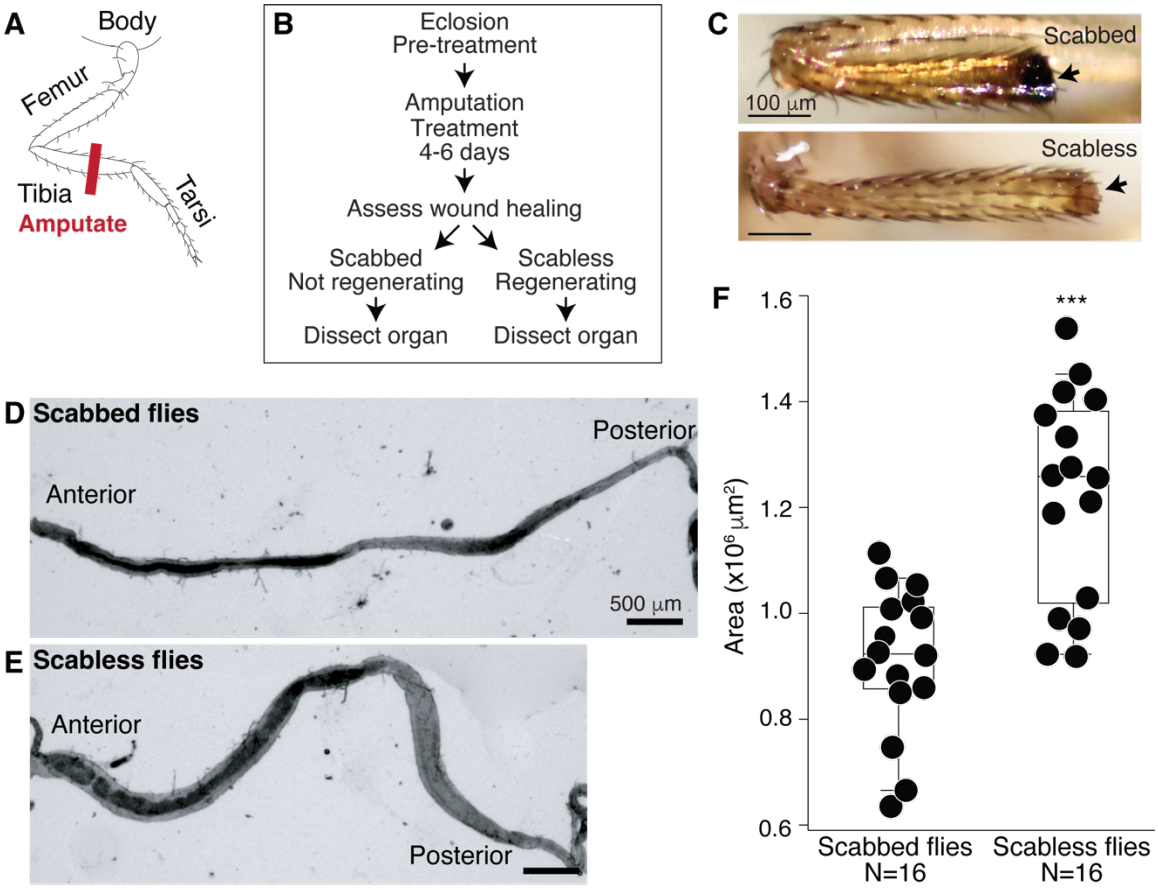


Figure 1. Flies that activate regeneration enlarge midguts.

(A-C) Flies were amputated across the tibia segment.

(B) Treatment was performed following Li et al. Newly eclosed flies were pre-treated with yeast for 3–5 days. After amputation, flies were treated with leucine, glutamine, insulin and yeast until they were assessed for wound healing and organ dissection at 4-6 days after amputation.

(C) Tibia segments that heal with a melanized scab (top) and without a melanized scab (bottom).

(D-E) Representative midguts from flies that heal scabbed **(D)** and flies that heal scabless **(E).**

(F) Midgut area. The datapoints are from three independent experiments. Area was measured from R2 to R5 (Buchon et al., 2013). Box plot: median and quartiles; whiskers: 95% confidence intervals. N: sample size. Statistical significance: Kruskall-Wallis, p-value = 0.00030. Figure A and C are modified from Li et al.

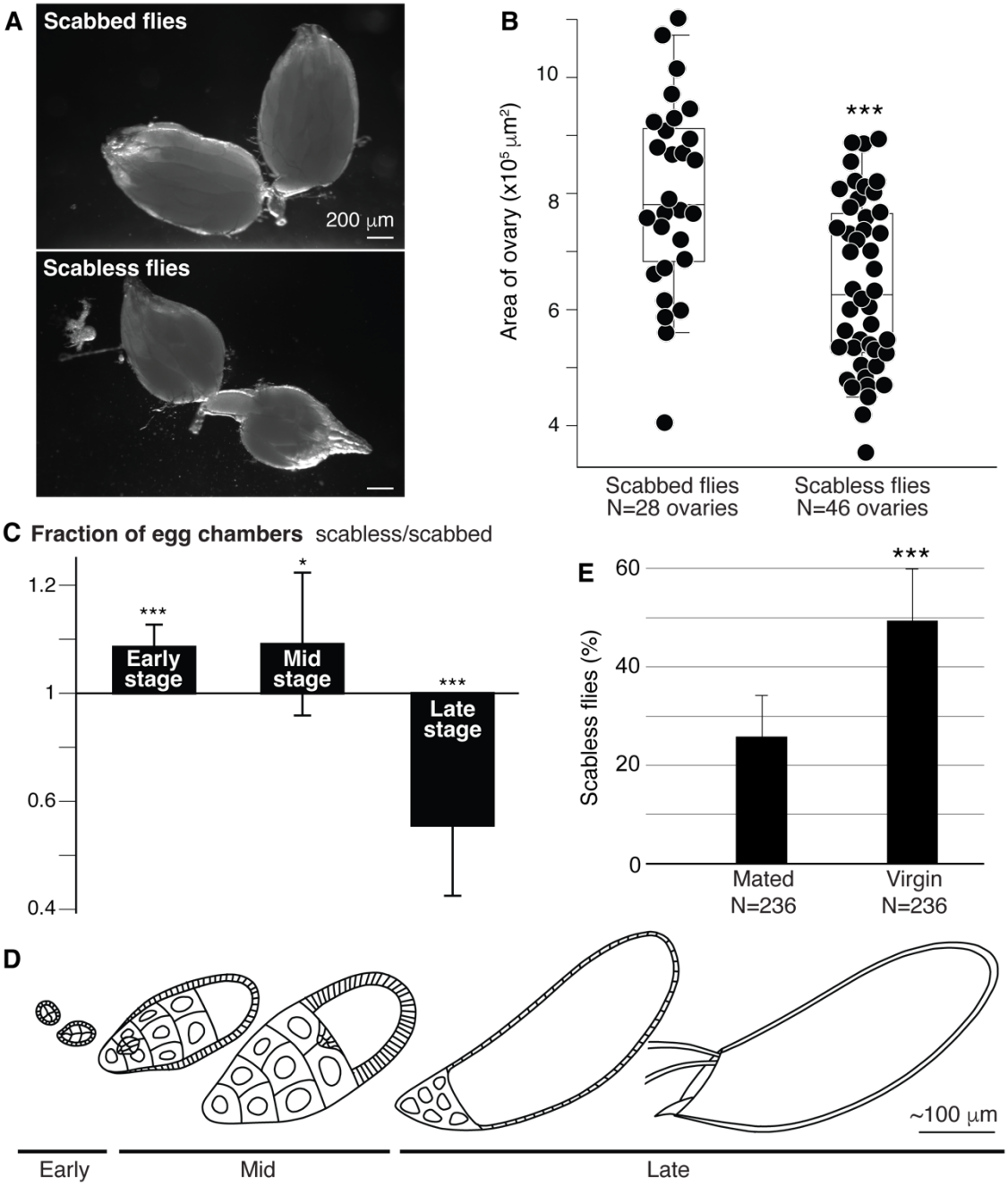


Figure 2. Flies that activate regeneration have smaller ovaries.

(A) Representative ovaries from scabbed (top) and scabless (bottom) flies.

(B) Areas of the ovaries. Each sample is an ovary, dissected 4-6 days after amputation. This dataset is from three independent experiments. Box plot: median and quartile; whiskers: 95% confidence intervals; N: sample size. Statistical test: Kruskall-Wallis, p-value = 0.0002.

(C-D) Egg chamber staging. Plotted here is the fraction of early, mid, and late stages with respect to the total egg chambers in each ovary. 16 ovaries from scabbed flies, and 17 ovaries from scabless flies were examined. Statistical significance: t-test, early, mid, late p-value = 1.9e-7, 0.024, and 6.5e-7 respectively. **(D)** Egg chamber illustration, by Ken Morrisey. Following the standard staging, early is the pre-vitellogenic stage 1–7; mid is the vitellogenic stage 8–10 with a visible oocyte; and late is stage 11–14, characterized by nurse-cell dumping and growth to mature size.

(E) Virgin and mated females were collected from the same fly cohorts. In these experiments, yeast was omitted, because yeast promotes egg laying in virgins (Gou et al., 2014; Ameku and Niwa, 2016). Wound healing was assessed 3–5 days after amputation. This dataset is from seven independent experiments. N: the total number of flies. Statistical test: t-test, p-value = 0.0007.

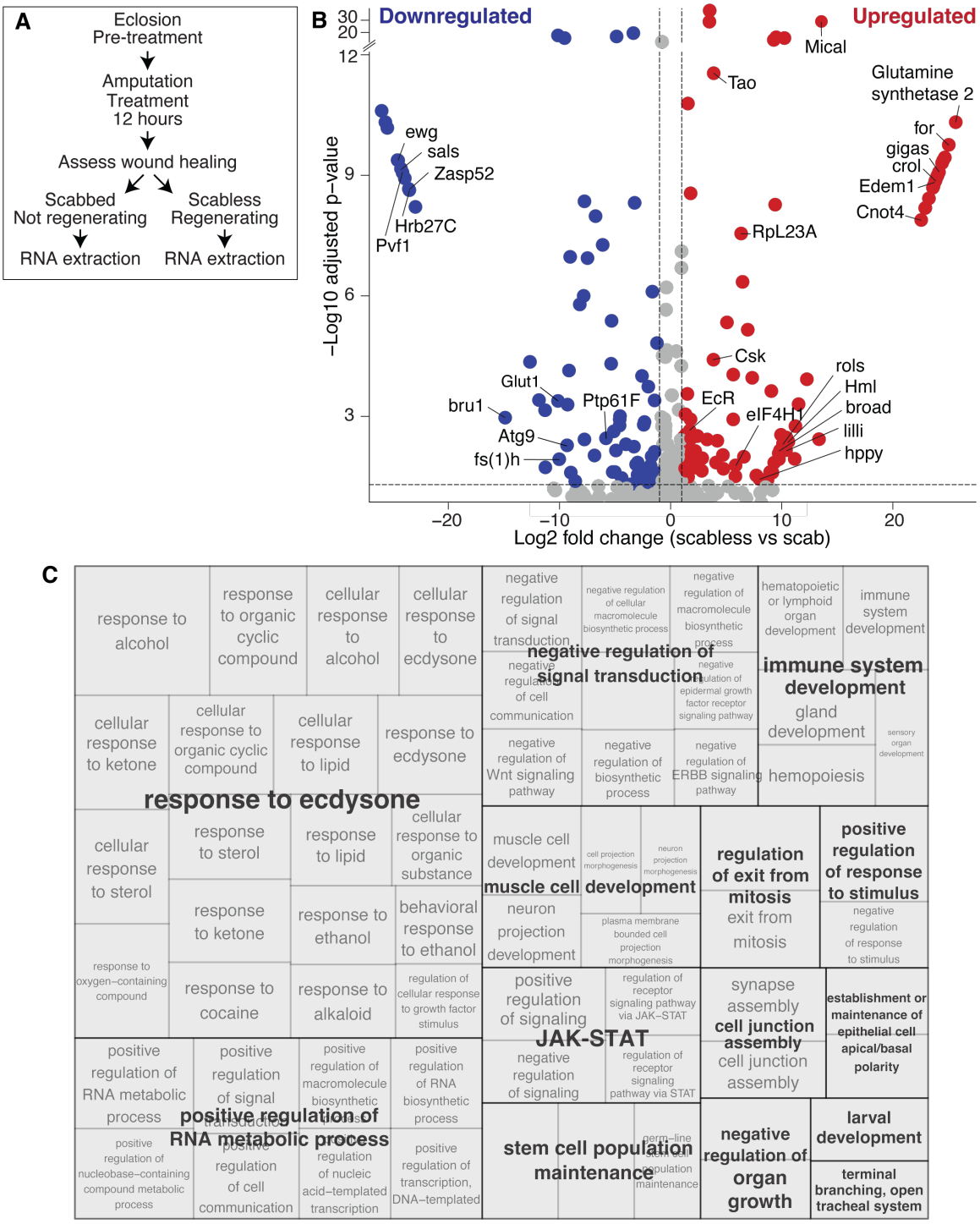


Figure 3. Early transcriptomic divergence between regenerating and non-regenerating flies is localized to few genes.

(A) To perform RNAseq, for each condition (scab vs scabless), four replicate samples were collected. For each sample, 20–30 flies were pooled. Only female flies were used to minimize transcriptional variations from sex.

(B) Volcano plot of differentially expressed (DE) genes, with cut p-value > 0.05 and log2 fold change > |1|.

(C) GO terms enriched in the upregulated genes, analyzed using *clusterProfiler* and plotted using rrvgo. The full list of the DE genes and GO term annotation is in Table S2. Heatmap of the DE genes is in Figure S1.

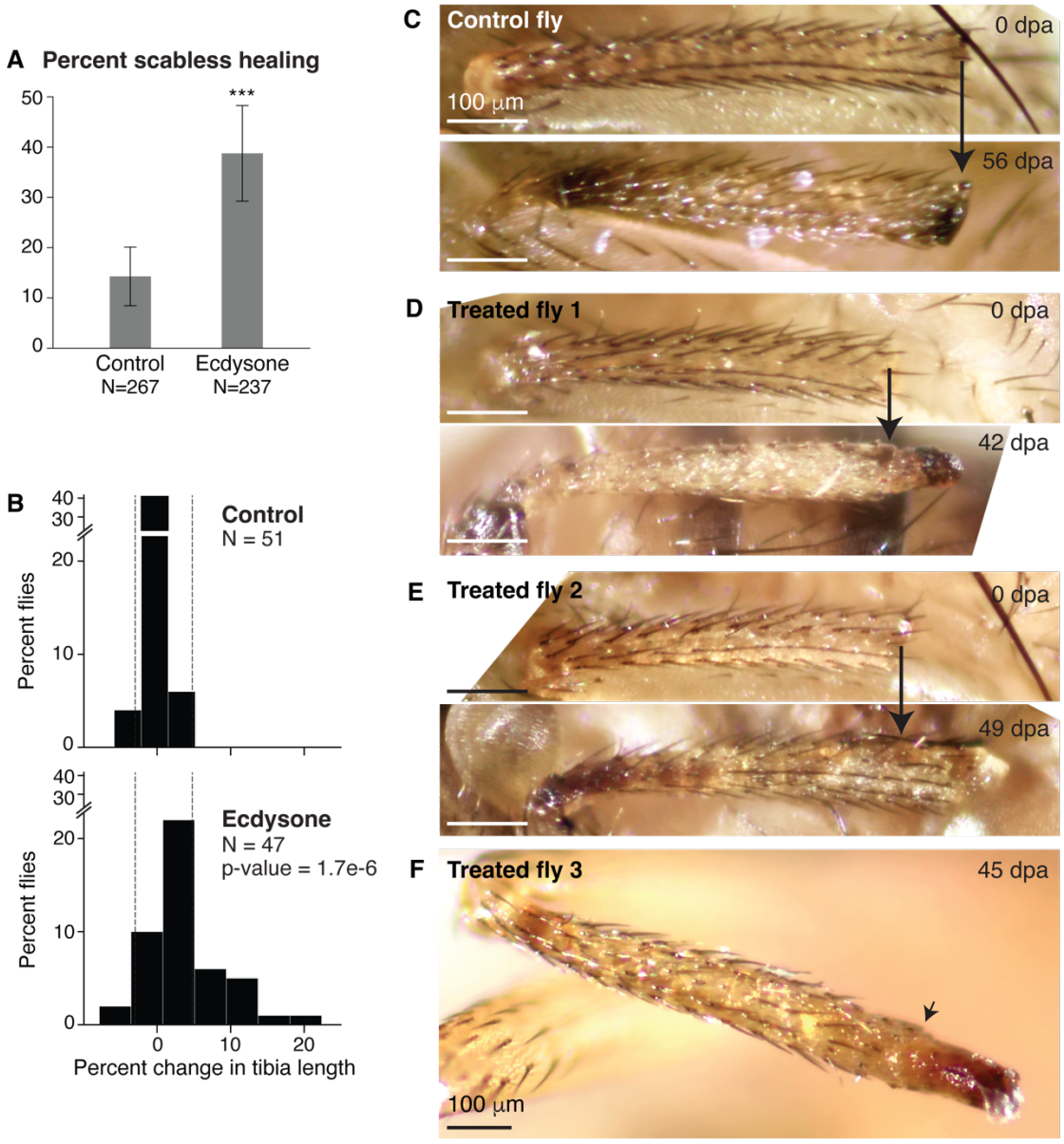


Figure 4. Ecdysone promotes activation of limb regrowth.

(A) Ecdysone (20-hydroxyecdysone, 0.3 mg/mL) was administered after amputation through the food. Wound healing was assessed 3 days after amputation. The concentration used is one that produces optimal growth in the imaginal disc (Karanja et al., 2022). This dataset comes from six independent experiments. N: total number of flies. Statistical analysis: t-test, p-value = 6e-4.

(B-E) Individual flies were tracked over several weeks to assess for tibia growth. To track individual flies, we housed in each vial up to 4 flies that were cut on different limbs, i.e., left vs right, mid vs hindlimb. Treated flies were placed on ecdysone treatment for 1 week, and then moved to regular food.

(B) Tibia length was measured between 0 and 4–6 weeks after amputation in control flies (top) and treated flies (bottom). Dashed lines are the 95% confidence intervals (CI) of the control data. Statistical analysis: Kruskal-Wallis test, p-value= 1.7e-6.

(C) A representative control fly.

(D-E) Two treated flies that show growth.

(F) Another example of growth, from a different experiment in which we did not image 0 dpa. The arrow indicates the end of cuticles, beyond which is a tubular-shaped growth. Dpa: days post amputation.

4.6 Supplemental information

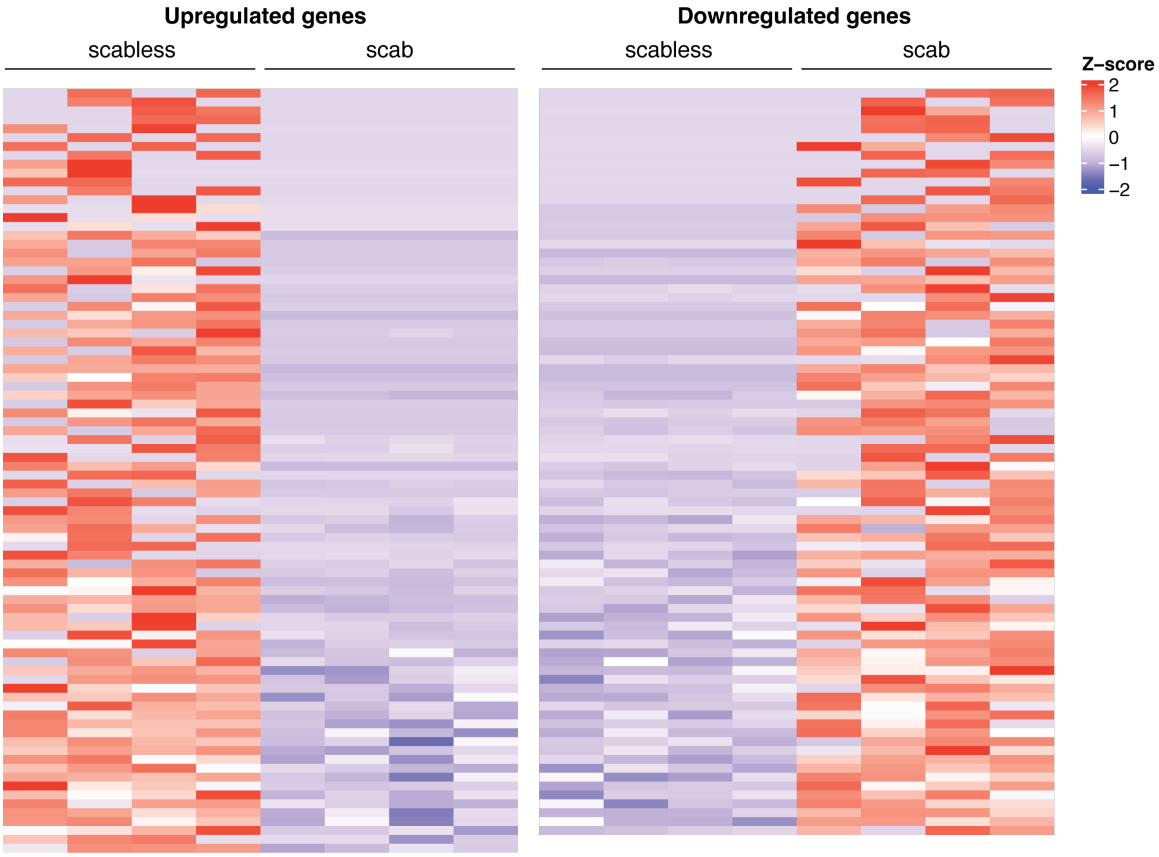


Figure S1. Heat map of the differentially expressed genes.

Within each list, upregulated and downregulated, each column is a replicate sample. Differential expression analysis was performed using DESeq2. Shown are differentially expressed genes with p-value < 0.05 and absolute fold change > 2.

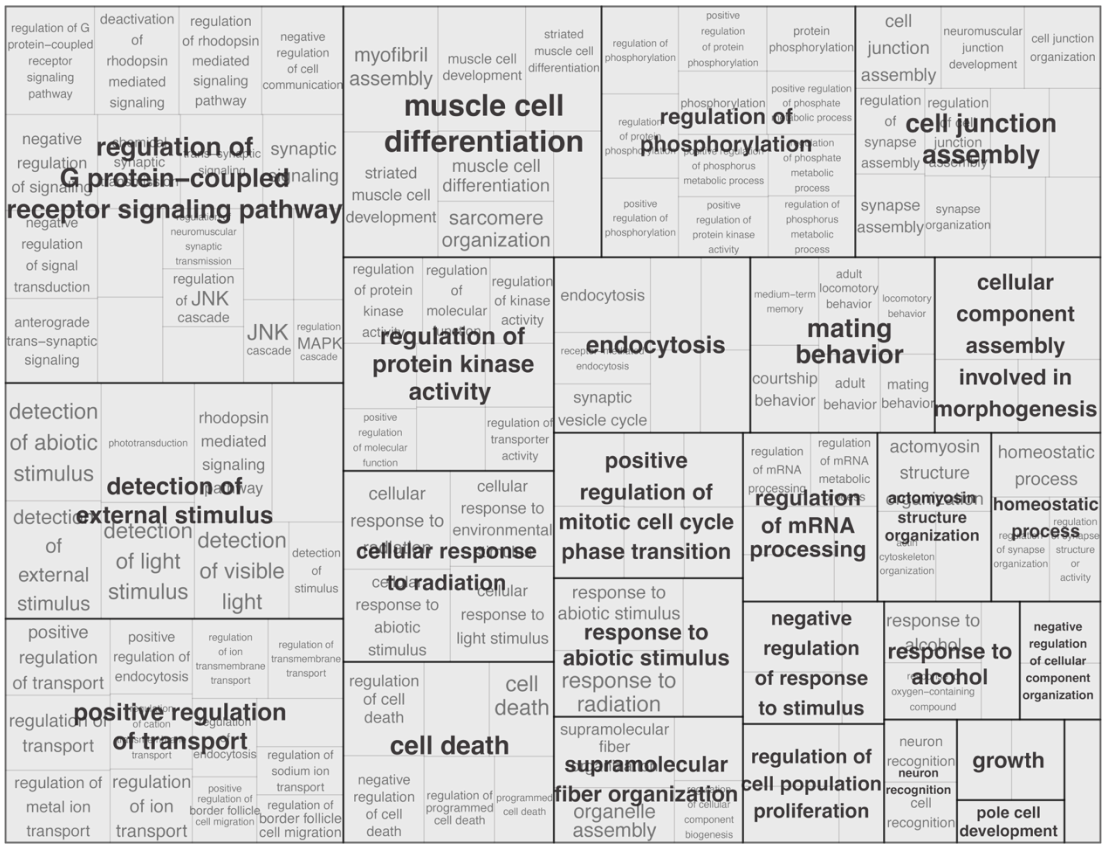


Figure S2. GO terms enriched in the downregulated genes.

GO enrichment analysis was performed using *clusterProfiler*. GO terms were clustered based on semantic similarity using rrvgo.

Table S1. Quantification of egg chambers.

Ovaries were dissected 4-6 days after amputation, fixed, and stored in 70% glycerin/PBS overnight. For staging, egg chambers were dissected apart with superfine tweezers, and staged under a microscope.

Average	**N**	**Total eggs**	**Number of ovarioles**	**Early stage**	**Mid stage**	**Late stage**
Scab	16	107.3	15.8	54.8%	19.0%	26.2%
Scabless	17	103.5	16.2	64.2%	22.4%	13.4%
Scab vs scabless, p-value, t-test, 2 tailed, unequal variance		0.58	0.70	1.9E-07	0.024	6.5E-07

Supplemental table S2 is available at: https://doi.org/10.22002/3e51h-09526

4.7 Materials and methods

Data Availability. RNA sequencing reads, analysis scripts, and raw data used in the study are deposited in CaltechDATA (https://doi.org/10.22002/hznne-der04). RNA sequencing reads are additionally deposited in NCBI (PRJNA1444877).

Fly lines. Wild-type CantonS (a gift from Kai Zinn lab at Caltech) were used in this study. Flies were kept at room temperature, with a 12h/12h light/dark cycle on Caltech food. In this study, to be consistent with the RNAseq design and ovary analysis, only female flies were used.

Amputation. Flies were gently anesthetized with CO_2. The CO_2 rate was kept at <4 liters per minute (the fly should still be awake, but sluggish) and anesthesia time was kept below a minute to minimize stress. Amputation was performed across the midlimb tibia segment using spring scissors (Fine Science Tools cat#91500-09). Only females were used in this study. In bulk RNA sequencing and single-fly tracking, midlimb and hindlimb were utilized to increase fly number. After amputation, flies were placed in treated food (see treatment next) at a density of 4–6 flies/vial.

Treatment. To supplement food with leucine, glutamine, and insulin, a master mix with 1.7 mM L-leucine (Sigma, L8912), 1.7 mM L-glutamine (Sigma, G8540), and 0.03 mg/mL insulin (Sigma, I0908) was prepared. Fly food was briefly microwaved to melt the top layer, then 200 μL of the master mix was added. To supplement food with yeast, dried yeast granules (Saf-Instant Yeast) was sprinkled to cover 30–40% of the food area. To supplement food with ecdysone, 100 uL of 0.3 mg/mL 20-Hydroxyecdysone (MP Bimedicals #157434) was added to the melted top layer of food. Ecdysone was administered for 1 week after amputation.

Gut analysis. Flies were amputated and treated as described above. Guts were dissected and mounted in 35 mm glass-bottom dishes (MatTek P35G-1.5-14-C) in ice cold Schneider's medium (Gibco, 21720-024). A 9x9 mm cover glass was placed on top of the gut, and excess

liquid was removed to keep the gut planar. Mounted gut was immediately imaged using Zeiss Axio.Zoom V16. To ensure consistency, because R1 was sometimes torn, midgut area was measured from R2, marked by the constriction, to the end of R5, marked by the Malphigian tubules (Buchon et al., 2013). To measure midgut area, gut images were imported into Fiji, a binary mask was generated by thresholding the midgut image, the freehand tool was used to remove excess parts (eg, esophagus, malpighian tubules), and the midgut area was measured using the "analyze particles" function.

Ovary and egg chamber analysis. Ovaries were dissected in ice cold Schneider's medium (Gibco, 21720-024) and immediately imaged using Zeiss Axio.Zoom V16. Ovary images were imported into Fiji, the freehand tool was used to separate the two ovaries, a binary mask was generated by thresholding the ovary image, and the ovary size was measured using the "analyze particles" function. To stage egg chambers, dissected ovaries were gently separated with superfine tweezers to allow better fixation, fixed in 4% PFA/0.1% PBST for 20 minutes at room temperature, rinsed thoroughly with PBS/0.1% Tween-20, and then stored in 70% glycerin/PBS overnight. For staging, fixed ovaries were placed on a slide, egg chambers further dissected apart with superfine tweezers, and staged under a microscope.

Virgin fly experiments. Virgin and mated females were collected from the same fly cohorts. To collect virgins, flies were assessed within 8 hours after eclosion and virgins were identified with pale bodies, unexpanded wings, and presence of meconium in the abdomen. Virgin females were collected and placed in vials at a density of 4–6 virgins per vial. Non-virgin females were collected, and placed together with males to ensure mating at a density of 4–6 flies per vial. Three to five days later, virgin and mated females were amputated and treated as described above.

Single fly tracking. To track individual flies, we housed up to four flies in each vial; each fly was amputated at a distinct limb: left midlimb, left hindlimb, right midlimb, and right hindlimb respectively. Flies were amputated one at a time, gently anesthetized with CO_2 (as described above) to minimize stress. CO_2 exposure to each fly was kept under 30 seconds to minimize stress. Flies were imaged immediately after amputation (0 dpa) and again at 4–6

weeks post amputation. To steady the fly, a customized chamber was made by placing 4 #1.5 coverslips as spacers on each end of a clear glass slide. The fly was placed under the chamber and recorded for 5-10 seconds with a Zeiss Discovery V8 stereomicroscope and Axiocam 208 color camera. Measurement of the tibia length was performed in Fiji. The length of the tibia is measured as the diameter of the smallest circle that encapsulates the tibia. Each datapoint was measured independently by two experimenters.

Statistical tests. For gut size, ovary size, and single-fly tracking, the non-parameteric Kruskal-Wallis test was used to assess statistical significance. For all other data with smaller sample size, unpaired, two-tailed Welch's t-test without assumption of equal variance was used.

RNA sequencing. Sample collection. Flies were amputated and treated with LGI as described above, and assessed at 12 hours post amputation for wound healing phenotype. Two conditions were compared: treated flies that heal scabbed and treated scabless that heal scabless. Four replicates were collected for each condition, with 20-30 flies pooled in each sample. RNA extraction was performed using Zymo Direct-zol RNA MiniPrep Kit (Zymo R2050). RNA samples were sequenced at the Caltech Millard and Muriel Jacobs Genetics and Genomics Laboratory using NextSeq 2000 platform, generating 20 million 50 base-pair paired-end reads. Data analysis. To align RNA-seq reads to the *Drosophila* genome, a *Drosophila* genome index was built using the genome FASTA file (6.32) and GTF annotation (6.32.52). Raw sequencing reads were paired and then trimmed with Trimmomatic (v0.39, Bolger et al., 2014), and quality-checked with fastqc (v0.11.9, Andrews, 2010). Reads were aligned to the *Drosophila* transcriptome using STAR (v2.7.7a, Dobin et al., 2013). Transcripts were quantified with StringTie (v2.2.1, Pertea et al., 2015) to generate the count matrix for downstream analysis. Differential gene expression was analyzed using DESeq2 (v1.34.0, Love et. al., 2014) on raw count matrices. GO enrichment analysis was performed with *clusterProfiler* (v4.2.2, Yu et. al., 2012), with background gene set as all genes detected in the sequencing experiment. GO terms were clustered based on semantic similarity using rrvgo (v1.6.0; Sayols, 2023).

Chapter 5

CONCLUSION AND FUTURE DIRECTIONS

The findings in this thesis support a model where regenerative capacity is not fully absent in poorly regenerating systems, but instead remains latent and can be reactivated under appropriate nutrient conditions. In adult *Drosophila melanogaster*, administering leucine, glutamine and insulin is sufficient to initiate limb regrowth that normally does not occur. Same nutrient treatment can be extended to induce regeneration in jellyfish and mice further supported the idea that although regenerative capacity varies across animal species, the underlying ability remains present, and that nutrients is a conserved factor that regulates this latent regeneration capacity.

Strikingly, in *Drosophila*, the decision to regenerate occurs as early as within 12 hours post amputation, and such decision is manifested by altered wound healing response. In flies with scabless wound healing, muscle degeneration upon injury has been largely reduced, and cellular replenishment programs have been activated. These early changes indicate that regeneration competence may be determined soon after injury, during an initial window when wound responses are still being established.

With the small body size, short life cycle, and genomic tools available in *Drosophila*, this thesis establishes adult fruit fly limb as a model for regeneration studies, and also expands the framework of such studies by integrating local tissue remodeling with whole-animal physiology. At the local level, nutrient treatment reshapes the cells in the injured limb to a more regenerative state. A subset of muscle cells begin to express cell cycle genes, and nearly all other cell types are highly expressing regenerative markers that has been recently identified as the key marker in larval disc regeneration.

At the organismal level, nutrient treatment also reprograms the entire animal. Flies that activate regeneration exhibit organ-level changes consistent with energy reallocation: regenerating flies expand their guts to adapt to the increased energy demands for tissue

rebuild. At the same time, they suppress reproductive behavior by reducing the size of ovaries, and slow down egg maturation. This suggests a trade-off between energy demanding processes: promoting regeneration and sustaining reproduction. Consistent with this trade-off, virgin flies are more responsive to nutrient treatment. Such organ remodeling indicates that regeneration is not simply a local repair process, but a whole-body response that integrates nutrient sensing and multi-organ communication.

In addition, the steroid hormone ecdysone was identified as one of the global mediators of early regenerative response. Ecdysone is a molting hormone best known for coordinating developmental progression in insects (Nijhout et al., 2014). Notably, in several arthropods, including crabs, appendage regeneration proceeds naturally through successive molting cycles (Das, 2015). These observations raise the possibility that nutrient-induced regeneration may stem from an ancient hormonal regulation that normally couple growth and tissue renewal.

There are still several directions to further study the mechanism underneath regeneration initiation. First of all, wound healing is likely to play a role. Scar formation has been widely studied in the context of wound healing: scar-like responses are associated with regeneration failure in some systems, whereas a slowed wound closure or even permissive wound supports regeneration in *Xenopus* limb (Murugan et al., 2022). In addition, *Drosophila* larval tissues are also capable of scar-free wound healing, suggesting that injury responses during larval stages may remain compatible with tissue regeneration (Bosch et al., 2005; Galko and Krasnow, 2004). But wound closure and melanization are decoupled processes controlled by distinct immune pathways. The downregulation of key melanization genes, including *PPO1/2/3* suggest that specific injury response may inhibit regeneration and could be modulated by nutrient treatment. More careful characterization of the immune pathways would be essential to understand the other key decision-making points underneath regeneration initiation.

Secondly, it is not fully understood how nutrient status is sensed and translated to regenerative competence. Although ecdysone signaling has been shown to be involved in

nutrient sensing, metabolism, and in regeneration (Schwedes et al., 2011), the detailed mechanism that links upstream nutrient detection to downstream organ responses remain unresolved. Some preliminary tests have already been conducted. Overexpression of ecdysone receptor gene, *EcR*, in the midgut, can already induce scabless wound healing in the injured limb.

Lastly, the limb growth observed in this thesis is substantial, but not complete. The strongest growth observed was a full regeneration of the tibia segment, and regrowth has not been observed in the tarsus segment. One possibility is that distinct limb segments differ in their cellular composition and regenerative potential. The tarsus lacks muscle tissues, which may be significant because muscle was among the earliest responding cell types identified in this work. Further investigations of tissue specific contributions may help explain current limits of regeneration and suggest strategies for more complete appendage regeneration.

BIBLIOGRAPHY

Abrams MJ, Basinger T, Yuan W, Guo CL, Goentoro L. Self-repairing symmetry in jellyfish through mechanically driven reorganization. Proc Natl Acad Sci U S A. 2015 Jun 30;112(26):E3365-73. doi: 10.1073/pnas.1502497112.

Abrams MJ, Tan FH, Li Y, Basinger T, Heithe ML, Sarma A, Lee IT, Condiotte ZJ, Raffiee M, Dabiri JO, Gold DA, Goentoro L. A conserved strategy for inducing appendage regeneration in moon jellyfish, *Drosophila*, and mice. Elife. 2021 Dec 7;10:e65092. doi: 10.7554/eLife.65092. Erratum in: Elife. 2023 Jun 22;12:e90007. doi: 10.7554/eLife.90007.

Adams MD, Celniker SE, Holt RA, Evans CA, Gocayne JD, Amanatides PG, Scherer SE, Li PW, Hoskins RA, Galle RF, George RA, Lewis SE, Richards S, Ashburner M, Henderson SN, Sutton GG, Wortman JR, … Venter JC. The genome sequence of *Drosophila melanogaster*. Science. 2000 Mar 24;287(5461):2185-95.

Ahmed SMH, Maldera JA, Krunic D, Paiva-Silva GO, Pénalva C, Teleman AA, Edgar BA. Fitness trade-offs incurred by ovary-to-gut steroid signalling in *Drosophila*. Nature. 2020 Aug;584(7821):415-419. doi: 10.1038/s41586-020-2462-y.

Álvarez-Fernández C, Tamirisa S, Prada F, Chernomoretz A, Podhajcer O, Blanco E, Martín-Blanco E. Identification and functional analysis of healing regulators in *Drosophila*. PLoS Genet. 2015 Feb 3;11(2):e1004965. doi: 10.1371/journal.pgen.1004965.

Ameku T, Niwa R. Mating-Induced Increase in Germline Stem Cells via the Neuroendocrine System in Female *Drosophila*. PLoS Genet. 2016 Jun 16;12(6):e1006123. doi: 10.1371/journal.pgen.1006123.

Andrews, S. (2010) FastQC: A Quality Control Tool for High Throughput Sequence Data. https://www.bioinformatics.babraham.ac.uk/projects/fastqc/

Bading KT, Kaehlert S, Chi X, Jaspers C, Martindale MQ, Javidpour J. Food availability drives plastic self-repair response in a basal metazoan- case study on the ctenophore Mnemiopsis leidyi A. Agassiz 1865. Sci Rep. 2017 Nov 27;7(1):16419. doi: 10.1038/s41598-017-16346-w.

Bassel-Duby R, Olson EN. Signaling pathways in skeletal muscle remodeling. Annu Rev Biochem. 2006;75:19-37. doi: 10.1146/annurev.biochem.75.103004.142622.

Beck CW, Christen B, Slack JM. Molecular pathways needed for regeneration of spinal cord and muscle in a vertebrate. Dev Cell. 2003 Sep;5(3):429-39. doi: 10.1016/s1534-5807(03)00233-8.

Belles X, Piulachs MD. Ecdysone signalling and ovarian development in insects: from stem cells to ovarian follicle formation. Biochim Biophys Acta. 2015 Feb;1849(2):181-6. doi: 10.1016/j.bbagrm.2014.05.025.

Bely AE, Nyberg KG. Evolution of animal regeneration: re-emergence of a field. Trends Ecol Evol. 2010 Mar;25(3):161-70. doi: 10.1016/j.tree.2009.08.005.

Bi P, Yue F, Sato Y, Wirbisky S, Liu W, Shan T, Wen Y, Zhou D, Freeman J, Kuang S. Stage-specific effects of Notch activation during skeletal myogenesis. Elife. 2016 Sep 19;5:e17355. doi: 10.7554/eLife.17355.

Bidla G, Lindgren M, Theopold U, Dushay MS. Hemolymph coagulation and phenoloxidase in *Drosophila* larvae. Dev Comp Immunol. 2005;29(8):669-79. doi: 10.1016/j.dci.2004.11.007.

Bolger AM, Lohse M, Usadel B. Trimmomatic: a flexible trimmer for Illumina sequence data. Bioinformatics. 2014 Aug 1;30(15):2114-20. doi: 10.1093/bioinformatics/btu170.

Borenstein M, Hedges LV, Higgins JP, Rothstein HR. *Introduction to Meta-Analysis.* John Wiley & Sons; 2021 Apr 6.

Bosch M, Bishop SA, Baguña J, Couso JP. Leg regeneration in Drosophila abridges the normal developmental program. Int J Dev Biol. 2010;54(8-9):1241-50. doi: 10.1387/ijdb.093010mb.

Bray NL, Pimentel H, Melsted P, Pachter L. Near-optimal probabilistic RNA-seq quantification. Nat Biotechnol. 2016 May;34(5):525-7. doi: 10.1038/nbt.3519. Epub 2016 Apr 4. Erratum in: Nat Biotechnol. 2016 Aug 9;34(8):888. doi: 10.1038/nbt0816-888d.

Buchon N, Broderick NA, Poidevin M, Pradervand S, Lemaitre B. *Drosophila* intestinal response to bacterial infection: activation of host defense and stem cell proliferation. Cell Host Microbe. 2009 Feb 19;5(2):200-11. doi: 10.1016/j.chom.2009.01.003.

Buchon N, Osman D, David FP, Fang HY, Boquete JP, Deplancke B, Lemaitre B. Morphological and molecular characterization of adult midgut compartmentalization in *Drosophila*. Cell Rep. 2013 May 30;3(5):1725-38. doi: 10.1016/j.celrep.2013.04.001.

Cao D, Lu H, Lewis TL, Li L. Intake of sucrose-sweetened water induces insulin resistance and exacerbates memory deficits and amyloidosis in a transgenic mouse model of Alzheimer disease. J Biol Chem. 2007 Dec 14;282(50):36275-82. doi: 10.1074/jbc.M703561200.

Carlson BM, editor. *Principles of Regenerative Biology.* Elsevier; 2011.

Carnevali MDC. Regeneration in echinoderms: repair, regrowth, cloning. Invertebr Surviv J. 2006;3.

Cary GA, Wolff A, Zueva O, Pattinato J, Hinman VF. Analysis of sea star larval regeneration reveals conserved processes of whole-body regeneration across the metazoa. BMC Biol. 2019 Feb 22;17(1):16. doi: 10.1186/s12915-019-0633-9.

Caskey M, Rich J, Weber R, Mortazavi A, Pachter L, Hallgrimsdottir IB. Single-Cell Genomics Decontamination with CellSweep. bioRxiv. 2026 Mar 4. doi:10.64898/2026.03.04.709349.

Chamberlain CS, Jeffery JJ, Leiferman EM, Yildirim T, Sun X, Baer GS, Murphy WL, Vanderby R. Level-specific amputations and resulting regenerative outcomes in the mouse distal phalanx. Wound Repair Regen. 2017 May;25(3):443-453. doi: 10.1111/wrr.12544.

Chapman T, Bangham J, Vinti G, Seifried B, Lung O, Wolfner MF, Smith HK, Partridge L. The sex peptide of *Drosophila melanogaster*: female post-mating responses analyzed by using RNA interference. Proc Natl Acad Sci U S A. 2003 Aug 19;100(17):9923-8. doi: 10.1073/pnas.1631635100.

Colombani J, Andersen DS, Léopold P. Secreted peptide Dilp8 coordinates *Drosophila* tissue growth with developmental timing. Science. 2012 May 4;336(6081):582-5. doi: 10.1126/science.1216689.
Cox BD, Yun MH, Poss KD. Can laboratory model systems instruct human limb regeneration? Development. 2019 Oct 2;146(20):dev181016. doi: 10.1242/dev.181016.
Das S. Regeneration in Crustaceans. Oxford University Press; 2015.
Dixon CT, Yang P, McCall K. Traumatic injury leads to ovarian cell death and reproductive disturbances in *Drosophila melanogaster*. Biol Open. 2025 Feb 15;14(2):BIO061825.
Dobin A, Davis CA, Schlesinger F, Drenkow J, Zaleski C, Jha S, Batut P, Chaisson M, Gingeras TR. STAR: ultrafast universal RNA-seq aligner. Bioinformatics. 2013 Jan 1;29(1):15-21. doi: 10.1093/bioinformatics/bts635.
Endo T, Bryant SV, Gardiner DM. A stepwise model system for limb regeneration. Dev Biol. 2004;270:135-145.
Eyal S, Rubin S, Krief S, Levin L, Zelzer E. Common cellular origin and diverging developmental programs for different sesamoid bones. Development. 2019 Feb 28;146(4):dev167452. doi: 10.1242/dev.167452.
Finco MG, Kim S, Ngo W, Menegaz RA. A review of musculoskeletal adaptations in individuals following major lower-limb amputation. J Musculoskelet Neuronal Interact. 2022 Jun 1;22(2):269-283.
Fuchs B, Wang W, Graspeuntner S, Li Y, Insua S, Herbst EM, Dirksen P, Böhm AM, Hemmrich G, Sommer F, Domazet-Lošo T, Klostermeier UC, Anton-Erxleben F, Rosenstiel P, Bosch TC, Khalturin K. Regulation of polyp-to-jellyfish transition in Aurelia aurita. Curr Biol. 2014 Feb 3;24(3):263-73. doi: 10.1016/j.cub.2013.12.003.
Galko MJ, Krasnow MA. Cellular and genetic analysis of wound healing in *Drosophila* larvae. PLoS Biol. 2004 Aug;2(8):E239. doi: 10.1371/journal.pbio.0020239.
Galliot B, Ghila L. Cell plasticity in homeostasis and regeneration. Mol Reprod Dev. 2010 Oct;77(10):837-55. doi: 10.1002/mrd.21206.
Garelli A, Gontijo AM, Miguela V, Caparros E, Dominguez M. Imaginal discs secrete insulin-like peptide 8 to mediate plasticity of growth and maturation. Science. 2012 May 4;336(6081):579-82. doi: 10.1126/science.1216735.
Goss RJ. The evolution of regeneration: adaptive or inherent? J Theor Biol. 1992 Nov 21;159(2):241-60. doi: 10.1016/s0022-5193(05)80704-0.
Gou B, Liu Y, Guntur AR, Stern U, Yang CH. Mechanosensitive neurons on the internal reproductive tract contribute to egg-laying-induced acetic acid attraction in *Drosophila*. Cell Rep. 2014 Oct 23;9(2):522-30. doi: 10.1016/j.celrep.2014.09.033.
Graham WM. Size-based prey selectivity and dietary shifts in the jellyfish, *Aurelia aurita*. J Plankton Res. 2001;23:67-74.
Gutiérrez-Gutiérrez Ó, Felix DA, Salvetti A, Amro EM, Thems A, Pietsch S, Koeberle A, Rudolph KL, González-Estévez C. Regeneration in starved planarians depends on TRiC/CCT subunits modulating the unfolded protein response. EMBO Rep. 2021 Aug 4;22(8):e52905. doi: 10.15252/embr.202152905.
Haddad GG, Sun Ya, Wyman RJ, Xu T. Genetic basis of tolerance to O2 deprivation in Drosophila melanogaster. Proc Natl Acad Sci U S A. 1997 Sep 30;94(20):10809-12. doi: 10.1073/pnas.94.20.10809.

Hariharan IK, Wake DB, Wake MH. Indeterminate growth: could it represent the ancestral condition? Cold Spring Harb Perspect Biol. 2016;8:a019174.
Han M, Yang X, Lee J, Allan CH, Muneoka K. Development and regeneration of the neonatal digit tip in mice. Dev Biol. 2008 Mar 1;315(1):125-35. doi: 10.1016/j.ydbio.2007.12.025. Epub 2007 Dec 27.
Herrera-Rincon C, Golding AS, Moran KM, Harrison C, Martyniuk CJ, Guay JA, Zaltsman J, Carabello H, Kaplan DL, Levin M. Brief Local Application of Progesterone via a Wearable Bioreactor Induces Long-Term Regenerative Response in Adult *Xenopus* Hindlimb. Cell Rep. 2018 Nov 6;25(6):1593-1609.e7. doi: 10.1016/j.celrep.2018.10.010.
Hirose K, Shiomi T, Hozumi S, Kikuchi Y. Mechanistic target of rapamycin complex 1 signaling regulates cell proliferation, cell survival, and differentiation in regenerating zebrafish fins. BMC Dev Biol. 2014 Dec 6;14:42. doi: 10.1186/s12861-014-0042-9.
Hopkins BR, Barmina O, Kopp A. A single-cell atlas of the sexually dimorphic *Drosophila* foreleg and its sensory organs during development. PLoS Biol. 2023 Jun 28;21(6):e3002148. doi: 10.1371/journal.pbio.3002148.
Illingworth CM. Trapped fingers and amputated finger tips in children. J Pediatr Surg. 1974;9:853-858.
Johnson K, Bateman J, DiTommaso T, Wong AY, Whited JL. Systemic cell cycle activation is induced following complex tissue injury in axolotl. Dev Biol. 2018 Jan 15;433(2):461-472. doi: 10.1016/j.ydbio.2017.07.010.
Jopling C, Sleep E, Raya M, Martí M, Raya A, Izpisúa Belmonte JC. Zebrafish heart regeneration occurs by cardiomyocyte dedifferentiation and proliferation. Nature. 2010 Mar 25;464(7288):606-9. doi: 10.1038/nature08899.
Karanja F, Sahu S, Weintraub S, Bhandari R, Jaszczak R, Sitt J, Halme A. Ecdysone exerts biphasic control of regenerative signaling, coordinating the completion of regeneration with developmental progression. Proc Natl Acad Sci U S A. 2022 Feb 1;119(5):e2115017119. doi: 10.1073/pnas.2115017119.
Katsuyama T, Comoglio F, Seimiya M, Cabuy E, Paro R. During *Drosophila* disc regeneration, JAK/STAT coordinates cell proliferation with Dilp8-mediated developmental delay. Proc Natl Acad Sci U S A. 2015 May 5;112(18):E2327-36. doi: 10.1073/pnas.1423074112.
Kaufman TC. A Short History and Description of *Drosophila melanogaster* Classical Genetics: Chromosome Aberrations, Forward Genetic Screens, and the Nature of Mutations. Genetics. 2017 Jun;206(2):665-689.
Kawakami Y, Rodriguez Esteban C, Raya M, Kawakami H, Martí M, Dubova I, Izpisúa Belmonte JC. Wnt/beta-catenin signaling regulates vertebrate limb regeneration. Genes Dev. 2006 Dec 1;20(23):3232-7. doi: 10.1101/gad.1475106.
Kawasaki F, Koonce NL, Guo L, Fatima S, Qiu C, Moon MT, Zheng Y, Ordway RW. Small heat shock proteins mediate cell-autonomous and -nonautonomous protection in a *Drosophila* model for environmental-stress-induced degeneration. Dis Model Mech. 2016 Sep 1;9(9):953-64. doi: 10.1242/dmm.026385.
Kimura W, Xiao F, Canseco DC, Muralidhar S, Thet S, Zhang HM, Abderrahman Y, Chen R, Garcia JA, Shelton JM, Richardson JA, Ashour AM, Asaithamby A, Liang H, Xing C, Lu Z, Zhang CC, Sadek HA. Hypoxia fate mapping identifies cycling

cardiomyocytes in the adult heart. Nature. 2015 Jul 9;523(7559):226-30. doi: 10.1038/nature14582.

Koyama LAJ, Aranda-Díaz A, Su YH, Balachandra S, Martin JL, Ludington WB, Huang KC, O'Brien LE. Bellymount enables longitudinal, intravital imaging of abdominal organs and the gut microbiota in adult *Drosophila*. PLoS Biol. 2020 Jan 27;18(1):e3000567. doi: 10.1371/journal.pbio.3000567.

Kress JP, Hall JB. ICU-acquired weakness and recovery from critical illness. N Engl J Med. 2014 Apr 24;370(17):1626-35. doi: 10.1056/NEJMra1209390.

Kübler IC, Kretzschmar J, Arredondo-Lasso MN, Keeley SD, Rößler LC, Ganss K, Sandoval-Guzmán T, Brankatschk M. Systemic and local lipid adaptations underlie regeneration in *Drosophila melanogaster* and *Ambystoma mexicanum*. NPJ Regen Med. 2024 Oct 29;9(1):33. doi: 10.1038/s41536-024-00375-x.

Lai AG, Aboobaker AA. EvoRegen in animals: Time to uncover deep conservation or convergence of adult stem cell evolution and regenerative processes. Dev Biol. 2018 Jan 15;433(2):118-131. doi: 10.1016/j.ydbio.2017.10.010.

Lehoczky JA, Robert B, Tabin CJ. Mouse digit tip regeneration is mediated by fate-restricted progenitor cells. Proc Natl Acad Sci U S A. 2011 Dec 20;108(51):20609-14. doi: 10.1073/pnas.1118017108.

Li H, Janssens J, De Waegeneer M, Kolluru SS, Davie K, Gardeux V, Saelens W, David FPA, Brbić M, Spanier K, Leskovec J, McLaughlin CN, Xie Q, Jones RC, Brueckner K, Shim J, Tattikota SG, Schnorrer F, Rust K, Nystul TG, … Zinzen RP. Fly Cell Atlas: A single-nucleus transcriptomic atlas of the adult fruit fly. Science. 2022 Mar 4;375(6584):eabk2432. doi: 10.1126/science.abk2432.

Li L, Messina JL. Acute insulin resistance following injury. Trends Endocrinol Metab. 2009 Nov;20(9):429-35. doi: 10.1016/j.tem.2009.06.004.

Lin G, Chen Y, Slack JM. Imparting regenerative capacity to limbs by progenitor cell transplantation. Dev Cell. 2013 Jan 14;24(1):41-51. doi: 10.1016/j.devcel.2012.11.017.

Liu G, Gao H, Liu X, Chen X, Cao N. Rejuvenating the damaged and aged heart: lessons from development. npj Biomed. Innov. 2026 Mar 24. doi: 10.1038/s44385-026-00080-y

Liu N, Nelson BR, Bezprozvannaya S, Shelton JM, Richardson JA, Bassel-Duby R, Olson EN. Requirement of MEF2A, C, and D for skeletal muscle regeneration. Proc Natl Acad Sci U S A. 2014 Mar 18;111(11):4109-14. doi: 10.1073/pnas.1401732111.

Love MI, Huber W, Anders S. Moderated estimation of fold change and dispersion for RNA-seq data with DESeq2. Genome Biol. 2014;15(12):550. doi: 10.1186/s13059-014-0550-8.

Lucas CH. Reproduction and life history strategies of the common jellyfish, *Aurelia aurita*, in relation to its ambient environment. In: Purcell JE, Graham WM, Dumont HJ, editors. *Jellyfish Blooms: Ecological and Societal Importance*. Springer Netherlands; 2001. p. 229-246.

Lynch CJ, Adams SH. Branched-chain amino acids in metabolic signalling and insulin resistance. Nat Rev Endocrinol. 2014 Dec;10(12):723-36. doi: 10.1038/nrendo.2014.171.

Mahmoud AI. Metabolic switches during development and regeneration. Development. 2023 Oct 15;150(20):dev202008. doi: 10.1242/dev.202008.

Malandraki-Miller S, Lopez CA, Al-Siddiqi H, Carr CA. Changing Metabolism in Differentiating Cardiac Progenitor Cells-Can Stem Cells Become Metabolically Flexible Cardiomyocytes? Front Cardiovasc Med. 2018 Sep 19;5:119. doi: 10.3389/fcvm.2018.00119.

Marik PE, Raghavan M. Stress-hyperglycemia, insulin and immunomodulation in sepsis. Intensive Care Med. 2004 May;30(5):748-56. doi: 10.1007/s00134-004-2167-y.

McClure KD, Sustar A, Schubiger G. Three genes control the timing, the site and the size of blastema formation in *Drosophila*. Dev Biol. 2008 Jul 1;319(1):68-77. doi: 10.1016/j.ydbio.2008.04.004.

McLeod MJ. Differential staining of cartilage and bone in whole mouse fetuses by alcian blue and alizarin red S. Teratology. 1980 Dec;22(3):299-301. doi: 10.1002/tera.1420220306.

Melsted P, Booeshaghi AS, Liu L, Gao F, Lu L, Min KHJ, da Veiga Beltrame E, Hjörleifsson KE, Gehring J, Pachter L. Modular, efficient and constant-memory single-cell RNA-seq preprocessing. Nat Biotechnol. 2021 Jul;39(7):813-818. doi: 10.1038/s41587-021-00870-2.

Mirth C, Akam M. Joint development in the Drosophila leg: cell movements and cell populations. Dev Biol. 2002 Jun 15;246(2):391-406. doi: 10.1006/dbio.2002.0593.

Moczek AP, Sultan S, Foster S, Ledón-Rettig C, Dworkin I, Nijhout HF, Abouheif E, Pfennig DW. The role of developmental plasticity in evolutionary innovation. Proc Biol Sci. 2011 Sep 22;278(1719):2705-13. doi: 10.1098/rspb.2011.0971.

Monici M. Cell and tissue autofluorescence research and diagnostic applications. Biotechnol Annu Rev. 2005;11:227-56. doi: 10.1016/S1387-2656(05)11007-2.

Morgan TH. *Regeneration*. New York: Macmillan and Co., Ltd.; 1901.

Morrow CS, Tweed K, Farhadova S, Walsh AJ, Lear BP, Roopra A, Risgaard RD, Klosa PC, Arndt ZP, Peterson ER, Chi MM, Harris AG, Skala MC, Moore DL. Autofluorescence is a biomarker of neural stem cell activation state. Cell Stem Cell. 2024 Apr 4;31(4):570-581.e7. doi: 10.1016/j.stem.2024.02.011.

Muneoka K, Allan CH, Yang X, Lee J, Han M. Mammalian regeneration and regenerative medicine. Birth Defects Res C Embryo Today. 2008 Dec;84(4):265-80. doi: 10.1002/bdrc.20137. PMID: 19067422.

Murugan NJ, Vigran HJ, Miller KA, Golding A, Pham QL, Sperry MM, Rasmussen-Ivey C, Kane AW, Kaplan DL, Levin M. Acute multidrug delivery via a wearable bioreactor facilitates long-term limb regeneration and functional recovery in adult *Xenopus* laevis. Sci Adv. 2022 Jan 28;8(4):eabj2164. doi: 10.1126/sciadv.abj2164.

Nakada Y, Canseco DC, Thet S, Abdisalaam S, Asaithamby A, Santos CX, Shah AM, Zhang H, Faber JE, Kinter MT, Szweda LI, Xing C, Hu Z, Deberardinis RJ, Schiattarella G, Hill JA, Oz O, Lu Z, Zhang CC, Kimura W, Sadek HA. Hypoxia induces heart regeneration in adult mice. Nature. 2017 Jan 12;541(7636):222-227. doi: 10.1038/nature20173.

Naviaux RK, Le TP, Bedelbaeva K, Leferovich J, Gourevitch D, Sachadyn P, Zhang XM, Clark L, Heber-Katz E. Retained features of embryonic metabolism in the adult MRL mouse. Mol Genet Metab. 2009 Mar;96(3):133-44. doi: 10.1016/j.ymgme.2008.11.164.

Nguyen LT, Schmidt HA, von Haeseler A, Minh BQ. IQ-TREE: a fast and effective stochastic algorithm for estimating maximum-likelihood phylogenies. Mol Biol Evol. 2015 Jan;32(1):268-74. doi: 10.1093/molbev/msu300.

Nicklin P, Bergman P, Zhang B, Triantafellow E, Wang H, Nyfeler B, Yang H, Hild M, Kung C, Wilson C, Myer VE, MacKeigan JP, Porter JA, Wang YK, Cantley LC, Finan PM, Murphy LO. Bidirectional transport of amino acids regulates mTOR and autophagy. Cell. 2009 Feb 6;136(3):521-34. doi: 10.1016/j.cell.2008.11.044.

Nijhout HF, Riddiford LM, Mirth C, Shingleton AW, Suzuki Y, Callier V. The developmental control of size in insects. Wiley Interdiscip Rev Dev Biol. 2014 Jan-Feb;3(1):113-34. doi: 10.1002/wdev.124.

O'Brien LE, Soliman SS, Li X, Bilder D. Altered modes of stem cell division drive adaptive intestinal growth. Cell. 2011 Oct 28;147(3):603-14.

Peng ZL, Yin BX, Ren RM, Liao YL, Cai H, Wang H. Altered metabolic state impedes limb regeneration in salamanders. Zool Res. 2021 Nov 18;42(6):772-782. doi: 10.24272/j.issn.2095-8137.2021.186.

Pertea M, Pertea GM, Antonescu CM, Chang TC, Mendell JT, Salzberg SL. StringTie enables improved reconstruction of a transcriptome from RNA-seq reads. Nat Biotechnol. 2015 Mar;33(3):290-5. doi: 10.1038/nbt.3122.

Pettersen AK, Marshall DJ, White CR. Understanding variation in metabolic rate. J Exp Biol. 2018 Jan 11;221(Pt 1):jeb166876. doi: 10.1242/jeb.166876.

Polezhaev L. *Neuron Structure of the Brain*. Cambridge: Harvard University Press; 1972.

Porrello ER, Mahmoud AI, Simpson E, Hill JA, Richardson JA, Olson EN, Sadek HA. Transient regenerative potential of the neonatal mouse heart. Science. 2011 Feb 25;331(6020):1078-80. doi: 10.1126/science.1200708.

Poss KD, Tanaka EM. Hallmarks of regeneration. Cell Stem Cell. 2024 Sep 5;31(9):1244-1261. doi: 10.1016/j.stem.2024.07.007.

Potthoff MJ, Olson EN. MEF2: a central regulator of diverse developmental programs. Development. 2007 Dec;134(23):4131-40. doi: 10.1242/dev.008367.

Rämet M, Lanot R, Zachary D, Manfruelli P. JNK signaling pathway is required for efficient wound healing in Drosophila. Dev Biol. 2002 Jan 1;241(1):145-56. doi: 10.1006/dbio.2001.0502.

Rennolds CW, Bely AE. Integrative biology of injury in animals. Biol Rev Camb Philos Soc. 2023 Feb;98(1):34-62. doi: 10.1111/brv.12894.

Rennolds CW, Bely AE. Investment in regeneration versus asexual reproduction is resource-dependent in a freshwater annelid. Funct Ecol. 2024 Apr;38(4):739–754. doi: 10.1111/1365-2435.14525.

Rodgers JT, King KY, Brett JO, Cromie MJ, Charville GW, Maguire KK, Brunson C, Mastey N, Liu L, Tsai CR, Goodell MA, Rando TA. mTORC1 controls the adaptive transition of quiescent stem cells from G0 to G(Alert). Nature. 2014 Jun 19;510(7505):393-6. doi: 10.1038/nature13255.

Rouse G. *Invertebrate Zoology*. Oxford University Press; 1998.

Sánchez Alvarado A. Regeneration in the metazoans: why does it happen? Bioessays. 2000 Jun;22(6):578-90. doi: 10.1002/(SICI)1521-1878(200006)22:6<578::AID-BIES11>3.0.CO;2-#.

Sanders JE, Fatone S. Residual limb volume change: systematic review of measurement and management. J Rehabil Res Dev. 2011;48(8):949-86. doi: 10.1682/jrrd.2010.09.0189.
Satija R, Farrell JA, Gennert D, Schier AF, Regev A. Spatial reconstruction of single-cell gene expression data. Nat Biotechnol. 2015 May;33(5):495-502. doi: 10.1038/nbt.3192.
Sayer AA, Cooper R, Arai H, Cawthon PM, Ntsama Essomba MJ, Fielding RA, Grounds MD, Witham MD, Cruz-Jentoft AJ. Sarcopenia. Nat Rev Dis Primers. 2024 Sep 19;10(1):68. doi: 10.1038/s41572-024-00550-w.
Sayols S. rrvgo: a Bioconductor package for interpreting lists of Gene Ontology terms. MicroPubl Biol. 2023 Apr 18;2023:10.17912/micropub.biology.000811. doi: 10.17912/micropub.biology.000811.
Schmid V, Alder H. Isolated, mononucleated, striated muscle can undergo pluripotent transdifferentiation and form a complex regenerate. Cell. 1984 Oct;38(3):801-9. doi: 10.1016/0092-8674(84)90275-7.
Schwedes C, Tulsiani S, Carney GE. Ecdysone receptor expression and activity in adult *Drosophila* melanogaster. J Insect Physiol. 2011 Jul;57(7):899-907. doi: 10.1016/j.jinsphys.2011.03.027.
Scorrano S, Aglieri G, Boero F, Dawson MN, Piraino S. Unmasking *Aurelia* species in the Mediterranean Sea: an integrative morphometric and molecular approach. Zool J Linn Soc. 2017;180:243-267.
Sepulveda S, Shojaeian P, Rauser CL, Jafari M, Mueller LD, Rose MR. Interactions between injury, stress resistance, reproduction, and aging in *Drosophila melanogaster*. Exp Gerontol. 2008 Mar;43(3):136-45.
Shyh-Chang N, Zhu H, Yvanka de Soysa T, Shinoda G, Seligson MT, Tsanov KM, Nguyen L, Asara JM, Cantley LC, Daley GQ. Lin28 enhances tissue repair by reprogramming cellular metabolism. Cell. 2013 Nov 7;155(4):778-92. doi: 10.1016/j.cell.2013.09.059.
Simkin J, Han M, Yu L, Yan M, Muneoka K. The mouse digit tip: from wound healing to regeneration. In: Gourdie RG, Myers TA, editors. *Wound Regeneration and Repair*. Vol. 1037. Humana Press; 2013. p. 419-435.
Singer M. The regeneration of body parts. Sci Am. 1958 Oct;199(4):79-80 passim. doi: 10.1038/scientificamerican1058-79.
Sinigaglia C, Peron S, Eichelbrenner J, Chevalier S, Steger J, Barreau C, Houliston E, Leclère L. Pattern regulation in a regenerating jellyfish. Elife. 2020 Sep 7;9:e54868. doi: 10.7554/eLife.54868.
Sousounis K, Baddour JA, Tsonis PA. Aging and regeneration in vertebrates. Curr Top Dev Biol. 2014;108:217-46. doi: 10.1016/B978-0-12-391498-9.00008-5.
Stipanuk MH. Leucine and protein synthesis: mTOR and beyond. Nutr Rev. 2007;65:122-129.
Stojanović O, Miguel-Aliaga I, Trajkovski M. Intestinal plasticity and metabolism as regulators of organismal energy homeostasis. Nat Metab. 2022 Nov;4(11):1444-1458.
Sullivan DK, Min KHJ, Hjörleifsson KE, Luebbert L, Holley G, Moses L, Gustafsson J, Bray NL, Pimentel H, Booeshaghi AS, Melsted P, Pachter L. kallisto, bustools and kb-python for quantifying bulk, single-cell and single-nucleus RNA-seq. Nat Protoc. 2025 Mar;20(3):587-607. doi: 10.1038/s41596-024-01057-0.

Sun F, Poss KD. Inter-organ communication during tissue regeneration. Development. 2023 Dec 1;150(23):dev202166. doi: 10.1242/dev.202166.
Sweeting A, Wong J, Murphy HR, Ross GP. A Clinical Update on Gestational Diabetes Mellitus. Endocr Rev. 2022 Sep 26;43(5):763-793. doi: 10.1210/endrev/bnac003.
Takayama K, Muto A, Kikuchi Y. Leucine/glutamine and v-ATPase/lysosomal acidification via mTORC1 activation are required for position-dependent regeneration. Sci Rep. 2018 May 29;8(1):8278. doi: 10.1038/s41598-018-26664-2.
Tanaka EM. The Molecular and Cellular Choreography of Appendage Regeneration. Cell. 2016 Jun 16;165(7):1598-1608. doi: 10.1016/j.cell.2016.05.038. PMID: 27315477.
Tanaka EM, Reddien PW. The cellular basis for animal regeneration. Dev Cell. 2011 Jul 19;21(1):172-85. doi: 10.1016/j.devcel.2011.06.016.
Togo J, Hu S, Li M, Niu C, Speakman JR. Impact of dietary sucrose on adiposity and glucose homeostasis in C57BL/6J mice depends on mode of ingestion: liquid or solid. Mol Metab. 2019 Sep;27:22-32. doi: 10.1016/j.molmet.2019.05.010.
Traag VA, Waltman L, van Eck NJ. From Louvain to Leiden: guaranteeing well-connected communities. Sci Rep. 2019 Mar 26;9(1):5233. doi: 10.1038/s41598-019-41695-z.
van den Berghe G, Wouters P, Weekers F, Verwaest C, Bruyninckx F, Schetz M, Vlasselaers D, Ferdinande P, Lauwers P, Bouillon R. Intensive insulin therapy in critically ill patients. N Engl J Med. 2001 Nov 8;345(19):1359-67. doi: 10.1056/NEJMoa011300.
Viechtbauer W. Conducting meta-analyses in R with the metafor package. J Stat Softw. 2010;36:e3.
Vieira WA, Wells KM, Raymond MJ, De Souza L, Garcia E, McCusker CD. FGF, BMP, and RA signaling are sufficient for the induction of complete limb regeneration from non-regenerating wounds on Ambystoma mexicanum limbs. Dev Biol. 2019 Jul 15;451(2):146-157. doi: 10.1016/j.ydbio.2019.04.008.
Vivien CJ, Hudson JE, Porrello ER. Evolution, comparative biology and ontogeny of vertebrate heart regeneration. NPJ Regen Med. 2016 Jul 28;1:16012. doi: 10.1038/npjregenmed.2016.12.
Wang W, Hu CK, Zeng A, Alegre D, Hu D, Gotting K, Ortega Granillo A, Wang Y, Robb S, Schnittker R, Zhang S, Alegre D, Li H, Ross E, Zhang N, Brunet A, Sánchez Alvarado A. Changes in regeneration-responsive enhancers shape regenerative capacities in vertebrates. Science. 2020;369:eaaz3090.
West-Eberhard MJ. *Developmental Plasticity and Evolution*. Cambridge: Oxford University Press; 2003.
Williams MC, Patel JH, Kakebeen AD, Wills AE. Nutrient availability contributes to a graded refractory period for regeneration in *Xenopus tropicalis*. Dev Biol. 2021 May;473:59-70. doi: 10.1016/j.ydbio.2021.01.005.
Wirtschafter ZT, Tsujimura JK. The sesamoid bones in Long-Evans strain rats. Anat Rec. 1961 Nov;141:195-204. doi: 10.1002/ar.1091410304.
Wolf FA, Angerer P, Theis FJ. SCANPY: large-scale single-cell gene expression data analysis. Genome Biol. 2018 Feb 6;19(1):15. doi: 10.1186/s13059-017-1382-0.
Wolfson RL, Chantranupong L, Saxton RA, Shen K, Scaria SM, Cantor JR, Sabatini DM. Sestrin2 is a leucine sensor for the mTORC1 pathway. Science. 2016 Jan 1;351(6268):43-8. doi: 10.1126/science.aab2674.

Wolock SL, Lopez R, Klein AM. Scrublet: Computational Identification of Cell Doublets in Single-Cell Transcriptomic Data. Cell Syst. 2019 Apr 24;8(4):281-291.e9. doi: 10.1016/j.cels.2018.11.005.

Worley MI, Everetts NJ, Yasutomi R, Chang RJ, Saretha S, Yosef N, Hariharan IK. Ets21C sustains a pro-regenerative transcriptional program in blastema cells of *Drosophila* imaginal discs. Curr Biol. 2022 Aug 8;32(15):3350-3364.e6. doi: 10.1016/j.cub.2022.06.040.

Worley MI, Hariharan IK. Imaginal Disc Regeneration: Something Old, Something New. Cold Spring Harb Perspect Biol. 2022 Nov 1;14(11):a040733. doi: 10.1101/cshperspect.a040733.

Worley MI, Setiawan L, Hariharan IK. Regeneration and transdetermination in Drosophila imaginal discs. Annu Rev Genet. 2012;46:289-310. doi: 10.1146/annurev-genet-110711-155637.

Wyart E, Bindels LB, Mina E, Menga A, Stanga S, Porporato PE. Cachexia, a Systemic Disease beyond Muscle Atrophy. Int J Mol Sci. 2020 Nov 14;21(22):8592. doi: 10.3390/ijms21228592.

Xin M, Kim Y, Sutherland LB, Murakami M, Qi X, McAnally J, Porrello ER, Mahmoud AI, Tan W, Shelton JM, Richardson JA, Sadek HA, Bassel-Duby R, Olson EN. Hippo pathway effector Yap promotes cardiac regeneration. Proc Natl Acad Sci U S A. 2013 Aug 20;110(34):13839-44. doi: 10.1073/pnas.1313192110.

Yokoyama H. Initiation of limb regeneration: the critical steps for regenerative capacity. Dev Growth Differ. 2008 Jan;50(1):13-22. doi: 10.1111/j.1440-169X.2007.00973.x.

Yu G, Wang LG, Han Y, He QY. clusterProfiler: an R package for comparing biological themes among gene clusters. OMICS. 2012 May;16(5):284-7. doi: 10.1089/omi.2011.0118.

Yu L, Dawson LA, Yan M, Zimmel K, Lin YL, Dolan CP, Han M, Muneoka K. BMP9 stimulates joint regeneration at digit amputation wounds in mice. Nat Commun. 2019 Feb 5;10(1):424. doi: 10.1038/s41467-018-08278-4.

Zhang J, Pavlova NN, Thompson CB. Cancer cell metabolism: the essential role of the nonessential amino acid, glutamine. EMBO J. 2017 May 15;36(10):1302-1315. doi: 10.15252/embj.201696151.

Zhang Y, Strehin I, Bedelbaeva K, Gourevitch D, Clark L, Leferovich J, Messersmith PB, Heber-Katz E. Drug-induced regeneration in adult mice. Sci Transl Med. 2015;7:290ra92.

Zhulyn O, Rosenblatt HD, Shokat L, Dai S, Kuzuoglu-Öztürk D, Zhang Z, Ruggero D, Shokat KM, Barna M. Evolutionarily divergent mTOR remodels translatome for tissue regeneration. Nature. 2023 Aug;620(7972):163-171. doi: 10.1038/s41586-023-06365-1.

Zipper L, Jassmann D, Burgmer S, Görlich B, Reiff T. Ecdysone steroid hormone remote controls intestinal stem cell fate decisions via the PPARγ-homolog Eip75B in *Drosophila*. Elife. 2020 Aug 10;9:e55795. doi: 10.7554/eLife.55795.